

Uncertainty in Well-to-Tank with Combustion Greenhouse Gas Emissions of Transportation Fuels Derived from North American Crudes

Giovanni Di Lullo, Hao Zhang, Amit Kumar*

Department of Mechanical Engineering, Donadeo Innovation Centre for Engineering, University
of Alberta, Edmonton, Alberta T6G 1H9, Canada.

Abstract

Many studies have calculated deterministic point estimates of well-to-combustion (WTC) emissions of transportation fuels from crude oil in an attempt to determine which crude oils have lower or higher emissions. However, there is considerable variation in the published results, resulting in uncertainty. The purpose of this study is to identify GHG emissions ranges for five conventional and two unconventional crudes by performing an uncertainty analysis using an improved version of the **FUNDamental ENgineering PrinciplEs-based ModeL** for Estimation of

*Corresponding Author. Tel.: +1-780-492-7797. Email: Amit.Kumar@ualberta.ca (A. Kumar).

°API, American Petroleum Institute gravity, API, American Petroleum Institute, FUNNEL-GHG-CCO, FUNDamental ENgineering PrinciplEs-based ModeL for Estimation of GreenHouse Gases in Conventional Crude Oils, FUNNEL-GHG-OS, FUNDamental ENgineering PrinciplEs-based ModeL for Estimation of GreenHouse Gases in Oil Sands, GHG, Greenhouse gas, GOR, Gas-to-oil ratio (m³/m³), GREET, Greenhouse Gases, Regulated Emissions, and Energy Use in Transportation, GWP, Global warming potential, LHV, Lower heating value (MJ/kg), OPGEE, Oil Production Greenhouse gas Emissions Estimator, P5, 5th percentile, P95, 95th percentile, PRELIM, Petroleum Refinery Life Cycle Inventory Model, SAGD, Steam assisted gravity drainage, SCO, Synthetic crude oil, SOR, Steam-to-oil ratio (cold water equivalent m³/m³), VFF, Venting, flaring and fugitive, WOR, Water-to-oil ratio (m³/m³), WTR, Well-to-refinery gate, WTT, Well-to-tank, WTC, Well-to-wheel + combustion

GreenHouse Gases (FUNNEL-GHG). Distributions for key inputs in the Monte Carlo simulation were determined based on values obtained from the literature. Eleven scenarios were developed, nine historical and two current, the former using life-long average production data from the oil fields studied and the latter using recent production data to illustrate how WTC emissions change as the fields age. The mean WTC emissions ranges for the eleven scenarios are 97.5-140 gCO₂eq/MJ. The uncertainty in the WTC emissions ranges from ±3% to ±11%. The largest source of uncertainty in the WTC emissions is from the venting, fugitive, and flaring volumes, fluid injection rates, and refinery yields.

Keywords: Life cycle assessment; well-to-combustion; CO₂ emissions; crude; uncertainty; Monte Carlo

1. Introduction

As climate change becomes a growing concern around the world, there is increased focus on the environmental impact of transportation fuel production. In 2014, the United States' greenhouse gas emissions (GHG) emissions for the petroleum and natural gas sector were 236 million tonnes CO₂eq with an additional 175 million tonnes CO₂eq from refineries [1, 2]. Growing concern over climate change has led to environmental policies such as the California Low Carbon Fuel Standard, which requires a 10% reduction in California's transportation fuels' 2007 carbon intensity by 2020 [3], and the European Union Fuel Quality Directive, which requires a 6% reduction in transportation fuels' 2010 carbon intensity by 2020 . One way to meet these reductions is to reduce the emissions generated during crude production and refining.

The well-to-combustion (WTC) emissions from different crudes vary widely depending on the production method used, the crude's properties, refining methods, regional regulations, and industry practices [4]. Additionally, as a crude reservoir ages, its pressure drops, and production decreases [5, 6]. Enhanced oil recovery methods, such as water flooding, gas injection, artificial pump lift, gas lift and steam flooding, are implemented to improve production rates [6, 7]. However, these methods increase the amount of energy required and emissions generated.

Well-to-wheel assessments, which are performed to compare gasoline vehicles to alternative drivetrain vehicles such as battery electric and hydrogen fuel cell, present their results in terms of gCO₂eq/km. However, well-to-wheel assessments that aim to compare the emissions from different crudes present their emissions in gCO₂eq/MJ. Here "MJ" refers to the lower heating value of the fuel that is released in the combustion chamber. The conversion from the fuel's lower heating value to km will depend on the efficiencies of the various components between the

combustion chamber and the wheel, and the driving cycle, which will be the same for all crudes. Therefore, ignoring the vehicle's overall fuel efficiency removes unnecessary uncertainty. Technically excluding the vehicle efficiency would make these studies a well-to-combustion assessment.

Current transportation fuel WTC assessments consist of either a high-level top-down analysis to determine industry average emissions or a bottom-up analysis to determine pathway-specific emissions. Top-down models such as the Greenhouse Gases, Regulated Emissions, and Energy Use in Transportation (GREET) and GHGenius use aggregated data, which makes it difficult to compare crudes and identify areas for improvement [8, 9]. Bottom-up models such as the Jacobs, TIAX, Oil Production Greenhouse gas Emissions Estimator (OPGEE), Petroleum Refinery Life Cycle Inventory Model (PRELIM), **FUNDamental ENgineering PrinciplEs-based ModeL for Estimation of GreenHouse Gases in the Oil Sands (FUNNEL-GHG-OS)**, and **FUNDamental ENgineering PrinciplEs-based ModeL for Estimation of GreenHouse Gases in Conventional Crude Oils (FUNNEL-GHG-CCO)** use engineering first principles to calculate the amount of energy required and emissions produced at each stage [10-16]. Bottom-up models have uncertainties as they focus only on the large pieces of equipment and do not capture every source of emissions; however, the models provide details on the emissions from specific sub-processes.

The previous transportation fuel WTC assessments produce deterministic point estimates (versus Monte Carlo, which uses distributions to determine inputs), which vary significantly among models. The variations are due to inconsistent boundaries, assumptions among the models, and differences in the model inputs. The Carnegie Endowment for International Peace published a report titled "Know Your Oil" on the WTC emissions from thirty different crudes with consistent system boundaries using the OPGEE and PRELIM models [4]; however, the

report does not include an uncertainty analysis, without which the confidence of the models is not determined. In order to compare crudes and determine which crudes have high and low emissions, a quantified uncertainty range is required. If the uncertainty in the emissions were larger than the difference in emissions between two crudes, it would not be possible to confidently state which crude has lower emissions.

Quantifying the effect each input uncertainty has on the total uncertainty will provide insight into how the model's accuracy can be improved. Furthermore, the assumptions made in WTC assessments are frequently questioned. Interested parties will ask how the results will change if certain parameters are varied and use the lack of information as justification to invalidate the work. By using ranges for the inputs we can show that with reasonable certainty, the emissions will be within the specified range. Input ranges also help reduce the effect of author bias (intentional or more often unintentional) as the ranges are generated from multiple data sources. Uncertainty has been examined in top-down models such as GREET [17, 18] and by Venkatesh et al. [17-19]; however, as mentioned earlier, the top-down models do not allow the examination of specific crude pathways. And although researchers like Spatari and MacLean performed a bottom-up uncertainty analysis, they focused on lignocellulose-based ethanol fuels and not conventional gasoline, diesel, and jet fuel [20].

Work by Vafi and Brandt [21] and Brandt et al. [22] assessed uncertainty in the regional well-to-refinery gate (WTR) emissions using smart defaults when crude-specific data are unknown. The goal of our work is to use crude-specific data as much as possible and focus on specific fields rather than regions. This will allow us to identify the high and low emission-intensive areas for comparison. The narrower scope will not only allow the examination of specific crude pathways but different technology pathways as well. Additionally, this work adds on the refinery-to-wheel

stages to complete the WTC scope. Adding the refinery is important as the refinery yields will magnify the pre-refinery emissions and have a significant effect on the final WTC emissions.

In conclusion, a model that can accurately calculate the WTC emissions of various crudes with uncertainty is needed to fill the current gap in the literature. This work focuses on the uncertainty and variability along a specific crude production pathway. Uncertainty from using alternative technologies, such as different refinery configurations, is outside the scope of the current work.

The main goal of this study is to quantify the uncertainty of the WTC emission estimates; this will be accomplished through the following three stages. The first is to perform an uncertainty analysis and determine the GHG emissions ranges of the five selected conventional crude oils and two unconventional crudes. The second is to identify what additional data are required to improve the accuracy of the emission estimates of each crude oil. The third is to examine how emissions change as the condition of the crude field declines near the end of its useful life. The results of this study will enhance the understanding of the accuracy of the WTC emission estimates that are used in developing GHG reduction policies. The results showing how emissions increase as a field ages will also be useful to policy makers and industry leaders when assessing whether to keep producing from an aging field.

2. Methodology

This study uses the FUNNEL-GHG-CCO&OS modules, published in 2014 [12-16, 23], as the basis for our uncertainty assessment. The goal of this study is to integrate the two previous models into a single universal model and enhance the model by adding an uncertainty analysis.

The Excel-based models are flexible and transparent, making them ideal for this study. First, we modified the original model to improve the accuracy of the WTC estimates. Then we performed

a sensitivity analysis to identify sensitive inputs and ran a Monte Carlo simulation to determine the uncertainty ranges in each crude's WTC emissions.

2.1 Base case model

Since our focus is an uncertainty analysis, this paper only gives a brief overview of the FUNNEL-GHG-CCO&OS modules, hereafter jointly referred to as the F-1 model. Readers are encouraged to refer to the previously published work for additional details [12-16, 23].

The F-1 bottom-up model uses engineering first principles to calculate energy use and emissions generated at each stage from raw material production to product end use.

Figure 1 shows the seven main sub-processes within the model boundary.

The production stage includes drilling the wells, injecting fluids to maintain reservoir pressure, and lifting the crude to the surface. Surface processing includes crude stabilization, gas treatment, and water treatment. Unconventional crudes need to be either upgraded or mixed with diluent prior to being transported to the refinery. Crude is transported by a combination of pipelines and marine vessels to refineries where it is processed into gasoline, diesel, and jet fuel. The finished products are distributed to bulk terminals by pipelines, trains, barges, and tankers and then distributed to fueling stations by truck. The final stage is combustion in a vehicle or aircraft.

This study uses a functional unit of $\text{gCO}_2\text{eq/MJ}$ of gasoline produced unless specified otherwise. The paper focuses on gasoline production emissions, as the emissions from diesel and gasoline are relatively similar. All of the emissions generated before the refinery stage are the same for all three fuels. The only variation is in the refinery, distribution, and combustion stages, and is

relatively small compared to the variation between crudes. Therefore, the diesel and jet fuel emissions are included in section A6 of the appendix for interested readers.

Figure 1: The FUNNEL-GHG model stages from well to combustion (*upgrading applies to Alberta synthetic crude oils [SCO] only)

The F-1 model analyzes five conventional and two unconventional crude oils with each crude oil using a unique production method (see Figure 1). Maya oil is a Mexican heavy crude, 22° API, produced from the Cantrell field located 100 km off the coast of the Yucatan Peninsula [23]. Mars crude is a light, 31.5° API, sour crude produced from an offshore platform in the U.S. Gulf Coast [23]. Bow River oil is a heavy, 23° API, conventional oil produced in Alberta, Canada [23]. Alaska North Slope (Alaska) crude is primarily produced from the Prudhoe Bay field and is a medium, 29° API, oil [23]. California Kern County crude is a heavy, 13° API, crude produced primarily from the Midway-Sunset oil field [23]. Athabasca crude has an API of 8.2 and is produced primarily via steam assisted gravity drainage (SAGD) and surface mining [12, 15, 16]. The Athabasca crude is either shipped to the U.S. as dilbit or upgraded in Alberta and shipped as synthetic crude oil (SCO). Thus, there are four Athabasca scenarios: SAGD-Bitumen, SAGD-SCO, Mined-Bitumen, and Mined-SCO.

This study assumes all crudes are refined in the U.S. The refineries are located in Los Angeles, California for Alaska and Kern; Cushing, Oklahoma for Mars, Bow River, and Athabasca; and Houston, Texas for Maya [23].¹⁵

The F-1 model focuses on assessing specific technology pathways; as a result, the model's uncertainty analysis does not capture variations from using different technology pathways such as different refinery configurations. The F-1 model assumes deep conversion refineries for all crudes as these are typical for North America, unlike "Know Your Oil," which uses different

refinery types for each oil [4, 23]. Future work will examine the effect of different refinery configurations and crude blending.

2.1.1 Base case model modifications

In order to improve the accuracy of the F-1 model we made five modifications, including using detailed calculations for sub-processes that are large sources of emissions and integrating new sources that are more accurate. The modified model will be referred to as the F-2 model. The modifications are described below.

The F-1 model only examined single stage rather than multistage compressors. Using single stage compressors would over-estimate the amount of energy required by the compressor when large compression ratios were required [13, 14, 23]. Compressors are used either to inject gas into the reservoir to maintain pressure or to aid in production using a gas lift system. The F-2 model calculations were modified using equations for multistage compressors from the OPGEE model described in the “Know Your Oil” report [4, 24]. The number of compressor stages is chosen such that the compressor ratio of each stage is below 5, as higher compression ratios result in excessive outlet temperatures, thereby decreasing efficiency [24, 25].

The original F-1 model assumed that 100% of California Kern and Athabasca steam is produced via cogeneration within the plant [23]. However, in reality the cogeneration capacity in the Midway-Sunset and Athabasca field can only provide approximately 30% and 18% of the field’s steam requirement, respectively. A once-through steam generator is added to the model to account for the remaining steam [12]. Additionally, data from OPGEE were used to update the cogeneration calculations to include a range of cogeneration configurations [26].

Because there were limited data on venting, flaring, and fugitive (VFF) emissions, the F-1 model used a simplistic estimate. Research by Canter et al. determined a range of venting and fugitive emissions for crude oils by examining several pieces of literature [27]. Canter et al. integrated the VFF ranges into the F-1 model to improve the accuracy of the VFF emissions. We expanded on the work done by Canter et al. and added fugitive emissions for reinjected produced gas. For the F-1-OS module, Alberta-specific data were used to determine the VFF emissions.

Excess produced gas was not considered in the original F-1 model. This gas, however, can be used to offset natural gas consumption. The OPGEE model applies a credit for the production of produced gas equal to the natural gas upstream emissions with the transportation emissions excluded [24]. This credit method is integrated in the F-2 model to align the model boundaries with those in existing literature.

The F-1 model assumed all crudes have the same energy content. The new model calculates the lower heating value (LHV) using a correlation from Speight [28]. This correlation depends on the crude's specific gravity and has been used by the GREET and PRELIM models [8, 29].

The F-1-OS module originally did not include land use emissions and now uses the F-1-CCO methodology to calculate land use emissions. Lastly, the F-2 model uses updated emission factors from GREET 2015, the F-1 model used GREET 2013. The crude transportation emissions have been updated to be consistent with work done by Di Lullo et al. which focused on non-North American crudes [30]. Detailed information on the modifications made to the original F-1 model is provided in section A1.

2.2 Uncertainty analysis methodology

Output uncertainty in this study has two parts, input uncertainty and input sensitivity [31]. Inputs with high sensitivity and high uncertainty will have a large effect on the output distribution.

Hence, a sensitivity analysis was first conducted to identify which key inputs should be further examined. Distributions for the key inputs were calculated from values obtained from the literature. ModelRisk, an Excel add-in software, was used to run a Monte Carlo simulation and determine the WTC emissions uncertainty [32]. Figure 2 provides an overview of the methodology used.

Figure 2: Methodology overview (WTT = well-to-tank)

2.2.1 Identify sensitive inputs

A +/-25% range of each input base case value was used in the sensitivity analysis on the WTT (well-to-tank) emissions, only one input is varied at a time. WTT emissions were analyzed instead of WTC emissions because combustion emissions, which represent 60%-90% of the total emissions and are constant for all of the scenarios, would minimize the input sensitivity [33].

Spider plots were used to identify any non-linear responses.

2.2.2 Determine distributions for key inputs

Due to the lack of publically available data, a conservative approach was used to determine the key input distributions. Triangle distributions require a most likely, minimum, and maximum estimates to generate and they favor extreme values [34], which results in a conservative output distribution. ModelRisk's copulas were used to link dependent inputs; for example, in the Alaska scenario, the produced gas volume is dependent on the injected gas volume. Figure 3 provides a

high-level overview of the identified key inputs; additional details are provided in section A4. Tables A4 to A6 show a summary of the Monte Carlo input distributions and their sources.

2.2.3 Determine distributions for insensitive inputs

The insensitive variables individually have little effect on the overall results but their combined effect could have a significant effect. As a result, all of the insensitive inputs are assigned an arbitrary triangle distribution wherein the maximum and minimum values are defined as +/- 10% of the base case value. The output distributions with and without the insensitive input distributions are then compared to determine if ignoring the uncertainty in the insensitive values will have a significant effect on the results. Ideally, every input should have an uncertainty distribution but due to the large number of inputs, this is not practical.

3. Monte Carlo Simulation

A Monte Carlo simulation allows us to examine how the resulting WTC emissions change as multiple key inputs are varied across a wide range of values. The Monte Carlo simulation ran with 50,000 samples, which ensures that the simulation sampling error has a 99% probability of being less than 0.1 gCO₂eq/MJ. The sampling error calculations and values for each crude are in section A2 [35]. The results are reported using the 5th and 95th percentiles (P5, P95). An iterative approach was used wherein the ModelRisk-generated tornado plots were used to determine which inputs should receive more focus.

The tornado plots are generated by calculating the output mean from a subgroup of Monte Carlo samples. Each subgroup contains only the samples where the input value is within a given percentile range. This study used a 5% range (20 tranches); therefore, the subgroups would be split into ranges of P0-P5, P5-P10, et cetera. The subgroups with the largest and smallest output

means are used as the tornado plot's maximum and minimum values [36]. Due to the number of inputs used and the accuracy of the tornado plots, only the key inputs are included. The tornado plots were further filtered to display only the significant inputs. An input was classified as significant if the input's tornado plot variance (maximum – minimum) was greater than 10% of the WTC variance (P95-P5).

Due to the complexity of the refinery portion of the model, an in-depth analysis was not performed for the refinery stage. The F-1 model uses Aspen HYSYS, an advanced refinery modeling software that is used globally by the oil and gas industry [37], to model the refinery. Aspen generates energy and mass balances for each process unit in the refinery [23], which are used by the F-1 model to allocate emissions to the transportation fuels. The Aspen model used was selected as it is based on a typical North American refinery. The uncertainty in the process units' mass and energy balances is not examined in this study due to the complexity of the refining process. However, boiler and heater efficiency as well as electricity emission factors are assigned Monte Carlo input distributions. The refinery yield is also assigned a range to reflect uncertainty from optimizing the refinery. Refinery emissions are determined using a Monte Carlo simulation that only examines the refinery portion of the model. Refinery output emissions are fed into the main model as Monte Carlo input distributions (Table A8). A second Monte Carlo simulation is run to find the WTC emissions.

3.1 Monte Carlo simulation inputs

The key inputs with their distributions and sources are listed in Table A5 and for general inputs that apply to all crudes and in Table A6 and A7 for the crude-specific inputs. The Monte Carlo inputs include emission factors, efficiencies, specific heat capacities, process temperatures, VFF volumes, fluid injection and production ratios, well depths, process pressures, and other

parameters (Figure 3). Additional information on how the distributions are determined for each input is in section A4.

Figure 3: Summary of key inputs identified by the sensitivity analysis and used in the Monte Carlo simulation; see section A4 of the appendix for additional details

3.2 Monte Carlo historical and current scenarios

Originally, one Monte Carlo scenario was run for each of the five crudes; however, for the Alaska and California Kern crudes the original results were 49 and 11% higher than the previous estimates from the F-1 model, respectively [23]. Additionally, the Kern scenario results were 25 and 41% higher than the Jacobs and TIAX results, respectively [10, 11]. Further investigation found that the discrepancy was from the assumed water and gas injection and production ratios. The Alaska and Kern fields have been using enhanced oil recovery for over 20 years [33, 38], and as the fields age the injection and production ratios have increased. Since the WTC emissions are sensitive to the injection and production ratios, two scenarios were developed for these fields, historical and current. The historical scenario uses cumulative ratios, which give an estimate of the average WTC emissions over the entire life of the field. The current scenario uses recent ratios to investigate how the WTC emissions rise as the field ages. Using two scenarios will provide more insight into how the WTC emissions can vary depending on the age of the data used.

Since we are interested in assessing how the WTC emissions change over time this analysis focuses specific oil fields. For Alaska this analysis focused on the Prudhoe Bay and Kuparuk fields as they represent 75% of Alaska current production and are adjacent [39]. The startup of the remaining fields in Alaska was not included. As a result of injecting lean gas the Prudhoe bay crude API has increased by 5° over the last 15 years [40]; hence, we used two crude assays to

determine the refinery emissions for the historical case (see section A3) [41, 42]. For Alaska, all of the wells in the Prudhoe Bay area are included as the water and gas injection affects the entire field. For California Kern this analysis focused on the Midway-Sunset field. Unlike Alaska the crude composition has not changed significantly with time [43, 44].

The only differences between the historical and current scenarios are the inputs for the injection WOR and GOR, and the production WOR and GOR, as well as the refinery crude assay for Alaska historical scenario only. Tables A3 and A4 show how the injection and production rates for Alaska and Kern have increased over time.

4. Results and Discussion

The resulting WTC distributions show that the Alaska and Kern current scenarios have the highest emission intensity (Figure 4A). Additionally, the Alaska and Kern current and historical scenarios show that emissions increased by 34% and 30%, respectively, as the fields aged. The Mars and Maya crudes have the lowest emission intensity due to their low energy intensive production methods (Figure 4A).

Figure 4: A) Gasoline WTC emissions and B) Venting fugitive and flaring emissions. Synthetic crude oil (SCO) pathways include upgrading. The additional Alaska and Kern scenarios are included to show the effect of reservoir age on the WTC emissions. P95, P75, P25, and P5 represent the respective percentile values.

Figure 4A additional data from the literature:

- Jacobs produced a bottom-up model that examined 9 crudes (2009) [10]
- TIAX's WTC bottom-up model focused on creating a detailed refinery model (2009) [11]
- Know Your Oil (KYO) performed a detailed bottom-up WTC model examining 30 crudes (2015) [4]
- GREET is a top-down model focused on determining regional averages (2015) [45, 46]
- F-1-CCO (2014) [13, 14, 23], and F-1-OS (2014) [12, 15, 16] are bottom-up models focusing on conventional crudes (CCO) and unconventional crudes (OS). The model developed in this study was built by combining and improving these two models

When the error bars of two crudes overlap, it is not possible to confidently conclude that one crude oil has lower emissions than the other does. The results in Figure 4A show an overlap

between most of the crudes studied; this is because of the conservative approach taken in defining input distributions for the Monte Carlo simulation. However, the current Alaska and Kern scenarios clearly produce higher emissions than the other scenarios. Additionally, even with the conservative uncertainty, the Kern historical scenario does not overlap the Mars and Maya scenarios. While it is not possible to definitively rank each crude based on its emission intensity, it is still possible to differentiate between high and low emission crudes.

Figure 5: Tornado plots of the gasoline WTC emissions for conventional crudes

Inj.: injection, **Eff:** efficiency **EF:** emission factor, **NG:** natural gas, **PG:** produced gas, **MD:** marine diesel

Figure 6: Tornado plots of the gasoline WTC emissions for conventional crudes

Inj.: injection, **Eff:** efficiency **EF:** emission factor, **NG:** natural gas, **Sep:** separation

Tornado plots (Figure 5&6 and Figure A3-A6) are used to identify which inputs have the largest effect on the output uncertainty; inputs with a wider range have a larger effect on the output uncertainty. The refinery and VFF emissions are a significant source of uncertainty for all crudes and represent 12- 2%, and 1-8% of the WTC emissions, respectively. Additional production specific parameters such as the injection SOR, injection GOR, and ore separation temperatures significantly affected the uncertainty for crudes that used an energy-intensive production method. Some inputs result in larger uncertainties than others do due to either a lack of information or a wide range of data in the literature. Additionally, inputs with higher sensitivity will have a larger effect on the WTC uncertainty. Importantly, tornado plots cannot accurately display dependent inputs that are linked with a copula. For example, the produced WOR has a relatively small effect on the WTC emissions, but since it is linked to the injection WOR, which does have a significant effect on the WTC emissions, it appears to be significant on the tornado plot.

Figure 7: Bow refinery and venting, fugitive, and flaring tornado plots

EF: emission factor, NG: natural gas, PG: produced gas. Refinery emissions are for gasoline, VFF emissions are the same for gasoline, diesel, and jet fuel. Tornado plots for the remaining crudes, diesel, and jet fuel are in section A6

4.1 Refinery uncertainty

The uncertainty in the refinery stage has two main sources, the refinery yield factor and emissions. The refinery yield factor is the ratio of crude oil energy content to the finished product's energy content. The yield factor depends on the crude properties and refinery configuration. For example, the yield factor for Alaska from PRELIM varies from 1.07 to 1.53, depending on the refinery configuration [29]. A yield factor of 1.5 means that 1.5 bbls of crude are required to produce 1 bbl of transportation fuels; therefore, as the yield factor increases, the production emissions increase, because more crude is required per barrel of product. The WTC variance of the yield factor ranges from 6.9 to 7.4 gCO₂eq/MJ for the Kern current and Alaska current scenarios.

Five of the six inputs in the refinery tornado plots (Figures 7 & A7) are related to the natural gas consumption, as natural gas is the primary energy source for the refinery. Therefore, efficiency improvements have the potential to significantly reduce the refinery emissions. The natural gas upstream emission factor is the first or second largest source of uncertainty for all eight crudes, therefore understanding where each refinery gets its natural gas from will have a significant effect on the results.

The large effect the refinery emissions have on the WTC emissions suggests that a more in-depth analysis is required to understand the emissions from the complex refinery processes.

Additionally, it should be noted that the refinery yield factor can decrease by using additional conversion processes to further upgrade the bottom-of-the-barrel products, which results in

higher emissions [29]. The current model does not include this correlation and provides a conservative range of WTC emissions.

4.2 Venting, fugitive, and flaring uncertainty

VFF emissions are one of the main sources of uncertainty. The VFF uncertainty is primarily due to fugitive volumes, flaring volumes, methane GWP, and produced gas methane concentrations (see Figure 7 for an example).

Canter et al. studied venting and fugitive gas volumes for North American crudes by examining multiple sources for the oil and gas industry [27]. However, there is a wide range of values in these sources, which rely on approximation methods. There are limited publically available data on directly measured fugitive volumes from crude oil production and refinement [27]. To accurately determine the WTC emissions for the various crudes, more information is needed on the amount of fugitive gas released, especially for gassy oils, as in the Alaska current scenario. The injected gas fugitives are calculated specifically for the Alaska scenarios and are described in section A4.5. As they are the largest source of uncertainty for the Alaska current scenario, more detailed data are required to reduce the uncertainty in the WTC emissions. Due to the unique process used for the Athabasca oil sands, crude-specific data were collected to model the VFF emissions (section A4.9).

Methane GWP values also affect the uncertainty of the model results. Methane GWP values have a $\pm 35\%$ uncertainty range [47, 48]. Usually a GWP of 34 is applied to the methane emissions to convert to GHG emissions (CO_2eq) [47, 48]. However, in an uncertainty analysis of total GHG emissions, a higher methane GWP value will have a relatively larger impact on the total GHG emissions for crudes with large VFF volumes compared to crudes with small VFF volumes.

VFF emissions depend on the concentration of methane in the produced gas. The data analyzed for California showed that methane concentrations could vary from 50-100%, with a mean of 84%. OPGEE and the original F-1 model used 84% for all of the crudes analyzed [23, 49]. Jacobs and TIAX use 75% and 80% methane for their produced gas, respectively [50, 51]. Methane gas concentrations for each well should be reported to get a better understanding of the produced gas emissions.

Flared gas volumes also have a wide range of uncertainty due to the limited data and range from $\pm 91\%$ to $\pm 382\%$ [52]. Though a wide conservative range of 80%-99% flaring efficiency was assumed, it resulted in a relatively small variance of 0.4 to 1.2 gCO₂eq/MJ for five of the eleven scenarios (Figure A8). However, for the Alaska historical and current scenarios the ranges were 3.4 and 3.3 gCO₂eq/MJ, respectively, as the larger flaring volumes amplified the effect of the flaring efficiency. Therefore, flaring efficiency should be closely monitored for gassy oil.

For the Alaska scenarios, the injection and production GOR values are significant since the venting and fugitive gas volumes are determined as a percentage of the produced gas volume. The produced gas volume also depends on the injected gas volume and is modelled using ModelRisk copulas.

The distribution of VFF emissions in Figure 4B shows that a significant amount of the uncertainty in WTC emissions is due to VFF emissions. The VFF variance (P95-P5) is 57%-88% of the WTC variance for the Mars, Maya, Bow, and Alaska crudes. For Kern, the VFF variance is less than 15% of the total variance as it produces less gas than the other scenarios. For the mining scenarios, the VFF variance is 40% due to the high pond and mine surface fugitive emissions, while for SAGD it is less than 1% due to the low produced gas volumes. This shows

that for crudes with a large production GOR, a better understanding of the VFF gas volumes is required to accurately estimate the WTC emissions.

4.3 Effect of field age on WTC emissions

Alaska and Kern current scenarios show emissions increases of 34% and 30%, respectively, from the historical scenarios (Figure 4A). These increases are a result of increased water and gas injection and production rates as discussed in section 3.2.

For the Kern scenario, the increase in emissions is primarily due to the production emissions, while VFF emissions are similar for the current and historical scenarios, as seen in Figure 4B. Kern has high production emissions because it requires thermal enhanced oil recovery methods. The other crudes use mechanical enhanced oil recovery methods, which are less energy intensive. The injection SOR, production WOR, steam energy, and natural gas emission factors are the largest sources of uncertainty for the Kern scenarios. For the Alaska scenarios, the mean VFF emissions increased from 6.8 to 30.0 gCO₂eq/MJ, while the mean well-to-refinery (WTR) emissions, excluding the VFF emissions, increased from 7.5 to 20.9 gCO₂eq/MJ. A better understanding of the VFF and production emissions will become increasingly important as Alaska gas and water volumes continue to increase.

4.4 Effect of insensitive inputs

The Monte Carlo gasoline WTC simulation results in Figure 4 include the key inputs only. A comparison of the WTC emissions with and without the insensitive inputs found that the insensitive inputs had a negligible effect, the variance increased by less than 1%. This confirms

the original assumption that detailed distributions are not required for the insensitive inputs as the effect will be negligible.

4.5 Model comparison with published literature

This study used an uncertainty analysis to determine the most likely range of emissions for each crude using a range of values for various inputs. If the input ranges used in this study cover all reasonable values, then the results from another model with the same model boundaries should be within the output ranges found in this study. Figure 4A compares the WTC emissions for gasoline from this study, Jacobs, TIAX, “Know Your Oil” (KYO), and the original F-1 model. The models in Figure 4A do not have the same boundaries, and as a result some of the WTC emissions are outside the range found in this study. The Jacobs and TIAX, F-1, and KYO models were developed in 2009, 2014, and 2015, respectively, and so did not use the same emission factors and methane GWP [4, 23, 50, 51]. The F-2 model and the KYO model use 34 as the methane GWP and the others use 25 [4, 10, 11, 23].

The TIAX emissions results are significantly lower than the other models’. This is because TIAX uses a simpler approach than the others when modeling well-to-refinery entrance emissions and focuses more on the refining emissions. TIAX uses medium conversion refineries; we used deep conversion, which results in lower refinery emissions.

The KYO and Jacobs results, except for the Jacobs Mars results, were within the range of values reported for all the crudes in this study. For Mars, the Jacobs results are higher than ours are due to the produced gas credit and the water injection ratio. This study calculated a 3.7 gCO₂eq/MJ

gas credit. Jacobs does not use a gas credit for produced gas, and it used a water injection ratio of $5.5 \text{ m}^3/\text{m}^3$, which is the highest water production ratio in our study [10].

Interestingly, the KYO, F-1, and Jacobs model results line up with the lower end of our Kern current scenario. This makes for KYO and the F-1 model since they use SORs of 5.79 and 5.13 m^3/m^3 while our scenario uses a mean SOR of $5.74 \text{ m}^3/\text{m}^3$ with a minimum of $4.72 \text{ m}^3/\text{m}^3$. It was initially unclear why the Jacobs Kern scenario is 7% lower than our current scenario as it uses a SOR of $5 \text{ m}^3/\text{m}^3$. Further investigation found that the variation was due to the refinery and electricity emissions. The Jacobs refinery emissions were lower due to differences in the refinery configurations used. The electricity emissions for the F-2 model were higher because the cogenerated electricity had a higher emission intensity than the grid electricity, which was used by Jacobs [10].

The original F-1 results differ from the F-2 results primarily due to the new VFF emissions. For example, the additional fugitive emissions for the reinjected gas increased the F-2 Alaska scenario emissions by 5 and 29% for the current and historical scenarios, respectively. This study's mining emissions tended to be higher than those from earlier studies due to the addition of land use and VFF emissions not included in the previous models and larger refinery emissions. The bitumen pathways also were found in this study to have high refinery yield factors, which magnified the upstream emissions. The F-1-OS emissions are shown as a range representing the cogen/no-cogen and coking/hydroconversion upgrading scenarios in the original F-1-OS model.

5. Policy implications

The uncertainty ranges determined by this study are important to policy makers and industry representatives as they show that even though these models have limitations, it is possible to

differentiate between high and low emission crudes. Our results also showed that there is a large variation in the WTC emissions between crudes. The top-down GREET model found that the North American average WTC emissions for gasoline are 92 gCO₂eq/MJ, which is 32% lower than our results for Alaska [45]. While GREET's high-level analysis is appropriate for a country-wide analysis, it lacks the detail required to form specific regional policy. For example, when attempting to determine how stricter venting, fugitive, and flaring regulations will affect the WTC emissions of Alaska crude, a detailed bottom-up model is required.

Additionally, Alberta's recently introduced Climate Leadership Plan limits GHG emissions from the oil and gas industry to 100 Mt/y [53]. The current scenarios for Alaska and Kern show that as fields age their production emissions can grow significantly. As the Athabasca SAGD oil sands wells age, policy makers should monitor the SOR to ensure a similar emissions increase does not occur. Our model can be used to identify poor performance wells and areas for potential emissions reduction. To limit emissions, governments may want to implement limits on the injection fluid ratios.

Using distributions for key inputs allowed our results to include estimates from several data sources. For example, KYO, Jacobs and the F-1 model assumed that the Mars production WOR was 0.2, 5.5 and 5.5, respectively [4, 13, 50]. By using a range of 0.02 to 5.5, we are able to produce a WTC estimate that was not dependent on whether we used data source A or B, reducing the effect of unintentional bias.

The Alaska and Kern current and historical scenarios further highlighted the advantage of using multiple scenarios and distributions for key inputs. The wide range in WTC emissions estimates in the literature, from 85-111gCO₂eq/MJ, and 101-135 gCO₂eq/MJ for Alaska and Kern, respectively, was a result of the assumed values used for the injection and production fluid ratios

[4, 11, 13, 50]. While all of the studies used similar data sources, variations in their assumed values resulted from the timeframe used. Since both crudes experienced periods of rapid decline, using an average over the last five years rather than the last ten years will provide significantly different values.

By determining the results as uncertainty distributions, rather than deterministic point estimates, we can reduce the severity the subjective assumption have on the WTC emissions. These ranges help policy makers understand how the assumed values affect the results and provide a more realistic overview of the differences in the crudes' WTC emissions. For example, the European Union's Fuel Quality Directive proposed grouping crudes in three categories (conventional crude, oil shale, and natural bitumen) and applying a default emission intensity for each group [54]. However, our analysis shows that due to the overlap in the WTC uncertainty ranges and the wide variation among crudes emissions, the use of generic defaults is unwise.

The VFF emissions were a large source of uncertainty in our model. While various government organizations provide high-level data on VFF gas volumes, the aggregated nature of the data makes it difficult to determine crude-specific VFF ratios. Additionally, some data sources such as the Alaska Oil and Gas Conservation Commission aggregate venting and flaring gas volumes [55]. Since the GHG emission intensity of venting is nearly 7 times higher than flaring, distinguishing between the two is essential to produce accurate WTC emission estimates. The VFF emissions, refinery natural gas consumption, refinery yield factors, natural gas upstream emission factors, and injection and production gas-to-oil ratios and water-to-oil ratios were found to have the largest effect on uncertainty. Policy makers interested in accurately determining the GHG emissions should focus on gathering additional data from industry related to these inputs.

When we compared our results to Di Lullo et al.'s, which examine the uncertainty in the WTC emissions for crudes extracted outside of North America [30], we found that there was no relation between crude WTC emissions and geographic location.

6. Conclusion

This study combined the FUNNEL-GHG-OS and FUNNEL-GHG-OS bottom-up life cycle assessment models into a single integrated Excel model, named F-2. This F-2 model was improved to expand its scope and updated to include current data. A sensitivity analysis was used to identify key inputs whose values have a significant effect on the WTC emissions. A Monte Carlo simulation using distributions for the key inputs was used to determine uncertainty ranges for the WTC emissions of eleven crude scenarios. Inputs that had a significant effect on the output uncertainty were determined using tornado plots. We found that while there is overlap between the WTC emission uncertainty ranges, it is still possible to differentiate between high and low emission crudes. The VFF emissions, refinery natural gas consumption, refinery yield factors, natural gas upstream emission factors, and injection and production gas-to-oil ratios and water-to-oil ratios were found to have the largest effect on uncertainty.

7. Acknowledgements

The authors thank the NSERC/Cenovus/Alberta Innovates Associate Industrial Research Chair Program in Energy and Environmental Systems Engineering and the Cenovus Energy Endowed Chair Program in Environmental Engineering (Grant No. IRCPJ 436795 & 436794 - 2011) for funding the research project. The authors are grateful to representatives from Cenovus Energy Inc., Suncor Energy Inc., Alberta Innovates Energy and Environment Solutions (AI-EES) and

Alberta Innovates Bio Solutions (AI-BIO) for their inputs and comments during the course of this study. The authors are thankful to Astrid Blodgett for editorial assistance with this paper.

9. References

1. Environmental Protection Agency, *Greenhouse Gas Reporting Program: Refineries*. 2014, EPA, <http://www.epa.gov/ghgreporting/ghgrp-2014-refineries> (Nov. 11, 2016).
2. Environmental Protection Agency. *Greenhouse Gas Reporting Program: Petroleum and Natural Gas Systems*. EPA, <http://www.epa.gov/ghgreporting/ghgrp-2014-petroleum-and-natural-gas-systems> (Nov. 11, 2015).
3. California Air Resources Board. *Low Carbon Fuel Standard Program Background*. Feb. 2, 2016 [cited Feb. 11, 2016]; Available from: <http://www.arb.ca.gov/fuels/lcfs/lcfs-background.htm>.
4. Gordon, D., et al., *Know Your Oil: Creating a Global Oil-Climate Index*. 2015, Carnegie Endowment for International Peace: Washington, http://carnegieendowment.org/files/know_your_oil.pdf (Feb. 18, 2016).
5. Alaska Oil and Gas Conservation Commission. *Prudhoe Bay Field, Prudhoe Oil Pool - EOR Injection*. 2004, Alaska Department of Administration: Anchorage, AK, http://doa.alaska.gov/ogc/annual/2004/Oil_Pools/Prudhoe%20Bay%20-%20Oil/Prudhoe%20Bay,%20Prudhoe%20Bay/Cht_Inj_EOR.pdf (Apr. 29, 2016).
6. Wikipedia. *Oil depletion*. Mar. 18, 2016 [cited June 28, 2016]; Available from: https://en.wikipedia.org/wiki/Oil_depletion.
7. Rigzone. *What Is EOR, and How Does It Work?* [cited June 28, 2016]; Available from: http://www.rigzone.com/training/insight.asp?insight_id=313.
8. Argonne, *GREET1*. 2015, Argonne National Laboratory: Argonne, IL, <https://greet.es.anl.gov/> (June 14, 2016).
9. (S&T)² Consultants Inc., *GHGenius*. 2012, (S&T)² Consultants Inc: Delta, BC, <http://www.ghgenius.ca/downloads.php> (May 16, 2016).
10. Keesom, W., S. Unnasch, and J. Moretta, *Life Cycle Assessment Comparison of North American and Imported Crudes prepared for Alberta Energy Research Institute*. July 2009, Jacobs Consultancy: Chicago, IL, <http://eipa.alberta.ca/media/39640/life%20cycle%20analysis%20jacobs%20final%20report.pdf> (June, 14, 2016).
11. Rosenfeld, J., et al., *Comparison of North American and Imported Crude Oil Lifecycle GHG Emissions - Final Report Prepared for Alberta Energy Research Institute*. July 6, 2009, TIAX LLC: Cupertino, CA, <http://eipa.alberta.ca/media/39643/life%20cycle%20analysis%20tiax%20final%20report.pdf> (Mar. 25, 2016).
12. Nimana, B., C. Canter, and A. Kumar, *Life cycle assessment of greenhouse gas emissions from Canada's oil sands-derived transportation fuels*. *Energy*, 2015. **88**: p. 544-554, doi: <http://dx.doi.org/10.1016/j.energy.2015.05.078>.
13. Rahman, M.M., C. Canter, and A. Kumar, *Well-to-wheel life cycle assessment of transportation fuels derived from different North American conventional crudes*. *Applied Energy*, 2015. **156**: p. 159-173, doi: <http://dx.doi.org/10.1016/j.apenergy.2015.07.004>.

14. Rahman, M.M., C. Canter, and A. Kumar, *Greenhouse gas emissions from recovery of various North American conventional crudes*. *Energy*, 2014. **74**: p. 607-617, doi: <http://dx.doi.org/10.1016/j.energy.2014.07.026>.
15. Nimana, B., C. Canter, and A. Kumar, *Energy consumption and greenhouse gas emissions in the recovery and extraction of crude bitumen from Canada's oil sands*. *Applied Energy*, 2015. **143**: p. 189-199, doi: <http://dx.doi.org/10.1016/j.apenergy.2015.01.024>.
16. Nimana, B., C. Canter, and A. Kumar, *Energy consumption and greenhouse gas emissions in upgrading and refining of Canada's oil sands products*. *Energy*, 2015. **83**: p. 65-79, doi: <http://dx.doi.org/10.1016/j.energy.2015.01.085>.
17. Elgowainy, A., et al., *Energy Efficiency and Greenhouse Gas Emission Intensity of Petroleum Products at U.S. Refineries*. *Environmental Science & Technology*, 2014. **48**(13): p. 7612-7624, doi: 10.1021/es5010347.
18. Han, J., et al., *A comparative assessment of resource efficiency in petroleum refining*. *Fuel*, 2015. **157**: p. 292-298, doi: 10.1016/j.fuel.2015.03.038.
19. Venkatesh, A., et al., *Uncertainty Analysis of Life Cycle Greenhouse Gas Emissions from Petroleum-Based Fuels and Impacts on Low Carbon Fuel Policies*. *Environmental Science & Technology*, 2011. **45**(1): p. 125-131, doi: 10.1021/es102498a.
20. Spatari, S. and H.L. MacLean, *Characterizing Model Uncertainties in the Life Cycle of Lignocellulose-Based Ethanol Fuels*. *Environmental Science & Technology*, 2010. **44**(22): p. 8773-8780, doi: 10.1021/es102091a.
21. Vafi, K. and A.R. Brandt, *Uncertainty of Oil Field GHG Emissions Resulting from Information Gaps: A Monte Carlo Approach*. *Environmental Science & Technology*, 2014. **48**(17): p. 10511-10518, doi: 10.1021/es502107s.
22. Brandt, A.R., Y. Sun, and K. Vafi, *Uncertainty in Regional-Average Petroleum GHG Intensities: Countering Information Gaps with Targeted Data Gathering*. *Environmental Science & Technology*, 2015. **49**(1): p. 679-686, doi: 10.1021/es505376t.
23. Rahman, M.M., *Life Cycle Assessment of North American Conventional Crudes for Production of Transportation Fuels*, in *Mechanical Engineering*. 2014, University of Alberta: Edmonton.
24. El-Houjeiri, H.M., et al., *OPGEE June 4, 2015*, Stanford School of Earth, Energy & Environmental Sciences: Stanford, CA, <https://pangea.stanford.edu/researchgroups/eao/research/opgee-oil-production-greenhouse-gas-emissions-estimator> (May 16, 2016).
25. Kidnay, A.J., W.R. Parrish, and D.G. McCartney, *Compression*, in *Fundamentals of Natural Gas Processing*. 2011, CRC Press: Boca Raton, Fl. p. 185-210.
26. El-Houjeiri, H.M., et al., *OPGEE V1.1 Draft D: User guide & Technical documentation*. Oct. 10, 2014, Stanford School of Earth, Energy & Environmental Sciences: Stanford, CA, <https://pangea.stanford.edu/researchgroups/eao/research/opgee-oil-production-greenhouse-gas-emissions-estimator> (June 14, 2016).

27. Canter, C. and A. Kumar. *Impact of fugitive emissions on the greenhouse gas emissions of conventional crudes*. in *AIChE Annual Meeting*. 2014. Atlanta: AIChE.
28. Speight, J.G., *The Chemistry and Technology of Petroleum*. 4th ed. Chemical Industries. 2014, Hoboken: CRC Press.
29. Bergerson, J., *Petroleum Refinery Life Cycle Inventory Model*. 2015, University of Calgary: Calgary, AB, <http://ucalgary.ca/lcaost/prelim> (May 16, 2016).
30. Di Lullo, G., H. Zhang, and A. Kumar, *Evaluation of uncertainty in the well-to-tank and combustion greenhouse gas emissions of various transportation fuels*. *Applied Energy*, 2016. **184**: p. 413-426, doi: 10.1016/j.apenergy.2016.10.027.
31. Loucks, D.P., et al., *Model Sensitivity and Uncertainty Analysis*, in *Water Resources Systems Planning and Management: An Introduction to Methods, Models and Applications*. 2005, UNESCO: Paris. p. 255-290, https://www.utwente.nl/ctw/wem/education/afstuderen/Loucks_VanBeek/09_chapter09.pdf (May 19, 2016).
32. Vose Software, *ModelRisk Software*. 2015, Vose Software: Belgium, <http://www.vosesoftware.com/> (May 16, 2016).
33. Di Lullo, G., M.M. Rahman, and A. Kumar. *Uncertainty analysis of transportation fuels from North American conventional oils GHG emissions*. in *65th Canadian Chemical Engineering Conference*. 2015. Calgary, Canada.
34. van Hauwermeiren, M. and D. Vose, *A Compendium on Distributions*. 2009, Vose Software: Ghent, Belgium.
35. Angevine, G. and V. Oviedo, *Ensuring Canadian Access to the Oil Markets in the Asia-Pacific Region*. July 17, 2012, Fraser Institute. p. 1-62, <https://www.fraserinstitute.org/studies/ensuring-canadian-access-oil-markets-asia-pacific-region> (Feb. 18, 2016).
36. *Tornado plots*. 2007 [cited Feb. 26, 2016]; Available from: http://www.vosesoftware.com/ModelRiskHelp/index.htm#Presenting_results/Other_plots/Tornado_charts.htm.
37. Aspen Technology Inc., *Aspen HYSYS Refiney Wide Model.hsc*. 2016, <http://www.aspentech.com/products/aspen-hysys/> (May 16, 2016).
38. Alaska Oil and Gas Conservation Commission. *AOGCC Pool Statistics - Prudhoe Bay Unit, Prudhoe Oil Pool*. 2004, Alaska Department of Administration: Anchorage, AK, http://doa.alaska.gov/ogc/annual/current/18_Oil_Pools/Prudhoe%20Bay%20-%20Oil/Prudhoe%20Bay,%20Prudhoe%20Bay/1_Oil_1.htm (Apr. 29, 2016).
39. Alaska Oil and Gas Conservation Commission. *Alaska Oil and NGL Production - December 2015*. Feb. 2, 2016, Alaska Department of Administration: Anchorage, AK, http://doa.alaska.gov/ogc/ActivityCharts/Production/2015_12-ProdChart.pdf (Apr. 29, 2016).
40. PetroWiki. *Prudhoe Bay field*. July 16, 2015 [cited Sept. 28, 2016]; Available from: http://petrowiki.org/Prudhoe_Bay_field.

41. Speight, J.G., *Crude Oil Assay Database*. Knovel, <http://app.knovel.com/hotlink/toc/id:kpCOAD0005/crude-oil-assay-database/crude-oil-assay-database> (Sept. 25, 2016).
42. *BP Crudes: Alaska North Slope*. July 2015 [cited July 20, 2016]; Available from: http://www.bp.com/en/global/bp-crudes/assays/americas/alaskan_north_slope.html.
43. Reynolds, J.G., et al., *Upgrading of heavy oil from the San Joaquin Valley of California by aqueous pyrolysis*. 1995, Lawrence Livermore National Lab.: Washington, <http://dx.doi.org/10.2172/266764> (Sept. 28, 2016).
44. Sheridan, M., *California Crude Oil Production and Imports*. 2006, California Energy Commission: Sacramento, California, <http://www.energy.ca.gov/2006publications/CEC-600-2006-006/CEC-600-2006-006.PDF> (Sept. 28, 2016).
45. Cai, H., et al., *Well-to-Wheels Greenhouse Gas Emissions of Canadian Oil Sands Products: Implications for U.S. Petroleum Fuels*. *Environmental Science & Technology*, 2015. **49**(13): p. 8219-8227, doi: 10.1021/acs.est.5b01255.
46. Englander, J.G. and A. R.Brandt, *Oil Sands Energy Intensity Analysis for GREET Model Update Technical Documentation*. 2014, Department of Energy Resources Engineering Stanford: Stanford, <https://greet.es.anl.gov/publication-lca-update-oil-sands>.
47. Myhre, G., et al., *Anthropogenic and Natural Radiative Forcing Supplementary Material*, in *Climate Change 2013: The Physical Science Basis. Contribution of Working Group to the Fifth Assessment Report of the Intergovernmental Panel on Climate Change*, T.F. Stocker, et al., Editors. 2013, Cambridge University Press: Cambridge and New York. p. 8SM-19, https://www.ipcc.ch/pdf/assessment-report/ar5/wg1/supplementary/WG1AR5_Ch08SM_FINAL.pdf (Nov. 15, 2016).
48. Myhre, G., et al., *Anthropogenic and Natural Radiative Forcing*, in *Climate Change 2013: The Physical Science Basis. Contribution of Working Group to the Fifth Assessment Report of the Intergovernmental Panel on Climate Change*, T.F. Stocker, et al., Editors. 2013, Cambridge University Press: Cambridge and New York, (Nov. 15, 2016).
49. El-Houjeiri, H.M., et al., *OPGEE V1.1 Draft E*. 2015, Stanford School of Earth, Energy & Environmental Sciences: Stanford, CA, <https://pangea.stanford.edu/researchgroups/eao/research/opgee-oil-production-greenhouse-gas-emissions-estimator> (May 16, 2016).
50. Keesom, W., S. Unnasch, and J. Moretta, *Life Cycle Assessment Comparison of North American and Imported Crudes prepared for Alberta Energy Research Institute*. 2009, Jacobs Consultancy: Chicago, IL, <http://www.eipa.alberta.ca/media/39640/life%20cycle%20analysis%20jacobs%20final%20report.pdf> (February 18, 2016).
51. Rosenfeld, J., et al., *Comparison of North American and Imported Crude Oil Lifecycle GHG Emissions - Final Report Prepared for Alberta Energy Research Institute*. 2009, TIAX LLC: Cupertino, CA, <http://eipa.alberta.ca/media/39643/life%20cycle%20analysis%20tiax%20final%20report.pdf> (March 25, 2016).

52. U.S. Energy Information Administration, *Crude Oil Production*. EIA: Washington, http://www.eia.gov/dnav/pet/pet_crd_crpdn_adc_mbbbl_a.htm (Feb. 17, 2016).
53. Alberta Government. *Climate Leadership Plan*. 2017 [cited Feb. 2, 2017]; Available from: <https://www.alberta.ca/climate-leadership-plan.aspx>.
54. ICF International, *Independent Assessment of the European Commission's Fuel Quality Directive's "Conventional" Default Value*. 2013, https://www.nrcan.gc.ca/sites/www.../EU_FQD_Study_Final_Report.pdf (Feb. 3, 2017).
55. Alaska Oil and Gas Conservation Commission. *Conservation Order 341D*. Nov. 30, 2001, Alaska Department of Administration: Anchorage, AK, http://doa.alaska.gov/ogc/orders/co/co300_399/co341d.htm (Apr. 29, 2016).

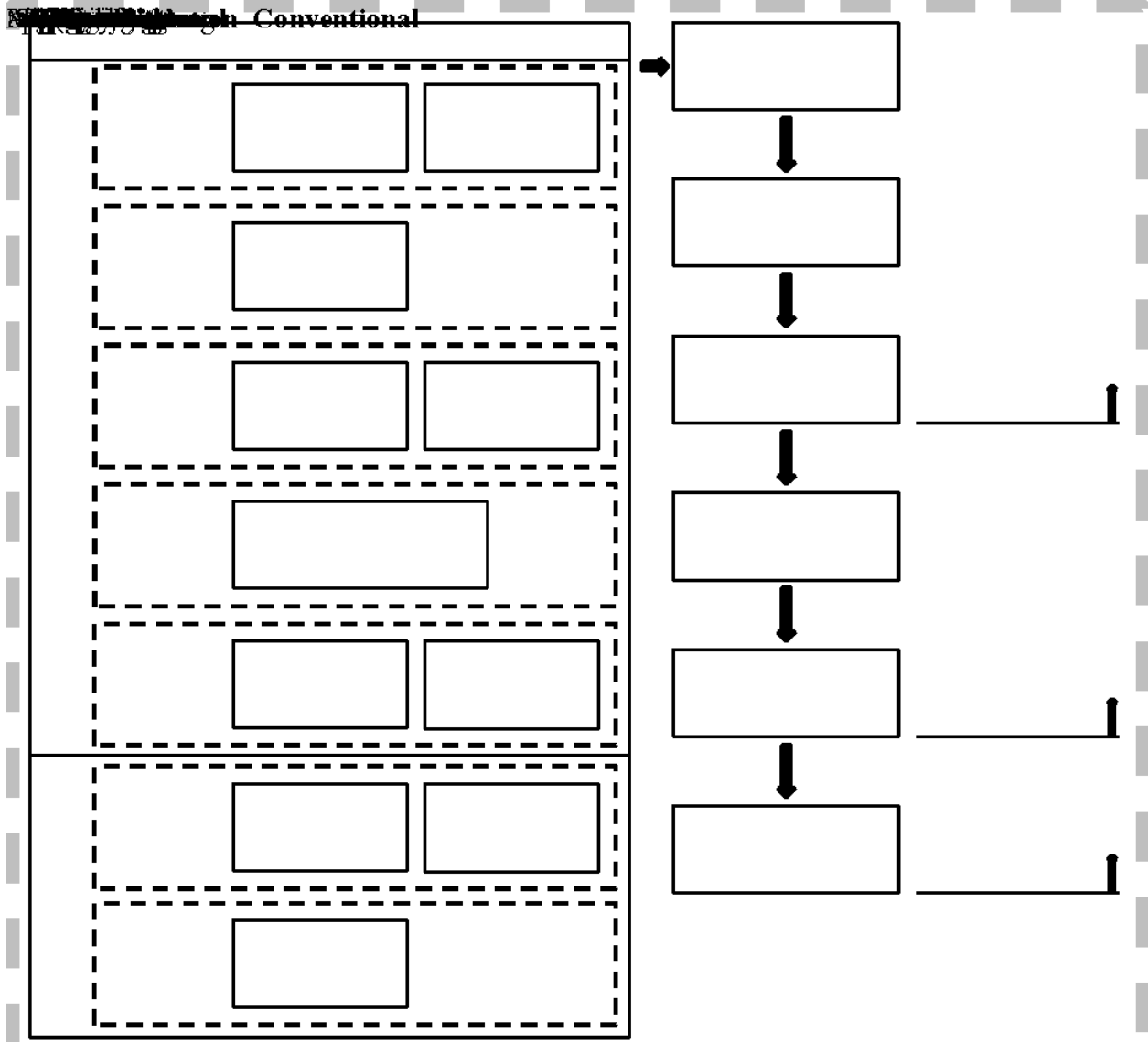


Figure 1: The FUNNEL-GHG model stages from well to combustion (*upgrading applies to Alberta synthetic crude oils [SCO] only)

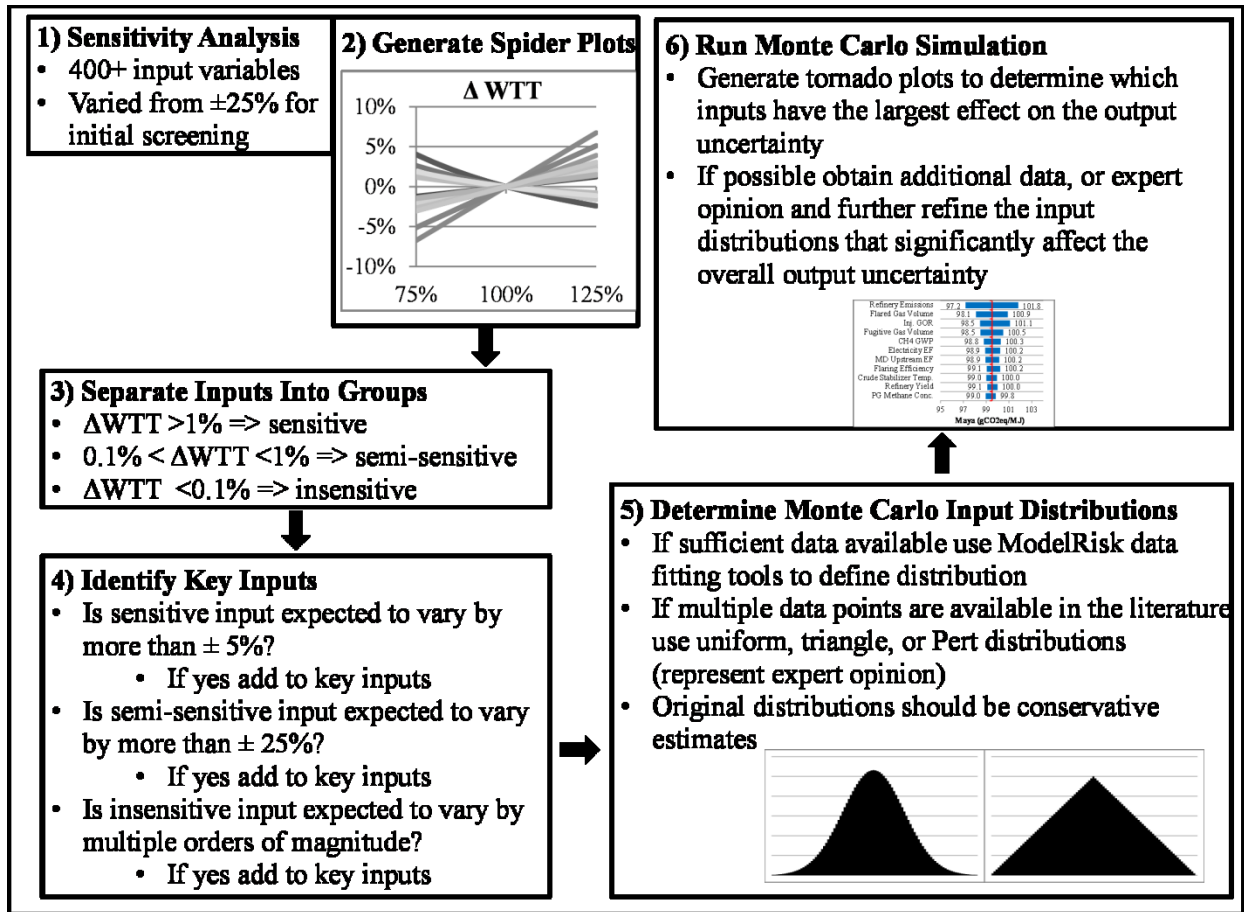


Figure 2: Methodology overview (WTT = well-to-tank)

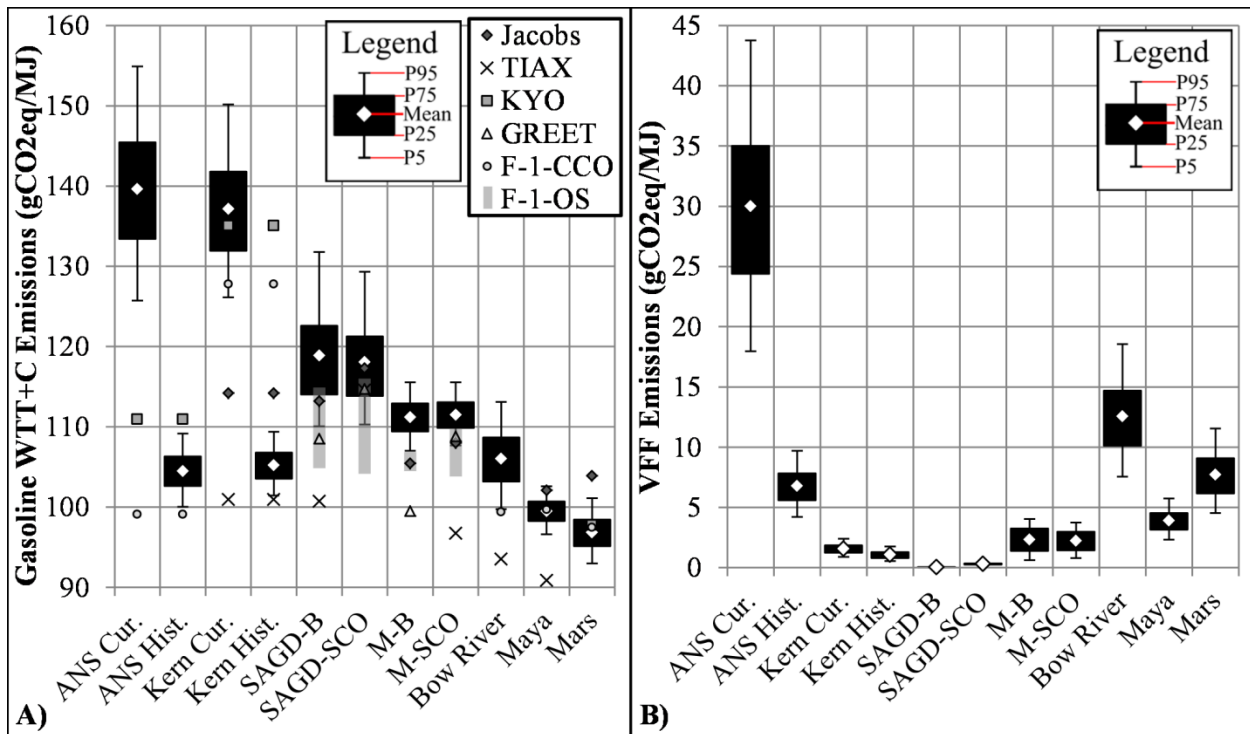


Figure 4: A) Gasoline WTC emissions and B) Venting fugitive and flaring emissions. Synthetic crude oil (SCO) pathways include upgrading. The additional Alaska and Kern scenarios are included to show the effect of reservoir age on the WTC emissions. P95, P75, P25, and P5 represent the respective percentile values.

Figure 4A additional data from the literature:

- Jacobs produced a bottom-up model that examined 9 crudes (2009) [10]
- TIAX's WTC bottom-up model focused on creating a detailed refinery model (2009) [11]
- Know Your Oil (KYO) performed a detailed bottom-up WTC model examining 30 crudes (2015) [4]
- GREET is a top-down model focused on determining regional averages (2015) [45, 46]
- F-1-CCO (2014) [13, 14, 23], and F-1-OS (2014) [12, 15, 16] are bottom-up models focusing on conventional crudes (CCO) and unconventional crudes (OS). The model developed in this study was built by combining and improving these two models

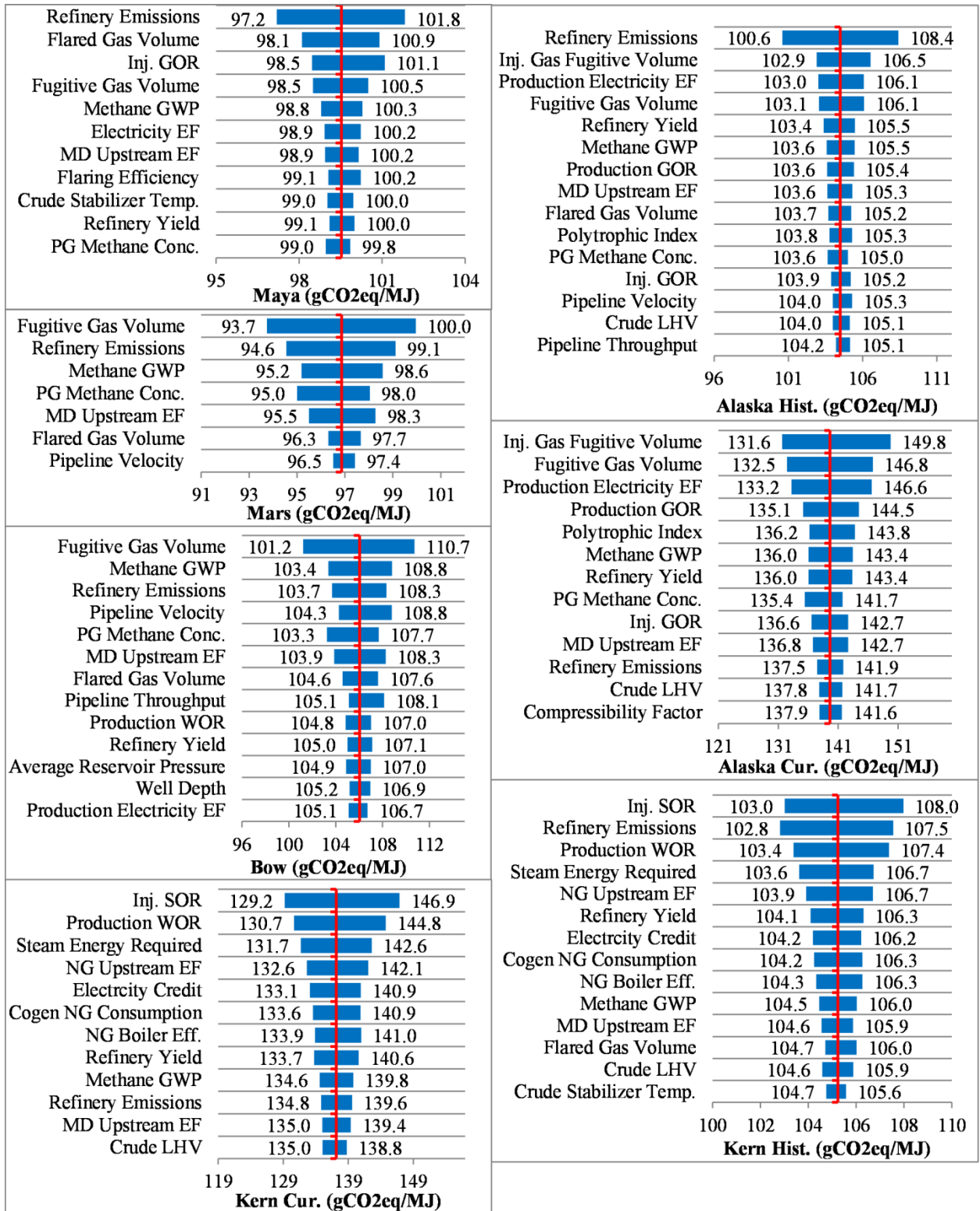


Figure 5: Tornado plots of the gasoline WTC emissions for conventional crudes
 Inj.: injection, Eff: efficiency EF: emission factor, NG: natural gas, PG: produced gas, MD: marine diesel

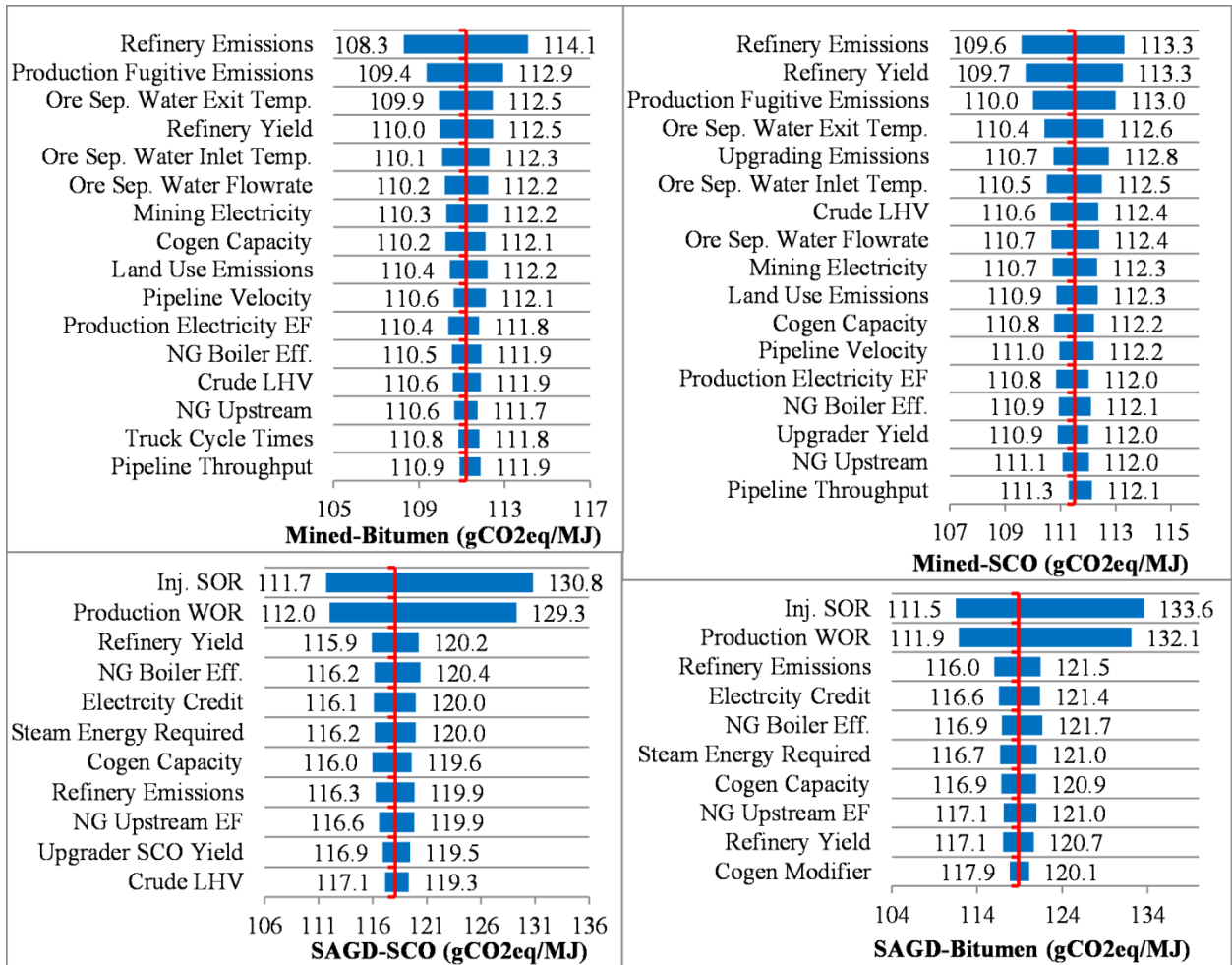


Figure 6: Tornado plots of the gasoline WTC emissions for conventional crudes
 Inj.: injection, Eff: efficiency EF: emission factor, NG: natural gas, Sep: separation

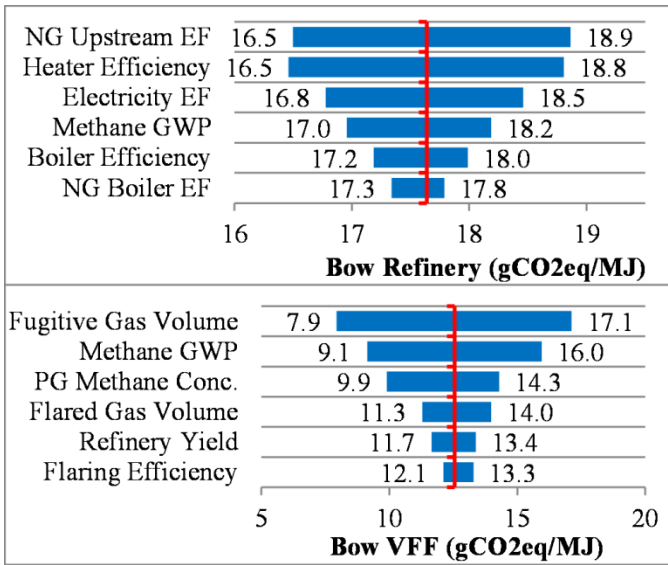


Figure 7: Bow refinery and venting, fugitive, and flaring tornado plots
 EF: emission factor, NG: natural gas, PG: produced gas. Refinery emissions are for gasoline, VFF emissions are the same for gasoline, diesel, and jet fuel. Tornado plots for the remaining crudes, diesel, and jet fuel are in section A6

Table of Contents

List of Tables	5
List of Figures	6
A1. Base case model modifications	8
A1.1 Multistage compressor	8
A1.2 Cogeneration calculations	10
A1.3 Venting, fugitive, and flaring	11
A1.4 Produced gas credit	11
A1.5 Crude energy content	11
A1.6 Land use emissions	12
A1.7 Updated base case defaults	12
A2. Monte Carlo sampling error	13
A3. Historical and current scenario justification	14
A4. Input distributions	15
A4.1 Common inputs distribution generation	20
A4.1.1 Emission factors inputs	20
A4.1.2 Electricity EF	21
A4.1.3 Process unit efficiency inputs	23
A4.1.4 Surface processing	25
	38

A4.1.5 Crude transportation	25
A4.1.5 Venting, fugitive, and flaring	26
A4.1.6 Other inputs	29
A4.2 Maya's input distribution generation	30
A4.3 Mars' input distribution generation	32
A4.4 Bow River's input distribution generation	34
A4.5 Alaska North Slope input distribution generation	34
A4.6 California Kern input distribution generation	36
A4.7 SAGD input distribution generation	38
A4.8 Mining input distribution generation	38
A4.9 Athabasca shared input distribution generation	40
A5. Input distributions data analysis	42
A5.1 Mars data	42
A5.2 Alaska data	42
A5.3 Kern data	44
A5.4 Kern cogeneration data	45
A5.5 SAGD data	46
A6. Gasoline, diesel and jet fuel results	46
A6.1 WTC tornado plots	47
A6.2 Refinery tornado plots	53
	39

A6.3 VFF tornado plots	56
A7. Abbreviations	1
A8. References	1

List of Tables

Table A1: Updated emission factors (g/MJ) [12]	12
Table A2: Monte Carlo sampling error for the WTC emissions SE (gCO ₂ eq/MJ)	13
Table A3: Alaska historical injection and production ratios	14
Table A4: Kern historical injection and production ratios	14
Table A5: Monte Carlo general inputs	17
Table A6: Monte Carlo conventional crude-specific inputs	18
Table A7: Monte Carlo unconventional crude-specific inputs	19
Table A8: Monte Carlo refinery inputs	19
Table A9: Flaring ratios	26
Table A10: Refinery emission tornado plots for diesel	55
Table A11: Refinery emission tornado plots for jet	55

List of Figures

Figure A1: Alaska North Slope water production ratio	44
Figure A2: WTC emissions	47
Figure A3: Conventional crude WTC emission tornado plots for diesel	50
Figure A4: Unconventional crude WTC emission tornado plots for diesel	51
Figure A5: Conventional crude WTC emission tornado plots for jet	52
	40

Figure A6: Unconventional crude WTC emission tornado plots for jet	53
Figure A7: Refinery emission tornado plots for gasoline	54
Figure A8: VFF emission tornado plots	0

A1. Base case model modifications

This section describes the modifications made to the original **FUNdamental ENgineering PrinciplEs-based Model for Estimation of GreenHouse Gases (FUNNEL-GHG)** conventional crude oil (CCO) and oil sands (OS) modules with the relevant equations.

A1.1 Multistage compressor

Oil and gas compressor efficiencies range from 65% to 90% depending on the type and size of the compressor [1, 2]. This study assumes polytropic compression with interstage cooling. The polytropic index is calculated from the compressor efficiency and is used to find the discharge temperature and compression energy requirements. The polytropic index is calculated using equation A1 [2]:

$$\eta_{\text{compressor}} = \frac{\left(\frac{n-1}{n}\right)}{\left(\frac{n-1}{n}\right)} \quad (\text{A1})$$

where n = polytropic index; k = heat capacity ratio of natural gas; and $\eta_{\text{compressor}}$ = compressor efficiency. The specific heat ratio for NG is 1.27 [3].

A polytropic index distribution with a mean, minimum, and maximum of 1.36, 1.31, 1.47 is used and represents polytropic efficiencies of 80%, 70%, and 90% [1, 2, 4]. A maximum compressor ratio (CR) of 5 is used for consistency with the published literature [5, 6]. The number of stages required is calculated using equation A2 [1]:

where m = the number of stages required; P_{out} = the out

$$m = \frac{\ln\left(\frac{P_{\text{out}}}{P_{\text{in}}}\right)}{\ln\left(\frac{n-1}{n}\right)} \quad (\text{A2})$$

let pressure [MPa]; P_{in} = the inlet pressure [MPa]; and CR_{max} = the maximum compression ratio.

The actual compression ratio is calculated using equation A3 [1]:

$$\frac{P_i}{P_{i-1}} = \left(\frac{P_{i+1}}{P_i} \right)^{\frac{1}{n}} \quad (A3)$$

The inlet temperature for each stage is calculated using equation A4 from OPGEE [1, 2, 5]:

$$T_i = [(1 - \eta_{cooling}) * T_{i-1} * (P_i/P_{i-1})^{(\frac{\gamma-1}{\gamma})} - 1] + T_{i-1} \quad (A4)$$

where T_i = the inlet temperature of the i th stage [$^{\circ}R$]; $\eta_{cooling}$ = interstage cooling efficiency; and T_{i-1} = the inlet temperature of the previous stage [$^{\circ}R$]. The interstage cooling efficiency is taken from OPGEE and assumed to be 80% [5]. Conservative minimum and maximum efficiencies were assumed to be 60% and 100%. The inlet temperature of the first stage is assumed for each crude.

The power of compressor is calculated using equation A5 [1, 2, 5]:

$$P_{Comp} = \left(\frac{P}{P_{atm}} - 1 \right) * 3.027 * \frac{P_{atm}}{Z} * \frac{P}{P_{atm}} * [(P/P_{atm})^{(\frac{\gamma-1}{\gamma})} - 1] * \sum_{i=1}^n T_i \quad (A5)$$

where P_{Comp} = the required compressor power [hp-d/MMscf]; P_{atm} = atmospheric pressure [psia], T_{atm} = atmospheric temperature [$^{\circ}R$]; and Z = the compressibility factor. The inlet pressure and temperature are assumed to be 101.4 kPa (14.7 psia) and 15.7 $^{\circ}C$ (520 $^{\circ}R$). The compressibility factor is examined for a temperature range of 15.7 to 171.3 $^{\circ}C$ (520 to 800 $^{\circ}R$) and a pressure range from 0.69 to 41.37 MPa (100psia to 6000 psia), to represent the industry, resulting in a compressibility factor range of 0.9 to 1.1 with a mean of 1 [7]. The constant 3.027 is a conversion constant with units of hp-d/MMscf-psia.

A1.2 Cogeneration calculations

The peak cogeneration steam production capacity of the Midway-Sunset field is 0.73 million m³/month [8] and steam consumption is 2.42 million m³/month [9]. Consequently, the cogeneration facilities can only produce 30% of California Kern steam. For Athabasca the capacity was determined using cogen electricity production data from the oil sands community alliance report and bitumen production data from Alberta Energy specifically for the Athabasca region [10, 11]. In 2013 the average cogeneration electricity production was 252 kWh/m³, which is used as the mean. Assuming crude production remains the same and using the projected cogeneration capacity in 2023 of 4,468 MWh, the maximum is calculated as 93 kWh/m³. Goal seek was used in the F-2 model to find the mean and max cogeneration capacity of 18% and 41% from the cogeneration electricity production. The minimum is assumed to be 0% and a triangle distribution is used, to be conservative. It is assumed in the current FUNNEL-GHG analysis that the remaining steam is produced with an NG once-through steam generator (OTSG) [12].

There are numerous cogeneration systems that produce varying electricity to steam ratios. While the original F-1 model performed a theoretical calculation based on thermodynamics and assumed conditions this work uses correlations from OPGEE to determine the cogen NG consumption and cogen electricity/steam ratio [5]. As OPGEE provides data for 4 different cogeneration systems each with different NG consumptions and electricity to steam ratios, a cogen modifier which varies from 1 to 4 was used to relate the two properties. The NG consumption in m³/MWh of combined steam and electricity is $-4.86 \times M + 144.4$, and the electricity to steam ratio is $0.125 \times M + 0.347$, where M is the cogen modifier.

A1.3 Venting, fugitive, and flaring

Additional data were collected to quantify the venting, fugitive, and flaring (VFF) emissions. Canter did a comprehensive examination of the literature and determined that the VFF gas volumes for typical North American crudes ranged from 2.1% to 7% of the produced gas volumes, with an average of 4.6% [13]. These values represent the crudes included in this study and are taken as is. The reinjected gas will also have venting and fugitive emissions, but since the reinjected gas is only partially processed, it will have lower emissions than the produced gas. More detail on the reinjected gas is given in section A4.5. For Alberta SAGD and mining crude specific data are used; see section A4.9.

A1.4 Produced gas credit

The gas credit is assumed to be the natural gas (NG) upstream emissions minus the transportation emissions. The transportation emissions are taken from GREET as 5.42 gCO₂eq/MJ [14]; the uncertainty in the credit is due to the uncertainty in the NG upstream emissions only.

A1.5 Crude energy content

The crude higher heating (HHV) value is calculated using equation A6 from Speight [15]:

$$HHV = a - b * SG^2 \tag{A6}$$

where HHV = higher heating value [cal/g], a and b = correlation coefficients, and SG = crude specific gravity. The correlation coefficients a and b are 11160 and 1890 cal/g [15]. PRELIM assumes that the lower heating value (LHV) is 90% of the HHV and converts the units to MJ/kg, which changes a and b to 46.693 and 7.908 MJ/kg [16].

A1.6 Land use emissions

The original F-1-OS module did not include land use emissions. The land use emissions depend on the drilling intensity and carbon richness of the area [17]. For both SAGD and mining, a high carbon richness is used, which corresponds to a forested area, and a moderate drilling intensity is used. The emission factors are taken from OPGEE with a 150 year timeframe as 0.79 and 1.28 gCO₂eq/MJ for SAGD and mining, respectively [5].

A1.7 Updated base case defaults

Table A1 shows the insensitive emissions factor (EF) inputs that have been updated from the previously published FUNNEL model. The updated values are from GREET1 2015 [14].

Table A1: Updated emission factors (g/MJ) [12]

Combustion EFs	CO ₂	CH ₄	N ₂ O
Diesel engine comb.	73.07	0.004	0.001
Industrial NG utility boiler comb.	56.23	0.001	0.001
Natural gas turbine comb.	56.21	0.001	0.000
Diesel upstream	13.06	0.076	0.000
NG upstream	8.04	0.279	0.001
Natural gas upstream transmission	1.70	0.098	0.001
Marine EFs	CO ₂	CH ₄	N ₂ O
Origin to dest. comb EF of res. fuel	80.06	0.004	0.002
Dest. to origin comb EF of res. fuel	80.06	0.004	0.002
Residual oil well to pump	10.35	0.069	0.000
Gasoline distribution EFs	CO ₂	CH ₄	N ₂ O
Ocean tanker	0.53	0.000	0.000
Barge	0.60	0.000	0.000
Pipeline	0.23	0.000	0.000
Rail	0.10	0.000	0.000
Truck	0.14	0.000	0.000
Diesel distribution EFs	CO ₂	CH ₄	N ₂ O
Ocean tanker	0.25	0.000	0.000
Barge	0.36	0.000	0.000
Pipeline	0.20	0.000	0.000
Rail	0.32	0.000	0.000

Truck	0.14	0.000	0.000
Jet distribution EFs	CO ₂	CH ₄	N ₂ O
Ocean tanker	0.25	0.000	0.000
Barge	0.36	0.000	0.000
Pipeline	0.19	0.000	0.000
Rail	0.31	0.000	0.000
Truck	0.14	0.000	0.000

The fuel combustion emissions have also been updated using GREET1 2015 to 73.3, 75.9, and 72.9 gCO₂eq/MJ for gasoline, diesel, and jet fuel, respectively [14].

A2. Monte Carlo sampling error

Monte Carlo simulations use random number generators to generate samples that give variations between model runs. This variation is calculated using equation A7 [18]:

$$SE = \frac{2.56 * \sigma}{\sqrt{N}} \quad (A7)$$

where SE = sampling error, σ = standard deviation of the modeled mean, and N= number of samples. The modeled mean then has a 99% probability of being $\mu \pm SE$. The resulting sampling error for each scenario is shown in Table A2

Table A2: Monte Carlo sampling error for the WTC emissions SE (gCO₂eq/MJ)

Crude	Gasoline	Diesel	Jet Fuel
Alaska Cur.	0.10	0.10	0.10
Alaska Hist.	0.03	0.03	0.03
Kern Cur.	0.08	0.08	0.08
Kern Hist.	0.03	0.03	0.03
SAGD-B	0.08	0.08	0.08
SAGD-SCO	0.07	0.07	0.07
M-B	0.03	0.03	0.03
M-SCO	0.03	0.03	0.03
Bow River	0.05	0.05	0.05
Maya	0.02	0.02	0.02
Mars	0.03	0.03	0.03

A3. Historical and current scenario justification

Alaska injects water and produced gas to maintain reservoir pressure. Table A3 shows Alaska’s historical annual production and injection GOR and WOR ratios for Alaska’s Prudhoe oil field [19-21]. California Kern uses steam injection. Table A4 gives its monthly historical SOR, WOR, and GOR for Kern’s Midway Sunset field [9]. As Table A3 and A show, the ratios have increased significantly over the last decade. It should be noted that the Jacobs and TIAX studies were published in 2009 and the F-1 model was published in 2014 [12, 22, 23].

Table A3: Alaska historical injection and production ratios

Date	Injection GOR	Production GOR	Injection WOR	Production WOR
1980	1,400	1,100	0.02	0.03
1990	3,300	3,200	1.33	0.64
2000	15,700	15,300	3.25	2.39
2010	26,000	28,300	5.74	3.61
Cumulative (2015)	2,200	2,200	0.22	0.33

Table A4: Kern historical injection and production ratios

Date	Injection SOR	Production WOR	Production GOR
Dec-96	2.92	4.42	27
Dec-00	2.63	4.78	37
Dec-05	4.10	5.95	38
Dec-10	4.80	7.81	155
Sep-15	6.60	10.75	190
Cumulative (2009)	1.64	1.92	93

For the Alaska historical scenario, two crude assays are used to determine the refinery emissions, as the crude composition has changed over time. The refinery model is run using both the Alaska crude assay used in the current scenario [24] and an assay from Prudhoe Bay from 1988 [25].

The resulting distributions are combined before being inserted into the main model. This gives a wider refinery emission range due to the uncertainty in the crude oils composition over time.

A4. Input distributions

The inputs with their distributions and sources are listed in Table A5 for general inputs that apply to all crudes and in Tables A6 and A7 for the crude-specific inputs. The Monte Carlo distributions use ModelRisk software notation [26]. The EFs are used to determine the GHG emissions from fuel and electricity consumption. The methane global warming potential (GWP) is used to convert methane emissions into carbon dioxide equivalent emissions. For the surface processing (SP) stage, crude stabilizer temperatures and crude-specific heat correction factors are used to calculate the energy requirement for crude stabilization, and water-electricity intensities are used to calculate the water filtering energy requirement. For the crude transportation emissions, the pipeline and tanker velocities are used to calculate the energy consumption. For VFF emissions, the flaring volume, flaring efficiency, and produced gas (PG) methane concentration are used to calculate the CO₂eq emissions. The yield factor represents the refinery's conversion efficiency. A yield factor of 1.3 means that 1.3 MJ of crude is required to produce 1 MJ of finished products (gasoline, diesel, and jet fuel); the remaining 0.3 MJ is converted into undesirable products such as fuel oils. The yield factor is important because pre-refinery emissions from extraction and surface processing are multiplied by the yield factor to determine final gasoline emissions. The "distributed to bulk terminals" input is used to determine which transportation method is used to distribute the gasoline from the refinery to the bulk terminals. Of the five transportation methods available; ocean tanker, barge, pipeline, rail, and truck; rail had the lowest emission intensity and barge had the highest emission intensity. Therefore, a zero means that only rail is used, and a one means that only barges are used.

Table A5: Monte Carlo general inputs

	Input	Monte Carlo distribution	Units	Source
	Methane GWP	Triangle(20.74,34,47.26)		[27, 28]
	NG Upstream	Triangle(71.2%,100%,140%)		[14, 29, 30]
	NG Boiler Comb.	Triangle(97.2%,100%,102.7%)		[14, 29]
	NG Turbine Comb.	Triangle(96.9%,100%,102.4%)		[14, 29]
	Maya N2 Inj.	Triangle(336,479,767)	gCO ₂ eq/kWh	[14, 31]
	Maya SP/Pipeline 1	Triangle(479,767,1140)	gCO ₂ eq/kWh	[14]
	Maya Refinery/Pipeline 2	Triangle(502,656,804)	gCO ₂ eq/kWh	[12, 14, 32, 33]
	Mars Pre-Refinery	Triangle(479,767,1140)	gCO ₂ eq/kWh	[14, 29, 34]
	Mars Pipeline 2	Triangle(502,669,961)	gCO ₂ eq/kWh	[14, 29]
	Mars/Bow/Athabasca Refinery	Triangle(479,741,1119)	gCO ₂ eq/kWh	[14, 29, 32]
	Bow/Athabasca Extraction/SP	Triangle(502,990,1119)	gCO ₂ eq/kWh	[14, 29, 33]
	Bow/Athabasca Pipeline	Triangle(502,834,1119)	gCO ₂ eq/kWh	[14, 32, 33]
	Alaska Pre-refinery	Triangle(502,721,972)	gCO ₂ eq/kWh	[14, 29] [34]
	Alaska/Kern/Refinery/Pipeline 2	Triangle(236,337,804)	gCO ₂ eq/kWh	[14, 32]
	Boiler	Triangle(62%,75%,88%)		[35-38]
	Heater	Triangle(70%,80%,90%)		[5, 12, 39, 40]
	Low Flow Pump	Triangle(50%,60%,70%)		[41]
	High Flow Pump	Triangle(50%,65%,85%)		[4, 5, 22, 41-43]
	Specific Heat Correction Factor	Triangle(0.84,1,1.5)		[44]
	Crude Stabilizer Inlet Temp.	Triangle(37.8,48.9,65.6)	°C	[45]
	Crude Stabilizer Outlet Temp.	Triangle(93.3,173.3,204.4)	°C	[45, 46]
	Produced Water Energy Intensity	Triangle(1.51,2.26,5.79)	kWh/m ³	[12, 47]
	Imported Water Energy Intensity	Triangle(1.26,1.51,3.90)	kWh/m ³	[12, 47]
C r	Heavy Crude Pipeline Velocities	Triangle(0.8,1.4,2.0)	m/s	[48, 49]

u d e T r a n s p o r t	Light/Medium Crude Pipeline Velocities	Triangle(1.3,2.0,3.1)	m/s	[48] [49]
	Pipeline Throughput	Triangle(15900,63600,127200)	m ³ /d	[48] [49]
	Tanker Velocity	Triangle(22.2,27.8,31.5)	km/hr.	[50-53] [49]
	Marine Fuel Comb. EF	Triangle(95%,100%,105%)		[14] [49]
	Residual Oil Energy Density	Triangle(37.7,39.5,41.6)	MJ/kg	[14] [49]
	Vented & Fugitive Gas Volumes	Triangle(2.1%,4.6%,7%)		[13]
	Maya Flared Gas Volume	Triangle(0,12.21,23.35)	m ³ /m ³	[54-57]
	Mars Flared Gas Volume	Triangle(0,2.31,11.13)	m ³ /m ³	[54-57]
	Bow Flared Gas Volume	Triangle(0,11.09,25.95)	m ³ /m ³	[54-57]
	Alaska Flared Gas Volume	Uniform(0,10.9)	m ³ /m ³	[54-59]
	Kern Flared Gas Volume	Triangle(0,2.31,11.13)	m ³ /m ³	[54-57]
	SAGD Extr. Flared Gas	Uniform(85,600)	gCO ₂ eq/m ³ Bit	[60] [61] [62, 63]
	Mining Extr. Flared Gas	Uniform(0,15000)	gCO ₂ eq/m ³ Bit	[60] [61] [62, 63]
	Upgrading Flared Gas	Uniform(4250,10000)	gCO ₂ eq/m ³ SCO	[60] [61] [62, 63]
	SAGD Extr. Fugitive Gas	Uniform(255,1000)	gCO ₂ eq/m ³ Bit	[60] [61] [62, 63]
	Mining Extr. Fugitive Gas	Uniform(3604,96220)	gCO ₂ eq/m ³ Bit	[60] [61] [62, 63]
	Upgrading Fugitive Gas	Uniform(0,2000)	gCO ₂ eq/m ³ SCO	[60] [61] [62, 63]
	Flaring Efficiency	PERT(80%,95%,99%)		[5, 14, 22, 42, 64]
	PG Methane Concentration	Beta(14.49,2.91,,XBounds(,0.989))	%mol	[5]
	Yield Factor	Pert(90%,100%,110%)		[12, 16, 22]
	Distributed to Bulk Terminals	Uniform(0,1)		[12, 14]

Table A6: Monte Carlo conventional crude-specific inputs

	Input	Monte Carlo distribution	Units	Source
M a y a	Nitrogen Driver Efficiency	Triangle(60%,82.3%,95%)		[5, 31, 65, 66]
	Nitrogen Injection Volume	Triangle(101.6,146.3,485.4)	m ³ /m ³	[31, 67-70]
M a r s	Injection WOR	Triangle(0.3,0.7,1.5)	m ³ /m ³	[6, 22, 71-73]
	Production WOR	Triangle(0.02,0.2,5.5)	m ³ /m ³	[6, 22, 71, 74, 75]
	Production GOR	Triangle(142.4,201.7,249.2)	m ³ /m ³	[75]
	Well Lifetime Productivity	Triangle(2.1e4,8.4e4,3.7e6)	m ³ /well	[6, 12, 76]
	Well Depth	Triangle(4267,4420,5791)	m	[70, 74]
	Pump Discharge Pressure	Triangle(37.9,42.1,47.2)	MPa	[22, 72, 77]
B o w	Well Depth	Triangle(600,1000,1800)	m	[78, 79]
	Reservoir Pressure	Triangle(4.1,7.8,17.2)	MPa	[12, 80, 81]
	Production WOR	Triangle(4,15,20)	m ³ /m ³	[82, 83]
A l s k a	Current Production WOR	Normal(4.25,0.60, WCopula, XBounds(0.5,6.5))	m ³ /m ³	[84, 85]
	Average Production WOR	Normal(0.97,0.137, WCopula, XBounds(0.1,3))	m ³ /m ³	[21, 86, 87]
	Current Injection WOR	Normal(6.33,1.8,WCopula)	m ³ /m ³	[84, 88]
	Average Injection WOR	Normal(1.35,0.38,WCopula)	m ³ /m ³	[21, 86, 87]
	Water Copula	CopulaBiFrank(5.6,1)		[84, 88]
	Current Production GOR	Normal(6070,390.7, GCopula)	m ³ /m ³	[85, 89]
	Average Production GOR	Normal(1137,73.2, GCopula)	m ³ /m ³	[19-21]
	Current Injection GOR	Normal(5571,464.2, GCopula)	m ³ /m ³	[85, 89]
	Average Injection GOR	Normal(1040,86.7, GCopula)	m ³ /m ³	[19-21]
	Gas Copula	CopulaBiFrank(35,1)		[85, 89]
	Compressor Inlet Temperature	Triangle(0,15,40)	C	[6, 22]
	Compressor Discharge Pressure	Triangle(15.5,18.6,21.7)	MPa	[90]
	Compressibility Factor	Triangle(0.9,1,1.1)		[7]

	Interstage Cooling Efficiency	Triangle(60%,80%,100%)		[5]
	Injection Gas Fugitives Emissions	Triangle(14.1,45.9,123.6)	gCO ₂ eq/m ³	[29, 91-93]
C a l i f o r n i a K e r n	Current Injection SOR	Triangle(4.72,5.74,7.82, WCopula)	m ³ /m ³	[9]
	Average Injection SOR	Triangle(1.35,1.64,2.23, WCopula)	m ³ /m ³	[9, 94]
	Current Production WOR	Triangle(6.6,8,12.1, WCopula)	m ³ /m ³	[9]
	Average Production WOR	Triangle(1.58,1.92,2.9, WCopula)	m ³ /m ³	[9, 94]
	Water Copula	CopulaBiFrank(13,1)		[9]
	Current Production GOR	Normal(31.65,3.20,,XBounds(21.36,42.72))	m ³ /m ³	[9]
	Average Production GOR	Normal(16.55,1.66,,XBounds(3.56,32.04))	m ³ /m ³	[9, 94]
	Cogen NG Consumption	Error(127.0,6.16,1,,VseXBounds(99.1,155.7))	/m ³ /MWh	[8, 94-96]
	Cogen Electricity/Steam Ratio	Normal(0.678,0.037,,VseXBounds(0.4,0.9))	MWh/MWh	[8, 95, 96]
	Cogen Steam Energy Required	Triangle(1682,1944,2321)	kJ/kg	[95, 96]
	Cogen Steam Capacity	Triangle(0%,30%,100%)		[8, 9]
	Cogen Electricity Credit	Triangle(236,337,502)	gCO ₂ eq/kWh	[14, 29]

Table A7: Monte Carlo unconventional crude-specific inputs

	Input	Monte Carlo distribution	Units	Source
S A C D	Injection SOR	JohnsonB(1.58,1.11,1.54,6.68,WCopula)	m ³ /m ³	[97]
	Production WOR	JohnsonB(1.52,1.10,1.58,6.41, WCopula)	m ³ /m ³	[97]
	Water Copula	CopulaBiNormal(0.9)		[97]
	Cogen Steam Energy Required	Triangle(1763,2051,2340)	kJ/kg	[96, 98]
	Produced Water Energy Intensity	Triangle(7.5,15.7,24.0)	kWh/m ³	[99]
	Well Depth	Triangle(165,639,818)	m	[100]
	Production GOR	Uniform(1,12)	m ³ /m ³	[60]
M i n i n g	Truck Fuel Consumptions	Uniform(0.406,0.580)	m ³ /hr.	[101]
	Truck Cycle Times	Triangle(15.8,22,44)	s	[102-104]
	Truck Rated Payload	Uniform(218,363)	tonnes	[101]
	Truck/Shovel Availability	Triangle(75%,85%,95%)	m ³ /m ³	[102]
	Shovel Fuel Consumptions	Uniform(0.375,0.740)	m ³ /hr.	[101]
	Shovel Cycle Times	Uniform(20,36)	s	[105]
	Shovel Rated Payload	Uniform(218,363)	tonnes	[101]
	Shovel Fill Factor	Uniform(85%,95%)		[102]
	Site Electricity Consumption	Triangle(94.8,122.6,162)	kWh/m ³ bit	[100]
	Bitumen Saturation	Triangle(10.61%,11.44%,12.12%)		[100]
	Ore Separation Water Flowrate	Uniform(6,9)	m ³ /m ³ bit	[106]
	Ore Separation Water Inlet Temp.	Uniform(2,25)	°C	[106, 107]
Ore Separation Water Exit Temp.	Uniform(50,75)	°C	[106, 107]	
S A C D / M i	Dilbit Kinematic Viscosity	Uniform(9.7,350)	cSt	[108]
	SCO Kinematic Viscosity	Triangle(5,15,250)	cSt	[109]
	Upgrading Emissions	Triangle(204,259,431,UpCopula)	kgCO ₂ eq/m ³ bit	[110, 111] [112]
	Upgrading Yield	Triangle(0.8,0.89,1.08,UpCopula)	m ³ SCO/m ³ bit	[110, 111] [112]

n i	UpCopula	CopulaBiFrank(10,1)		[110, 111] [112]
n g	Cogen Steam Capacity	Triangle(0%,18%,41%)		[10, 11]
	Cogen Electricity Credit	Uniform(418,990)	gCO ₂ eq/kWh	[113]
	Cogen Modifier	Uniform(1,4)		[93]

Refinery emissions are determined using a Monte Carlo simulation that only examines the refinery portion of the model. The refinery output emissions are fed into the main model as the Monte Carlo input distributions shown in Table A8.

Table A8: Monte Carlo refinery inputs

Crude	Gasoline	Diesel	Jet
Maya	Normal(18.84,1.04)	Normal(15.29,0.83)	Normal(9.55,0.52)
Mars	Normal(16.60,0.93)	Normal(12.52,0.70)	Normal(8.02,0.45)
Bow	Normal(17.43,0.98)	Normal(13.85,0.77)	Normal(9.10,0.51)
Alaska Hist.	Normal(16.44,1.87)	Normal(12.81,2.23)	Normal(8.15,1.27)
Alaska Cur.	Normal(14.95,1.02)	Normal(10.79,0.73)	Normal(7.02,0.48)
Kern	Normal(16.73,1.02)	Normal(12.19,0.73)	Normal(7.73,0.46)
Bitumen	Normal(20.97,1.40)	Normal(17.15,1.14)	Normal(11.84,0.78)
SCO	Normal(13.51,0.89)	Normal(6.49,0.43)	Normal(5.66,0.37)
Units	gCO ₂ eq/MJ Gasoline	gCO ₂ eq/MJ Diesel	gCO ₂ eq/MJ Jet Fuel

A4.1 Common inputs distribution generation

The inputs that are used by multiple crudes are categorized into emission factors (EF), electricity EFs, process unit efficiency, surface processing, crude transportation, VFF, and “Other.”

A4.1.1 Emission factors inputs

Methane emissions are of special interest as they have a larger effect on global warming than CO₂. Previous studies use a methane **Global Warming Potential (GWP)** of 25 [6, 29, 114]; this

means that one tonne of methane has the same global warming effect as 25 tonnes of CO₂. The 2014 Fifth Assessment Report of the Intergovernmental Panel on Climate Change updated the GWP of methane to $34 \pm 39\%$ [27, 28]. This will primarily affect produced gas venting and fugitive emissions as the produced gas is mainly methane (78.8%), though it will also affect the natural gas upstream EF. The combustion EFs and electricity EFs will be minimally affected as methane contributes to less than 4% and 0.2%, respectively, of the overall emissions [29, 115].

Natural gas (NG) and produced gas are the main sources of heat for crude recovery and refining, and as a result the **NG Upstream EF** has a significant effect on the results. Weber and Calvin found that shale gas emissions range from 11.0-21.0 gCO₂eq/MJ with a mean of 14.6 gCO₂eq/MJ, and conventional gas ranges from 12.4-19.5 gCO₂eq/MJ with a mean of 16.0 gCO₂eq/MJ [29]. Since 40% of U.S. NG production comes from shale wells [116], this study used a weighted mean of 15.44 gCO₂eq/MJ. To be conservative, a minimum and maximum of 11.0 and 21.0 gCO₂eq/MJ were used. These emission factors use the former global warming potential (GWP) of 25 for methane and need to be updated to use the new GWP of 34 [27, 28].

The breakdown of emissions from CO₂, CH₄, and N₂O were not available in the Weber and Calvin paper, so the breakdown from GREET was used as an approximation. GREET finds that the U.S. average NG upstream emissions are 52.1% CO₂, 45.1% CH₄, and 2.8% N₂O [115].

Using the GREET ratios, we broke down the original mean of 15.44 gCO₂eq/MJ to 8.04gCO₂/MJ, 0.28 gCH₄/MJ, and 1.45e-3 gN₂O/MJ. For ease of calculation, the minimum and maximum values are converted to 71.2% and 136% of the mean. Assuming a constant share of CO₂, CH₄, and N₂O emissions will introduce error, as the higher upstream emissions tend to have more methane emissions [117]. As a result the maximum is increased to 140% to compensate.

For the **NG Combustion EF**, Weber and Clavin found that the uncertainty was due to the energy content of the NG and ranged from 55 to 58.1 gCO₂eq/MJ [29]. GREET values of 56.6 and 56.8 gCO₂eq/MJ are used as the mean values for industrial utility boilers and NG turbines, respectively [115]. Weber's and Calvin's values are used as the minimum and maximum values for both combustion EFs since the authors do not specify ranges for specific technologies. The minimum and maximum values are converted to percentages of the mean to account for the change in the GWP of methane.

A4.1.2 Electricity EF

The electricity EF used is dependent on the crude's location and the technology adopted. The mean electricity EF is determined based on the local grid EF; the minimum and maximum are based on the EF for generation technologies that are realistic for the area. GREET 2015 is used to determine the electricity EF for various technologies; the upstream EF for the NG, oil, and coal to run the power plants adds an additional 17.4%, 14.7% and 6.4% to the combustion emissions [14]. When electricity is generated offsite a 6.5% transmission loss is included. The electricity EFs were updated to match those found in Di Lullo et al.'s F-3 update for consistency [118]. In general a wide range is used to be conservative.

For Maya, which uses nitrogen injection and gas lift to extract oil, electricity is the primary energy source. For injection, the Maya nitrogen production facility currently uses an NG combined heat and power plant [119]; therefore the **Nitrogen Compressor Electricity EF** mean is assumed to be an on-site NG combined cycle (NG CC) plant. The minimum and maximum are assumed to be 70% of the mean and a NG simple cycle turbine (NG SC) is assumed. For the **Gas Lift Compressor and Surface Processing**, it was assumed that electricity is generated on the floating platform. An on-site NG SC turbine is assumed as the mean due to space limitations on

the platform. An optimistic on-site NG CC is assumed as the minimum and an on-site oil internal combustion engine (ICE) is assumed as the maximum.

As Mars is also a floating platform, the **Mars Electricity EF** used for the artificial pump lift and surface processing will be the same as the Maya gas lift compressor.

For **Bow River Electricity EF**, the Alberta grid average from 2011-2013 was 990 gCO₂eq/kWh [120]. This study assumed the Alberta grid average as the mean and off-site NG CC and coal plants as the minimum and maximum, respectively.

For **Alaska Electricity EF**, the local grid EF is 224 gCO₂eq/kWh [29]. However, a large amount of hydro is used along the southern coast; the only power plants located in the Alaska county are petroleum liquids, NG ICEs, and NG turbines [121]. Therefore, the GREET EFs for off-site NG ICE, oil ICE, and NG CC plants are used as the mean, maximum, and minimum values [14].

Refinery electricity is assumed to be drawn from the grid; therefore, the **Refinery Electricity EF** is dependent on the refinery location. The original FUNNEL-GHG-CCO model assumed that the refineries were located in Los Angeles (L.A.), California for Alaska North Slope and California Kern, Cushing, Oklahoma for Mars, Bow River, and Athabasca, and Houston, Texas for Maya. eGrid data from 2004, 2005, 2007, 2009, 2010, and 2012 are averaged to find the mean electricity EFs, which were 337, 741, and 654 gCO₂eq/kWh for L.A., Cushing, and Houston, respectively [29]. For L.A., a conservative minimum and maximum of 3 standard deviations below the average [29] and an off-site NG SC turbine [14] were assumed. For Cushing, a minimum and maximum for an off-site NG CC and coal steam turbine were assumed. For Houston, a minimum and maximum for an off-site NG combined cycle and oil ICE were assumed [14].

A4.1.3 Process unit efficiency inputs

Extraction, surface processing, and refining require a large amount of process heat and steam; therefore, **Boiler and Heater Efficiencies** have a significant effect on the WTC emissions. This study assumes only NG boilers are used. Manufacturer data from Cleaver-Brooks found that small (less than 800Bhp) 860 kPa (125 psig) boilers have efficiencies between 80% and 88% [35]. Larger boilers have lower efficiencies (between 70% and 75%) [36-38]. This study uses a mean of 75% and a maximum of 88% for boiler efficiency. No information was available on the minimum boiler efficiency; however, due to economic and environmental factors, low boiler efficiencies are unlikely and a conservative minimum of 62% (symmetric) is used. Heaters are used to heat various fluids throughout the refinery and surface processing units; this study assumes only NG-fired heaters are used. Drevco Process Heaters advertises heater efficiencies from 70-85% and up to 90% when heat recovery is added [39]. OPGEE [5] and FUNNEL-GHG-CCO [12] assumed an 80% heater efficiency. A report from AMETEK Process Instruments found that energy costs are 65% of the operating costs, thus providing incentives for operators to improve efficiency and making low efficiency heaters unlikely [40]. A mean of 80% a minimum of 70%, and a maximum of 90% are used.

Low Flow Pump Efficiencies are used for smaller pumps during the surface processing stage. Evans reports that smaller centrifugal pumps have efficiencies between 50% and 70% (this range includes motor efficiency) and that motor efficiencies range from 90-97% [41]. Karassik shows that a pump with a gpm/rpm ratio of 0.01 (31gpm glycol pump operating at 1750rpm) would have a maximum hydraulic efficiency of 70% and a minimum efficiency of 40% depending on the pump's specific speed [43]. Due to economics, low efficiencies are unlikely; hence we

selected a mean of 60%, a minimum of 50%, and maximum of 70% for the overall pump efficiency.

High Flow Pump Efficiencies are used for extraction pumps and main pipeline pumps. OPGEE, Jacobs, and FUNNEL-GHG-CCO use a 65% efficiency for extraction pumps [5, 22, 42].

Flowserve pumps for the oil and gas sector have gpm/rpm ratios of 0.1 to 10 [122]. Using performance charts from Karassik, we found that ratios of 0.1-10 correspond to peak hydraulic efficiencies for centrifugal pumps of 80% and 85% [43]. Evans stated that medium to large centrifugal pumps have overall efficiencies ranging from 75% to 93% [41]. Additionally, Campbell states that oil and gas centrifugal pumps operate between 70% and 90%, while reciprocating pumps operate between 85% and 92% [4]. These efficiencies are for water. When viscous fluids are pumped, the pump efficiency will drop. Conservative mean, minimum, and maximum efficiencies of 65%, 50%, and 85% were selected.

A4.1.4 Surface processing

After the crude oil reaches the surface, it goes through crude oil stabilization to separate out the gases and water from the crude. The energy required depends on the crude specific heat capacity, the inlet temperature, and the outlet temperature. Wright developed a correlation for the **Crude Specific Heat Capacity** based on the API and temperature [44]. He also found that the specific heat capacity required a correction factor based on its UOP K factor from 0.84 to 1.5, which was used as the Monte Carlo distribution minimum and maximum. The crude stabilizer **Inlet Temperature** was assumed to have a mean temperature of 48.9 °C [45]. Limited information is available on the crude inlet temperature, and as a result a minimum and maximum of 37.8 and 65.6 °C are assumed. The **Outlet Temperature** mean is assumed to be 173.3 °C [45], with a minimum and maximum of 93.3 and 204.4 °C [46].

For crude oil production both **Produced and Imported Water** needs to be treated to remove impurities. Rahman used an average electricity consumption [12] based on work from Vlasopoulos et al. [47], which examined several water treatment technologies. Water treatment involves four stages for produced water and two stages for imported water [12]. To determine a range of energy intensities, the processes with the lowest and highest energy intensities are selected for each stage. Minimum and maximum energy intensities were found to be 1.51 and 5.79 kWh/m³ of water for produced water and 1.26 and 3.90 kWh/m³ of water for imported water. We selected the averaged values of 2.26 and 1.51 kWh/m³ used by Rahman as the mean values.

A4.1.5 Crude transportation

Input distributions for the crude transportation stage were added as part of the F-3 model expansion by Di Lullo et al. examining crudes from outside North America [49]. They were included as part of this work for consistency. For Alberta bitumen, the scenarios for the heavy crude group pipeline velocities are used.

A4.1.5 Venting, fugitive, and flaring

The **Vented and Fugitive Gas Volumes** for typical North American crudes range from 2.1% to 7% of the produced gas volume with an average of 4.6%, as stated in section A1.3 [13].

Flared Gas Volumes were determined using country-specific flaring estimates from the National Oceanic and Atmospheric Administration (NOAA) using data from 2004 to 2009 [54]. Oil production data were collected from the Energy Information Administration (EIA) [56, 123] and the National Energy Board (NEB) [57]; the data are shown in Table A9. It is assumed that there is no error in the oil production data and the flaring intensity error is based only on the

satellite measurement error from the NOAA [54]. Alaska-specific flaring emissions are included in section A4.5. Athabasca-specific VFF emissions are included in section A.9.

Table A9: Flaring ratios

Crude	Years	Total oil (m ³)	Total flaring (BCM) [54]	NOAA error (BCM) [54]	Flaring intensity (m ³ /m ³)	Flaring intensity error (m ³ /m ³)	NOAA region
Maya	2004-2009	1,220,476,050 [55]	14.91	13.62	12.21	11.14	Mexico
Mars	2004-2009	1,544,005,434 [56]	3.56	13.62	2.31	8.81	USA Conus
Bow	2004-2009	916,077,380 [57]	10.16	13.62	11.09	14.86	Canada
Alaska	2004-2009	265,095,771 [56]	9.00	13.62	33.93	51.34	USA Alaska
Kern	2004-2009	1,544,005,434 [56]	3.56	13.62	2.31	8.81	USA Conus

An examination of OPGEE’s in-depth analysis of **Flaring Efficiency** found that efficiencies below 80% only occur when there are both high wind speeds and a high gas velocity at the flare tips; this aligns with Carleton University research that found that Alberta’s average flaring efficiency is 95%. GHGenius, OPGEE, and the original FUNNEL-GHG-CCO used flaring efficiencies of 95% [5, 42, 64], while GREET used 98% [14], and Jacobs used 99% [22]. High flaring efficiencies are common, but as flare efficiency can degrade quickly at high wind speeds a minimum of 80% is used to be conservative. Since wind speeds follow a Rayleigh distribution [5], wherein high wind speeds have a low probability of occurring, a PERT distribution, which favors values closer to the mean, is used in the Monte Carlo simulation. A mean of 95% and a maximum of 99% are used to align with previous research.

The **Produced Gas Composition** affects the surface processing, venting, and fugitive emissions as these depend on the concentration of methane. The default composition is taken from OPGEE, which examined 135 oil wells in California [5]. To develop a beta distribution for the methane concentration, ModelRisk data fitting tools were used on the 118 wells that had methane

concentrations above 50%. To ensure the gas composition totals 100%, the following method is used.

The component input mol% is generated from the user inputs and the Monte Carlo distributions. The methane concentration is determined from the OPGEE beta distribution, and the remaining components use the insensitive input triangle distributions. The mid calculation concentrations are then calculated as described here. If the methane concentration is higher than 78.8% (the default), then the sum of the component concentrations would be greater than 100%. As a result, the concentrations of nitrogen and heavier hydrocarbons will be reduced. The nitrogen and heavier hydrocarbons components are reduced first because they do not affect the surface processing or VFF calculations. The CH₄ concentration has a maximum of 98.9%; this ensures there is always room for H₂S gas, as this gas will affect the surface processing amine treater emissions. Carbon dioxide emissions are reduced last as they effect the VFF emissions and amine treater emissions.

$$x_{CO_2}^{total} = x_{CO_2} [x_{CO_2} (x_{CO_2}, 1 - x_{CH_4} - x_{C_2H_6}), 0] \quad (A8)$$

$$x_{CO_2}^{total} = x_{CO_2} [x_{CO_2} (x_{CO_2}, 1 - x_{CH_4} - x_{C_2H_6} - x_{C_2H_2}), 0] \quad (A9)$$

$$x_{CO_2}^{total} = x_{CO_2} [x_{CO_2} (x_{CO_2}, 1 - x_{CH_4} - x_{C_2H_6} - x_{C_2H_2} - x_{C_2H_4}), 0] \quad (A10)$$

$$x_{CO_2}^{total} = x_{CO_2} [x_{CO_2} (x_{CO_2}, 1 - x_{CH_4} - x_{C_2H_6} - x_{C_2H_2} - x_{C_2H_4} - x_{C_3H_8}), 0] \quad (A11)$$

$$x_{CO_2}^{total} = x_{CO_2} [x_{CO_2} (x_{CO_2}, 1 - x_{CH_4} - x_{C_2H_6} - x_{C_2H_2} - x_{C_2H_4} - x_{C_3H_8} - x_{C_4H_{10}}), 0] \quad (A12)$$

If the methane concentration is below 78.8%, then the sum of the components will be less than 100%; therefore the remainder shown below is split evenly between the five remaining gases.

$$x_{CO_2}^{total} = 1 - x_{CH_4} - x_{C_2H_6} - x_{C_2H_2} - x_{C_2H_4} - x_{C_3H_8} - x_{C_4H_{10}} - x_{C_2H_2} \quad (A13)$$

$$x_{CO_2}^{total} = \frac{x_{CO_2}^{total}}{5} \quad (A14)$$

$$x_{CO_2}^{total} = x_{CO_2} + x_{CO_2}^{total} \quad (A15)$$

$$x_{CO_2}^{total} = x_{CO_2} + x_{CO_2}^{total} \quad (A16)$$

$$x_{CO_2}^{total} = x_{CO_2} + x_{CO_2}^{total} \quad (A17)$$

$$x_{CO_2}^{total} = x_{CO_2} + x_{CO_2}^{total} \quad (A18)$$

$$x_{CO_2}^{total} = x_{CO_2} + x_{CO_2}^{total} \quad (A19)$$

The output mol% is used by the model to calculate the VFF and amine treater emissions.

A4.1.6 Other inputs

The **Refinery Yield Factor** is the amount of crude, in terms of energy (MJ), required to produce 1 MJ of transportation fuel. Due to losses and the generation of by-products such as fuel oils, the yield factor is greater than one. The refinery yield factor depends on the type of refinery used, the crude properties, and the refinery operating practices. This study assumes a deep conversion refinery is being used, but the yield factor still depends on the refinery configuration [16]. The crude-specific FUNNEL-GHG-CCO value is used as the mean [12]. A PERT distribution with maximums and minimums of $\pm 10\%$ are used based on the variation in refinery yield factors observed when alternative assays are used in Aspen HYSYS for each crude.

Finished products are **Distributed to Bulk Terminals** via ocean tankers, barges, pipelines or freight trains. FUNNEL-GHG-CCO used GREET defaults [115] to calculate the distribution emissions [114, 115]. For gasoline distribution, barges have the highest emission intensity, 0.616 gCO₂eq/MJ, while rail has the lowest, 0.104 gCO₂eq/MJ. Therefore, to determine uncertainty in distribution, a uniform distribution from zero to one was used for the share of gasoline transported by barges. It is also assumed that the only other transportation method used is rail. This same method is used to calculate diesel and jet fuel distribution emissions.

The correlation used to calculate the **Crude's Lower Heating Value (LHV)** was taken as 90% of the higher heating value from Speight, who claimed it was generally accurate to within $\pm 1\%$ [15, 124]. To be conservative, a range of $\pm 5\%$ is used.

A4.2 Maya's input distribution generation

For **Nitrogen Generation and Compression** a MAN turbomachinery report states that 573,957 hp was required to generate and compress 33.98 million m³/d of nitrogen to 121 bar [119]. An

article in Modern Power Systems stated that the entire N₂ generation and compression facility is powered by a 520 MW combined heat and plant [125]. The compressors are driven by a combination of electric motors and steam turbines; a natural gas turbine cogeneration unit is used to produce the electricity and steam [119]. With equations A8 to A10 and the facility information, we calculated the compressor energy intensity (EI), driver efficiency, and facility energy intensity (EI).

$$EI_{\text{Compressor}} = \frac{P_{\text{Compressor}} * 1000 \frac{\text{kWh}}{\text{h}} * 24 \frac{\text{h}}{\text{d}}}{\dot{V}_{\text{N}_2}} = 0.3023 \frac{\text{kWh}}{\text{m}^3 \text{N}_2} \quad (\text{A20})$$

$P_{\text{Compressor}}$ = the compressor power required [428 MW] [119] and \dot{V}_{N_2} = the nitrogen production rate [33,980 m³/d] [119].

$$\eta_{\text{Driver}} = \frac{EI_{\text{Compressor}}}{EI_{\text{Facility}}} = 82.3\% \quad (\text{A21})$$

P_{Facility} = the facility power consumption [520MW] [125]. The driver efficiency of 82.3% is reasonable as large electric motors have efficiencies above 95% [93], while steam turbine drivers have peak efficiencies from 60% to 80% [66].

$$EI_{\text{Facility}} = \frac{P_{\text{Facility}} * 1000 \frac{\text{kWh}}{\text{h}} * 24 \frac{\text{h}}{\text{d}}}{\dot{V}_{\text{N}_2}} = 0.367 \frac{\text{kWh}}{\text{m}^3 \text{N}_2} \quad (\text{A22})$$

The overall N₂ generation and compression energy intensity (kWh/m³) is calculated by multiplying the required nitrogen injection rate (m³ N₂/m³) by the facility intensity (kWh /m³ N₂)

To calculate the uncertainty in the overall N₂ generation and compression energy intensity, we assume that the compressor energy intensity is constant and vary the driver efficiency from 60% to 95%, with a mean of 82.3%.

The **Volume of Nitrogen Injected** is dependent on the field production rate. The fully operational Maya facility injects 33.98 million m³/d of nitrogen [119]. Limón-Hernández et al. stated that in 1996 production was 222,600 m³/d prior to gas injection. Gas injection was initiated in May, 2000 and fully operational by December 2000 [126]. By October 2000, oil production was up to 267,120 m³/d with a target production rate of 318,000 m³/d [126]. In 2005 production peaked at 333,900 m³/d and has steadily declined to 232,140 m³/d in 2008 [68]. In 2013 production had decreased to 69,960 m³/d [69]. Hence an N₂ injection ratio of 146.3 m³ N₂/m³ oil is used as the mean with a minimum and maximum of 101.6 and 485.4 m³ N₂/m³ oil. The original FUNNEL-GHG-CCO model used 176.2 m³ N₂/m³ oil [42] and Jacobs used 213.6 m³ N₂/m³ oil [70], which are included within the selected range.

Maya also uses a gas lift compressor to enhance oil recovery. Although the gas compressibility factor, polytrophic index, and interstage cooling efficiency are insensitive inputs, the same Monte Carlo distributions as for Alaska crude are used for consistency.

A4.3 Mars' input distribution generation

Mars uses water flooding to maintain reservoir pressure. The **Water Injection Ratio** was difficult to determine as water was not injected continuously [76]. The planned water injection rate for the field is 13,750 m³/d [74]. Between 2005 and 2011 production was at a minimum and maximum of 11,290 and 19,100 m³/d [76], which gives injection ratios of 1.21 m³/m³ and 0.72 m³/m³. Jacobs and Know Your Oil used higher injection ratios of 3 m³/m³ and 1.5 m³/m³ [6, 70]. Using production and injection plots for the N/O layer of the Mars field gave an approximate ratio of 0.32 m³/m³ from June 2005 to June 2008, which is reasonable as Mars has experienced technical difficulties [74]. Data from the Bureau of Safety and Environmental Enforcement (BSEE) were used for the mean and gave an average water injection ratio of 0.70 m³/m³ [75].

The data analysis is in section A5.1. The minimum and maximum are assumed to be $0.32 \text{ m}^3/\text{m}^3$, from the N/O layer, and $1.5 \text{ m}^3/\text{m}^3$, from Know Your Oil. Jacobs' ratio of $3 \text{ m}^3/\text{m}^3$ was ignored as it uses a worldwide average [70].

The **Water Production Ratio** affects how much water needs to be treated at the surface. Jacobs uses $5.5 \text{ m}^3/\text{m}^3$ and references a personal communication [70], while Know Your Oil used $0.2 \text{ m}^3/\text{m}^3$ [6]. Reported data from Sousa [76] and Lach [74] showed ratios ranged from 0.04 to 0.22 m^3/m^3 , and 0.02 to 0.05 m^3/m^3 . Data from the BSEE gave an average ratio of $0.20 \text{ m}^3/\text{m}^3$ [75].

To cover the wide range, mean, minimum and maximum values of 0.2, 0.02, and 5.5 are used.

The **Gas-to-Oil Ratio** (GOR) was determined from the BSEE data [75]. The mean of $202 \text{ m}^3/\text{m}^3$ is from the 2012-20105 data. To be conservative, a minimum and maximum of 1 and $249 \text{ m}^3/\text{m}^3$ are used. More detail is available in section A5.1.

The **Well Lifetime Productivity** is used to amortize the well drilling emissions. For the minimum and mean, values from Know Your Oil ($20,670 \text{ m}^3/\text{well}$) and the original FUNNEL-GHG-CCO model ($84,883 \text{ m}^3/\text{well}$) were used [6, 114]. Data from Sousa showed that 41 wells produced a cumulative 151 million m^3 of oil as of 2011 [71], which gave $3.69 \text{ million m}^3/\text{well}$. This is a conservative maximum as it does not include injection and exploration wells. The field production rate was updated to $15,100 \text{ b m}^3/\text{d}$ for constituency with the new data [71].

The **Well Depth** will affect the amount of fuel used during drilling, though the fuel amount will have a small effect. A range of 3,048 to 5791 m was taken from Jacobs [22]. These data agree with the data taken from Lach [74].

The water flood injection **Pump Discharge Pressure** effects the pumping energy consumption. Jacobs used 37.9 MPa, while a paper from Weiland found a range of 42.1 to 43.0 MPa [70, 77].

Lach found higher pressures at 42.7 to 47.2 MPa [74]. This study used a mean, minimum, and maximum of 42.0, 37.9, and 47.2 MPa.

A4.4 Bow River's input distribution generation

The **Well Depth** effects the drilling and artificial pump lift emissions. Data from the Alberta Energy Regulator show the average well depth for areas 3 and 4 from 2002 to 2013 is 954m, with a minimum and maximum of 712m and 1306m [78]. Areas 3 and 4 are used as the Bow River crude is extracted from both areas. The National Energy Board (NEB) found the average depth was 1047m with a minimum and maximum of 880m and 1720m for the Bow River Pekisko field [79]. Due to the limited data coverage, a mean, minimum, and maximum of 1000m, 600m, and 1800m were used.

The **Reservoir Pressure** is used to determine the energy requirements of the artificial pump lift and water injection pump. FUNNEL-GHG-CCO used an average pressure of 7.83 MPa, which is used as the mean [114]. Data from a Viking field well show a minimum pressure of 4.39 MPa [127], while Pekisko data show a range of 11.03 to 17.24 MPa [81]. To be conservative, a minimum and maximum of 4.14 and 17.24 MPa are assumed.

The **Water Production Ratio** was determined from data for typical heavy oil water floods in Alberta and Saskatchewan. Renouf et al. found the average WOR was $15 \text{ m}^3/\text{m}^3$, with the average field operating with a WOR greater than $4 \text{ m}^3/\text{m}^3$ for 53% of the time [82, 83]. This study uses a mean, minimum and maximum of 15, 4, and $20 \text{ m}^3/\text{m}^3$.

A4.5 Alaska North Slope input distribution generation

Alaska uses gas alternating water injection, and data show a large amount of water and gas in the production streams [84]. The **Water Production and Injection Ratios** and the **Gas Production**

and Injection Ratios have a significant effect on the results. Monthly production data for Prudhoe Bay and Kuparuk were used as these two fields are responsible for approximately 75% of the Alaska North Slope Production [88]. The analysis of the Alaska data can be found in section A5.2. ModelRisk fitting tools were used to develop the distributions, and ModelRisk copulas were used to relate the production and injection ratios. The gas production and injection ratios were strongly correlated with a correlation coefficient of 0.99. The water production and injection ratios showed a weaker correlation with a 0.69 correlation coefficient.

Alaska injects large amounts of gas into the reservoir; hence, the compressor inputs have a significant effect on the results. The mean compressor **Inlet Temperature** is assumed to be 15 °C [6, 70]. A conservative minimum of 0 °C (cold day) and maximum of 40 °C (hot day) are assumed for this study. The **Discharge Pressure** for the injection and gas lift compressors uses a mean, minimum, and maximum of 18.6, 15.5, and 21.7 MPa. The maximum and mean are from the Alaska Department of Administration [128], and the minimum is determined assuming a symmetric distribution due to lack of data.

For the compressor calculations the **Polytropic Index**, **Compressibility Factor**, and **Interstage Cooling Efficiency** are required. A polytropic index distribution with a mean, minimum, and maximum of 1.36, 1.31, 1.47 is used and represents polytropic efficiencies of 80%, 70% and 90% [1, 4, 129]. A compressibility factor range of 0.9 to 1.1 is assumed with a mean of 1 for this study [7]. The interstage cooling efficiency is assumed to be 80% with a minimum and maximum efficiency of 60% and 100%.

The venting and fugitive analysis by Canter only examines the produced gas that is not reinjected and assumes there are no venting and fugitive emissions from the reinjected gas. It is expected that the **Reinjected Gas Venting and Fugitive** volumes will be lower than the remaining

produced gas since the reinjected gas is not processed to the same extent as the produced gas, but the volume will not be negligible. The reinjected gas has the natural gas liquids and water removed prior to reinjection [91]. A GHGenius model update found that oil well fugitives and basic surface processing losses are 0.316% of the produced gas [130]; which correspond to 45.9 gCO₂eq/m³ of gas processed. OPGEE found that a dehydrator can emit up to 14.1 gCO₂eq/m³ [93]. Weber and Clavin found that a typical natural gas plant produces an average of 95.3 gCO₂eq/m³ of fugitive emissions at the well and a minimum of 28.3 gCO₂eq/m³ at the plant [29]. The lower estimate was chosen for the plant since the injected gas is not treated as thoroughly. As a result, mean, minimum, and maximum values of 45.9, 14.1, and 123.6 gCO₂eq/m³ are used. The non-injected gas equivalent emissions are 656 gCO₂eq/m³ when a venting and fugitive loss of 4.6% is used.

Since the Alaska Oil and Gas Conservation Commission (AOGCC) implemented strict flaring regulations in the 1970s [131] additional data were collected from the EIA to determine the **Flaring** volumes for the Alaska scenario [58, 59]. The new data found that the flaring ratio was 1.4 - 10.9 m³/m³ for the State of Alaska, which is significantly lower than the NOAA value of 33.9 m³/m³. Since the NOAA has a large error range, which includes zero flaring, data from the EIA will be used for Alaska. A uniform distribution with a minimum and maximum of 0 and 10.9 m³/m³ are used to be conservative. The Alaska fugitive gas volume is left as is as the calculation only examines the venting and fugitive gas volumes from the sold produced gas, excluding the reinjected produced gas.

A4.6 California Kern input distribution generation

Kern uses steam injection to extract the heavy oil. The **Steam Injection Ratio**, **WOR**, and **GOR** were determined from monthly production data for the Midway Sunset oilfield [9]. A detailed

analysis is provided in section A5.3. The WOR and SOR were also found to have a correlation coefficient of 0.91; a BiFrank copula was determined using the same methodology used in the Alaska scenario.

Since Kern requires a large amount of heat for steam injection, cogeneration can be used to increase efficiency. The California Department of Conservation found that 415MW of NG cogenerated electricity is produced in the Midway Sunset field [132]. The **Natural Gas Consumption** and **Electricity/Steam Ratio** were determined from the data; the analysis is in section A5.4.

The **Steam Energy Required** is used to convert the steam injection ratio to steam energy. The mean value of 1944 kJ/kg was determined from a typical Midway Sunset Cogeneration facility with a steam quality of 80%. The steam energy required was most sensitive to the quality of steam produced; hence, the minimum and maximum values of 1682 kJ/kg and 2321 kJ/kg are for 60% and 100% quality steam.

The **Cogeneration Steam Capacity** determines the percentage of Kern's steam generation that uses cogeneration. The mean uses 30% from the average monthly steam consumption of 2.4 million m³/month and the total cogeneration steam production rate of 0.7 million m³/month [9, 132]. The minimum and maximum assumptions are no cogeneration and 100% cogeneration.

The cogeneration unit produces more electricity than the extraction and surface processing facilities require; the excess electricity is sold to the grid and receives a credit for offsetting the grid electricity. The **Electricity Credit** uses the local grid EF, which for California is 318 gCO₂eq/kWh [29]. A minimum of 200 gCO₂eq/kWh is assumed as a conservative lower limit. The maximum is assumed to be 471 gCO₂eq/kWh (NG combined cycle turbine) [115].

A4.7 SAGD input distribution generation

The SAGD **Injection SOR** and **Production WOR** were determined for the Athabasca oil sands area from the Alberta Energy Regulator Thermal In Situ Water Publication [97]. The **Steam Energy Required** is used to convert the steam injection ratio to steam energy. The mean value of 2051 kJ/kg was determined for a SAGD injection well with a steam quality of 80% at 8 MPa [98]. The steam energy required was most sensitive to the quality of steam produced; hence, the minimum and maximum values of 1763 kJ/kg and 2340 kJ/kg are for 60% and 100% quality steam. The **Produced Water** is filtered using evaporators, which have power consumptions from 1.2 to 3.8 with an average of 2.5 kWh/bbl [99].

For Athabasca SAGD the **Well Depth** was determined from AER ST 39 data using the 75 and 76 field codes and resulted in min, average, and max depths of 165, 639, and 818 m.[100] The well depth was modeled with a triangle distribution.

A4.8 Mining input distribution generation

Shovels and trucks are used to extract bitumen ore and transport it to the separation plant. The **Truck Cycle** times were determined from multiple sources and range from 15.8 and 44, with an average of 22 mins/cycle, and were modeled with a triangle distribution [102-104]. Nimana et al. surveyed shovel brochures and found **Shovel Cycle** times between 20 and 36 s [105]. The **Truck/Shovel Capacity** and **Fuel Consumption** were taken from Ordorica-Garcia et al. and modeled as uniform distributions [101]. Truck fuel consumption varied from 406 to 580 L/h and capacity varied from 218 to 363 tonnes. Shovel fuel consumption varied from 375 to 740 L/h and capacity varied from 45 to 85 tonnes. **Truck and Shovel Availability** was assumed to range

from 75% to 95% with a mean of 85% and is modeled as a triangle distribution [102]. The **Shovel Fill Factor** was assumed to range uniformly from 85% to 95% [102].

The mining **Land Use Emissions** depend on the intensity of the land disturbance. With a low, medium, and high intensity corresponding to land use emissions of 0.83, 1.28, and 2.33 gCO₂eq/MJ which are modeled as a triangle distribution.

It is difficult to calculate **Mining Electricity Consumption** for the min conveyor belts and froth treatment unit; therefore, electricity data from ST39 for Shell Canada's Jackpine mine and Albian Sands were used. The electricity intensity for the mining and ore separation stage ranged from 94.8 to 162 with an average of 123 kWh/m³ in 2014 [100]. The **Bitumen Ore Saturation** for Shell Canada was also determined from ST39 and ranged from 10.6% to 12.1% with an average of 11.44% [100].

Hot water is required for ore preparation and froth production. **Hot Water Consumption** was calculated from Total's report on the Joslyn North Mine Project that states that 6705 tph of hot water are required for an oil sands capacity of 8600 tph. Varying the oil sands grade gives 6 to 9m³ of hot water/m³ of bitumen, with an average of 7.5 [106]. The hot water enters the heater at 2 - 25°C depending on the season and is heated to 50 - 75°C [106, 107]. Uniform distributions are used to model both temperature ranges.

Data from the Alberta government were used to determine the **Fugitive Emissions** from the mine surface and tailings ponds [63]. The data were too coarse to use data fitting; hence, a uniform distribution was used between the min and max values. Data from the Imperial Kearn mine and upgrader were not considered as this facility just started up in 2013 and has relatively low production at the moment.

A4.9 Athabasca shared input distribution generation

No Alberta-specific cogeneration data were available and so the correlations from OPGEE were used to determine the **Cogen NG Consumption** and **Cogen Electricity/Steam Ratio** as described in section A1.2 [5]. The **Cogen Modifier** is modelled as a uniform distribution from 1 to 4. Cogenerated electricity can be sold back to the grid and receive a **Cogeneration Credit**. The Alberta government currently uses a 418 gCO₂eq/kWh credit [113]. Since the grid emission intensity in Alberta averaged 990 gCO₂eq/kWh, the government credit is conservatively small [33]. Hence, a uniform distribution between 418 and 990 gCO₂eq/kWh is used.

For crude transportation, the dilbit **Kinematic Viscosity** for Athabasca dilbit was calculated as 9.7 cSt in Aspen HYSYS. The kinematic viscosity must be below 350 cSt to meet pipeline requirements [108]. To be conservative, a uniform distribution from 9.7 to 350 cSt is used for the bitumen scenarios. Data from Enbridge give a kinematic viscosity range of 5 to 250 cSt for SCO, with the majority of crudes below 15 cSt [109]. Therefore, a triangle distribution with a min, mean, and max of 5, 15, and 250 cSt is used.

Alberta bitumen can be upgraded to SCO using either a coking or hydroconversion upgrader. Coking upgraders typically have lower emissions and yields, while hydroconversion upgraders have higher emissions and yields [111]. GHOST found that approximately 78% of Alberta SCO is produced using coker upgraders [112]. Nimana et al. found that coking upgraders produce between 205 and 236 kgCO₂eq/m³ bitumen while hydroconversion produces 362 to 431 kgCO₂eq/m³ depending on the extent of cogeneration used [110, 111]. For this study the average **Upgrading Emissions** are assumed to be 259 kgCO₂eq/m³, which is the production weighted average using 78% coking and 22% hydroconversion upgrading. A triangle distribution is used with a min and max of 205 and 431 kgCO₂eq/m³, respectively. The **Upgrader Yield**, m³

SCO/m³ bitumen, varies from 80% to 95% and 95% to 108% for coking and hydroconversion refineries, respectively. The production weighted average of 89% is used as the mean for a triangle distribution, with a min and max of 85% and 108%. The upgrader emissions and yield dependence were modeled by a BiFrank copula.

Due to Alberta bitumen's composition and extraction techniques, the VFF emissions and produced gas ratios cannot be approximated using the same methods as for conventional crudes.

Due to the aggregated nature of the Alberta Energy Regulator (AER) data, it is not possible to accurately determine the GOR and VFF volumes for SAGD and mining. However, GHOST collected information through NDA in 2011 paper [60]. For SAGD, the **GOR** was determined from GHOST as 1 - 12 m³/m³ [60]. For mining it is assumed that the GOR is approximately zero.

SAGD Flaring and Fugitive Emissions ranged from 100 - 600, and 300 - 1000 gCO₂eq/m³ bitumen, respectively. However, due to regulations, the percentage of produced gas conserved increased from 94.5% in 2011 to 95.3% in 2013, which means that venting and fugitive emissions decreased by 15% [61]. However, it is unclear what portion of that increase is associated with SAGD production due to the aggregated nature of the data. To be conservative, the flaring and fugitive emissions are modeled with a uniform distribution; the lower end emissions will drop by 15% and the upper end emissions will remain the same. For the mining scenario, the mine face and tailings ponds are the largest sources of fugitive emissions. Data from the Alberta government were used to determine the **Fugitive Emissions** from the mine surface and tailings ponds [63]. The data were too coarse to use data fitting; hence, a uniform distribution was used between the min and max values of 106 and 2830 gCH₄/m³ (3604 and 96220 gCO₂eq/m³ with GWP of 34). Data from the Imperial Kearn mine and upgrader were not included as this facility started up in 2013 and has relatively low production at the moment. The

Alberta government data are higher than the GHOST range of 3000 - 24000 gCO₂eq/m³; however, this is expected as the measurement scope has been expanded in recent years [62, 63]. The **Flaring Emissions** are taken from GHOST as 0 - 15000 gCO₂eq/m³ and modeled as a uniform distribution [62]. When an upgrader is included, the **Flaring and Fugitive Emissions** increase by 5000 - 10000 and 0 - 2000 gCO₂eq/m³ SCO, respectively.

For the Athabasca bitumen scenarios, the Athabasca thermal assay from Alberta Energy is used [133]. For the SCO scenarios, the Suncor Synthetic A crude assay was used [134].

A5. Input distributions data analysis

In order to determine some of the Monte Carlo distributions, the raw data had to first be filtered, combined, or adjusted. The following sections summarize how the distributions were determined from the raw data.

A5.1 Mars data

The Mars offshore field is defined by the BSEE codes 764 and 807 [76]. Well statuses codes were filtered to include only 04 (water injecting) and 08 (oil producing) wells [135]. Data were analyzed for the years 2012-2015 [75]. The average injection WOR was determined to be 0.70 m³/m³ and was constant over the four-year period. The GOR data showed a wider range of values that oscillated over the four-year time period. As a result, a wider range was used for the GOR distribution to be conservative.

A5.2 Alaska data

Monthly production data were gathered for the period January 2013 to December 2015 from the Alaska Department of Administration [84]. The data included the monthly crude, water, and gas production volumes and water and gas injection volumes [89]. Only the data from Prudhoe Bay

and Kuparuk were used, as these two fields are responsible for approximately 75% of Alaska North Slope's production [85]. Over the three years analyzed, there was no correlation to time. The data showed that for the high production wells the ratios were relatively stable, but for the low production wells there was a significant amount of variation. This can be seen for the Production WOR in Figure A1. Consequently, wells producing less than 477,000 m³/d (3 million bpd), approximately 20% of the total production, were excluded from the analysis. ModelRisk data fitting tools were used to produce distributions from the remaining data. Due to limitations in the data fitting software and the data coverage, the standard deviation for the distributions was multiplied by 1.5, making the distribution wider to be more conservative.

Excel's Data Analysis correlation function was used to examine the relationship between the production and extraction ratios. The gas production and injection ratios were strongly correlated with a correlation coefficient of 0.99. The water production and injection ratios showed a weaker correlation with a 0.69 correlation coefficient. ModelRisk BiFrank copulas were used to model the dependence between the production and injection ratios. The BiFrank copula requires the correlation parameter theta. The simulated Injection/Production ratio was determined using the copula and compared to the actual Injection/Production ratio in an iterative method until an acceptable theta was determined. For the gas ratios theta is assigned the maximum value of 35 due to the strong correlation. For the water ratios a theta of 5.6 was used; a more conservative approach was used for water as it is less sensitive variable.

For the historical scenarios the data from Prudhoe Bay are used as its cumulative production is five times larger than Kuparuk River's [89]. Similar to the current scenarios, the ratios are modelled as normal distributions. The mean values are determined from the 2015 cumulative production and injection volumes. Due to the lack of information, the standard deviation is

assumed to be the same as the current scenario's. For example, the injection WOR standard deviation was $\pm 28\%$ for the current scenario, so the historical scenario standard deviation is assumed to also be $\pm 28\%$.

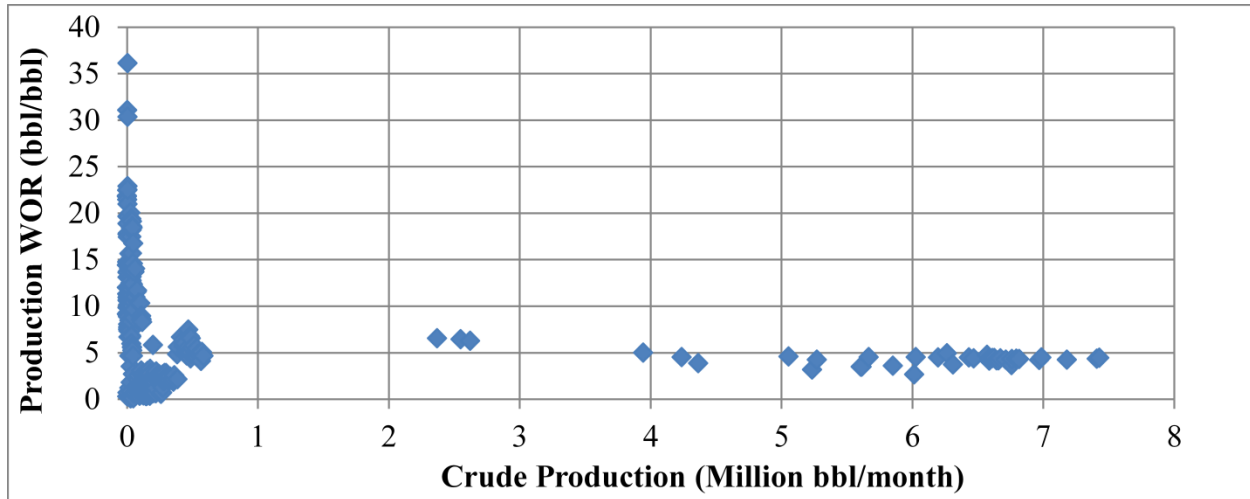


Figure A1: Alaska North Slope water production ratio

A5.3 Kern data

Data were collected from monthly production reports from January 2011 to September 2015 for the Midway Sunset oilfield [9]. The data included monthly volumes of crude, GOR, and water cut production data. For the steam injection data, the volume of steam injected was collected for both steam flooding and cyclic steam injection. The data showed an increasing trend with time; hence the December data were used and were collected for 1996 and 2005 to 2010. The additional data confirmed that the crude production has been steadily declining while steam injection and water production have been increasing. The GOR showed a sharp rise in 2009 but leveled off afterwards.

Due to the strong time dependence of the steam injection and WOR, ModelRisk data fitting tools were not used. The Monte Carlo distribution mean and minimum are determined from the averages and minimums in the 2011-2015 data. The maximum is determined by projecting a

linear trend five years into the future. Since the GOR stabilized during the 2011-2015 timeframe, it was possible to fit a normal distribution to the data. The standard deviation was doubled to be conservative and account for the limited data availability. The steam injected and water produced showed a strong dependence with a correlation coefficient of 0.91. Using the same method as for the Alaska scenario, we created a BiFrank copula with a theta of 13.

Historical scenario ratios are determined from the Midway Sunset field cumulative data [9]. The minimum and maximum values are determined using the same methodology as for the Alaska historical case.

A5.4 Kern cogeneration data

The data from the California Department of Conservation included the peak power consumption, mass flow rate of steam produced, and the volume of natural gas used. The amount of electricity produced was determined assuming a 90% use. The energy added to the steam was calculated from the change in enthalpy. It was assumed that the boiler is a constant pressure system and the water entered at 100 °C and exited at 285 °C [95]. The system produces 80% quality steam at 6.89 MPa [95], resulting in an enthalpy change of 1944 kJ/kg [96]. The electricity/steam ratio (MWh/MWh) was used to eliminate the three outliers that had large ratios (9.9) or small ratios (0.2) compared to the remaining plants, which had ratios between 0.54 and 0.75. The three outliers represented 16% of the peak power production. The natural gas consumption in m³/MWh was determined from the natural gas volume divided by the electricity and steam energy. ModelRisk data fitting tools were used to produce distributions for the natural gas consumption intensity and the electricity/steam ratio.

A5.5 SAGD data

The monthly water use data were filtered to include only SAGD operations in the Athabasca oil sands area from 2012 to 2016. Data points with SOR over 5.91 and WOR over 5.1 were considered outliers and represented less than 0.5% of the bitumen extracted. The SOR and WOR from each month were assigned a frequency equal to the bitumen volume (m³) divided by 100,000 and rounded to the nearest integer. This gives a higher weight to SORs and WORs from facilities with a larger production. The resulting data were fitted to a bounded Johnson distribution using the ModelRisk data fitter tool. The produced WOR and injected SOR had a correlation coefficient of 0.92; hence, a normal copula was used to link the two data sets.

A6. Gasoline, diesel and jet fuel results

Additional results for the gasoline scenarios, as well as results for the diesel and jet fuel scenarios are presented here. The diesel and jet fuel results are similar to the gasoline emissions. The VFF and WTR emissions are the same for all three fuels. The only difference between the gasoline, diesel, and jet fuel emissions is in the refining, distribution and combustion emissions. Figure A2 shows the WTC emissions for each fuel using a functional unit of gCO₂eq/MJ of fuel, where fuel is diesel or jet for each respective scenario.

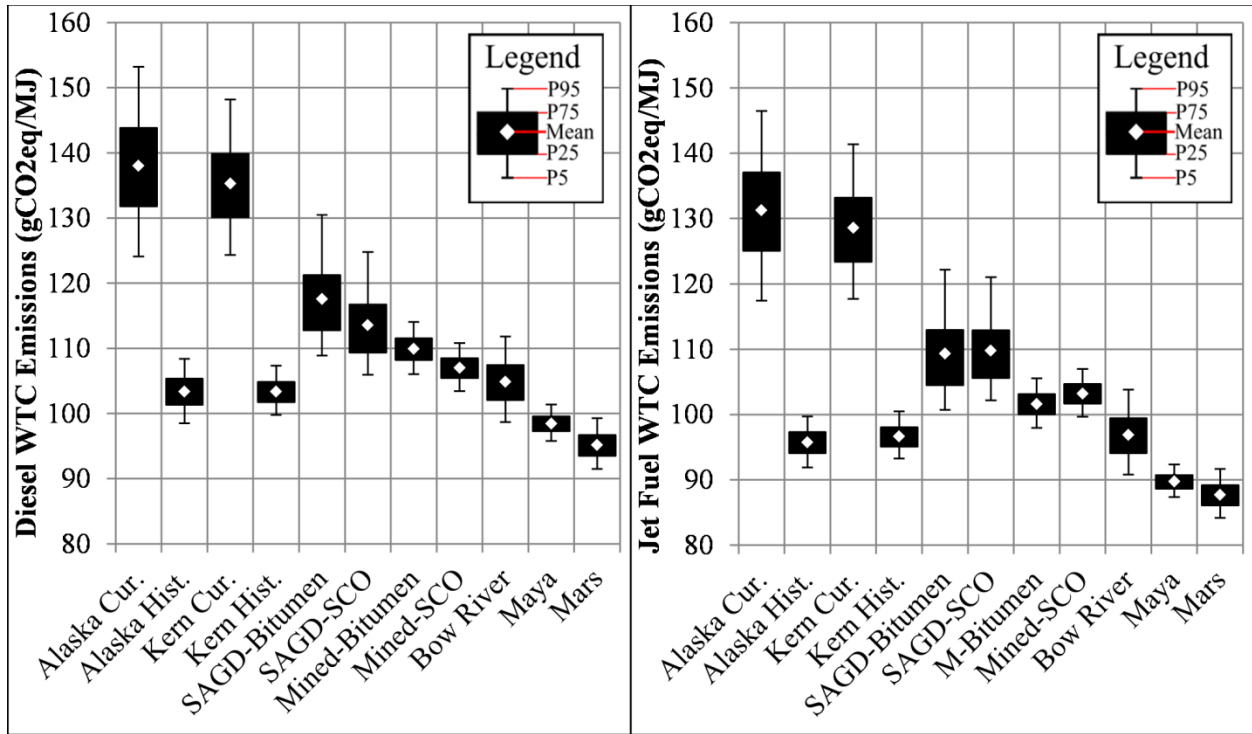


Figure A2: WTC emissions

A6.1 WTC tornado plots

The inputs that have a significant effect on the diesel and jet fuel WTC emission uncertainty are shown using tornado plots in Figure A3 to A6. The inputs at the top of the tornado plot have the largest effect on the overall uncertainty while inputs at the bottom are less significant.

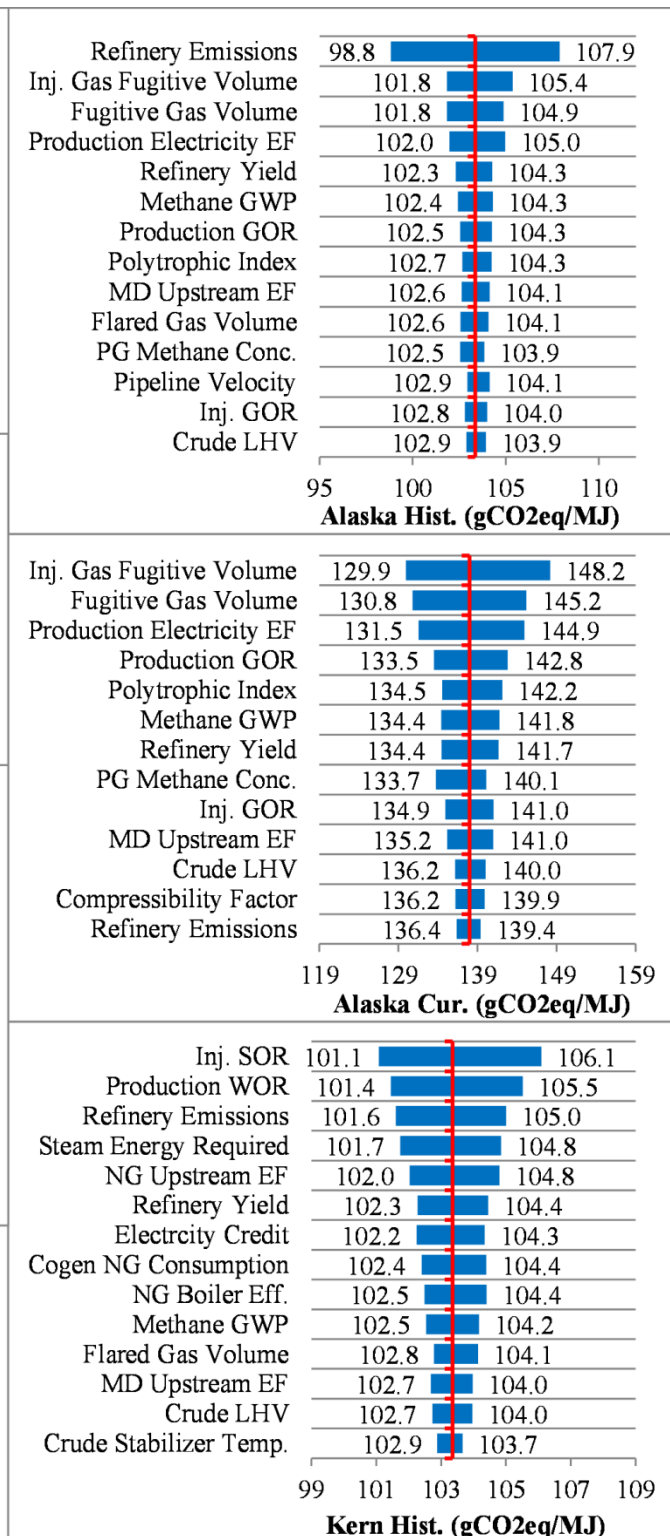
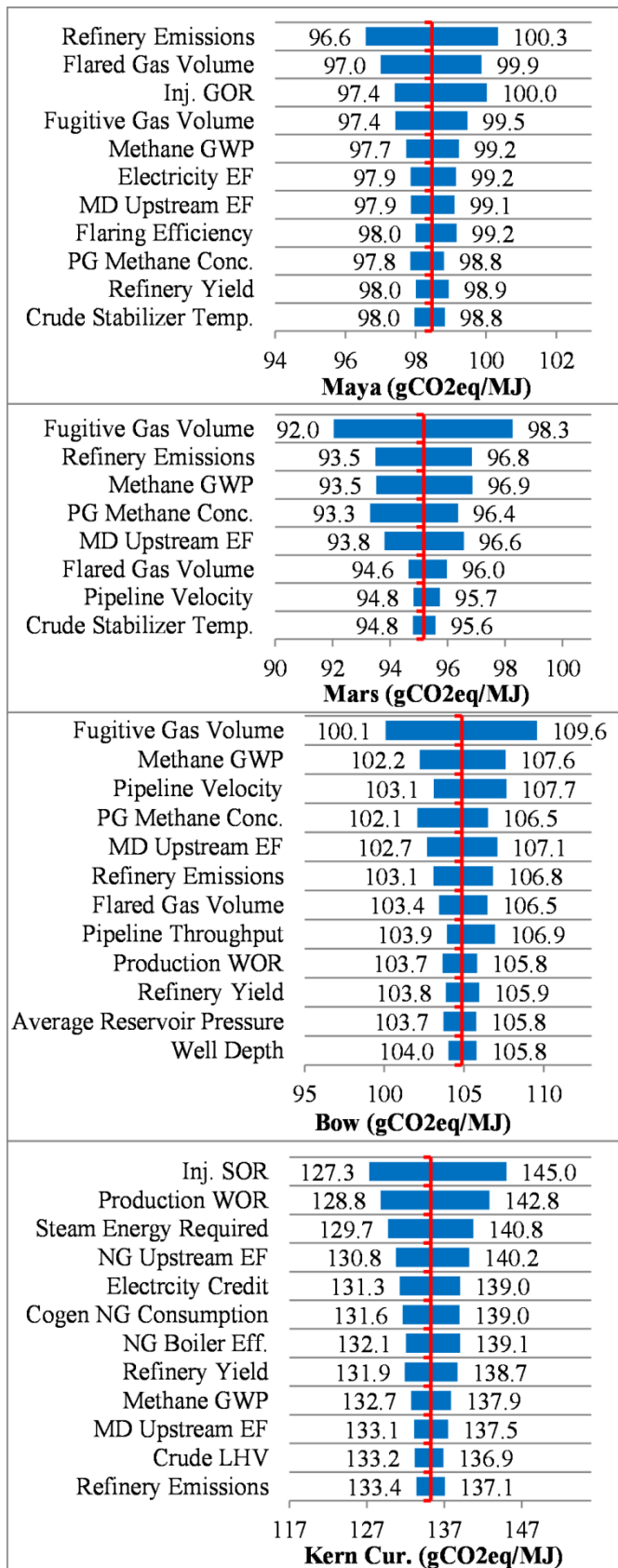


Figure A3: Conventional crude WTC emission tornado plots for diesel

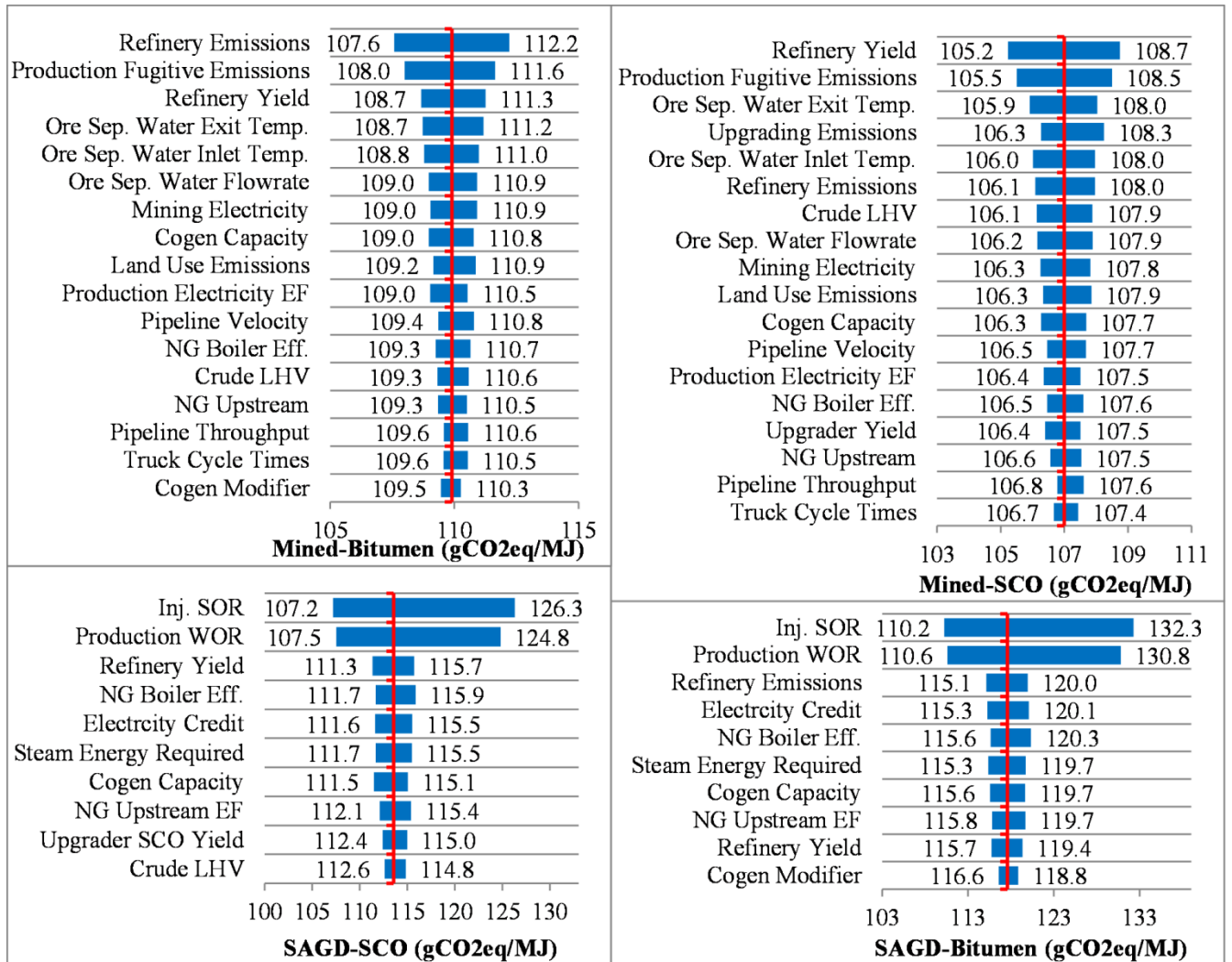


Figure A4: Unconventional crude WTC emission tornado plots for diesel

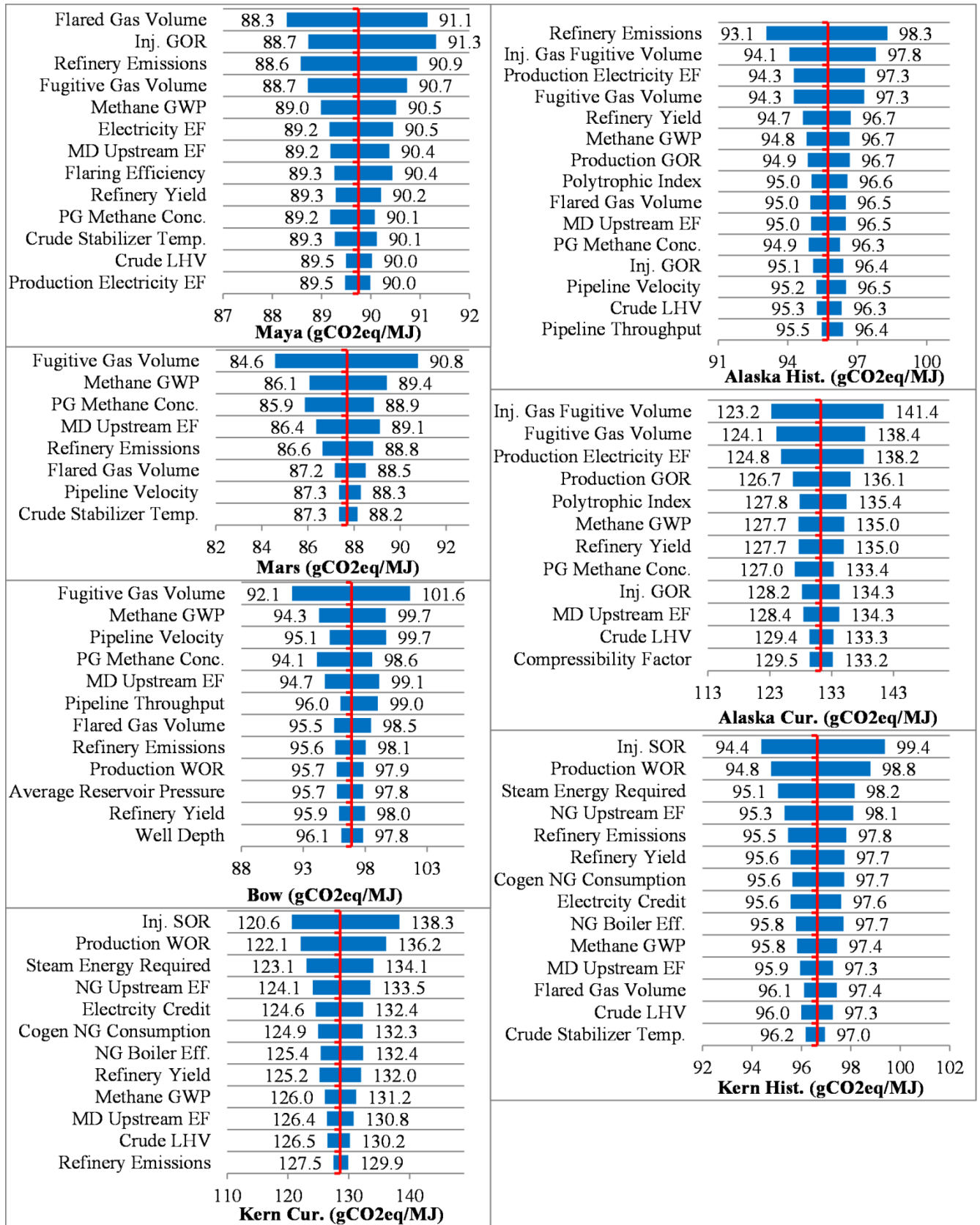


Figure A5: Conventional crude WTC emission tornado plots for jet

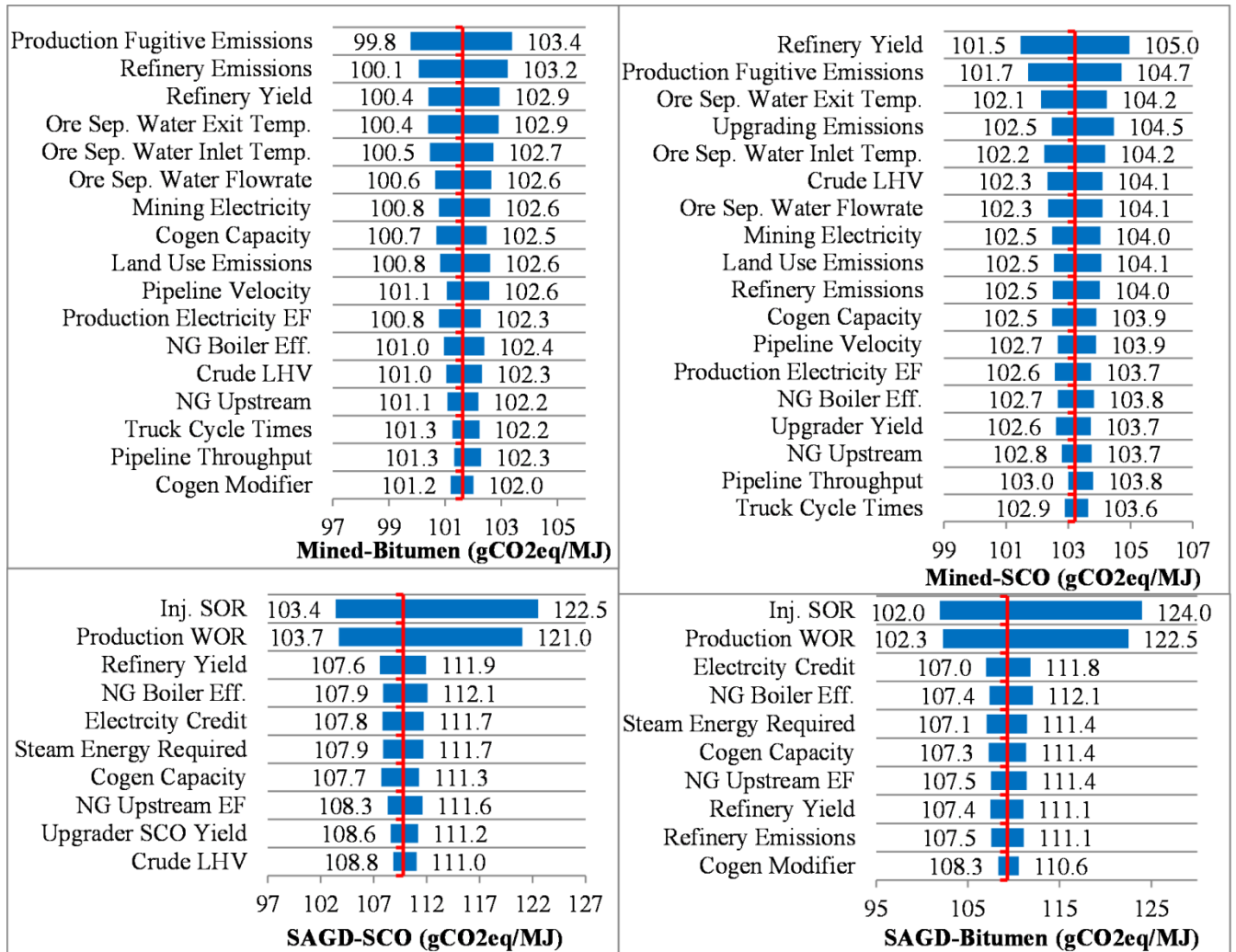


Figure A6: Unconventional crude WTC emission tornado plots for jet

A6.2 Refinery tornado plots

The inputs that have a significant effect on the refinery emission uncertainty are shown in Figure A7 and Tables A10 and A11 for the gasoline, diesel, and jet fuel scenarios, respectively. For Alaska, the current scenario uses the Alaska North Slope assay, while the historical scenario uses the average from the Alaska North Slope and Prudhoe Bay assays. The Alaska refinery tornado plot represents the Alaska North Slope assay, while the Prudhoe plot represents only the Prudhoe Bay assay. A tornado plot was not generated for the averaged Alaska North Slope and Prudhoe Bay scenario.

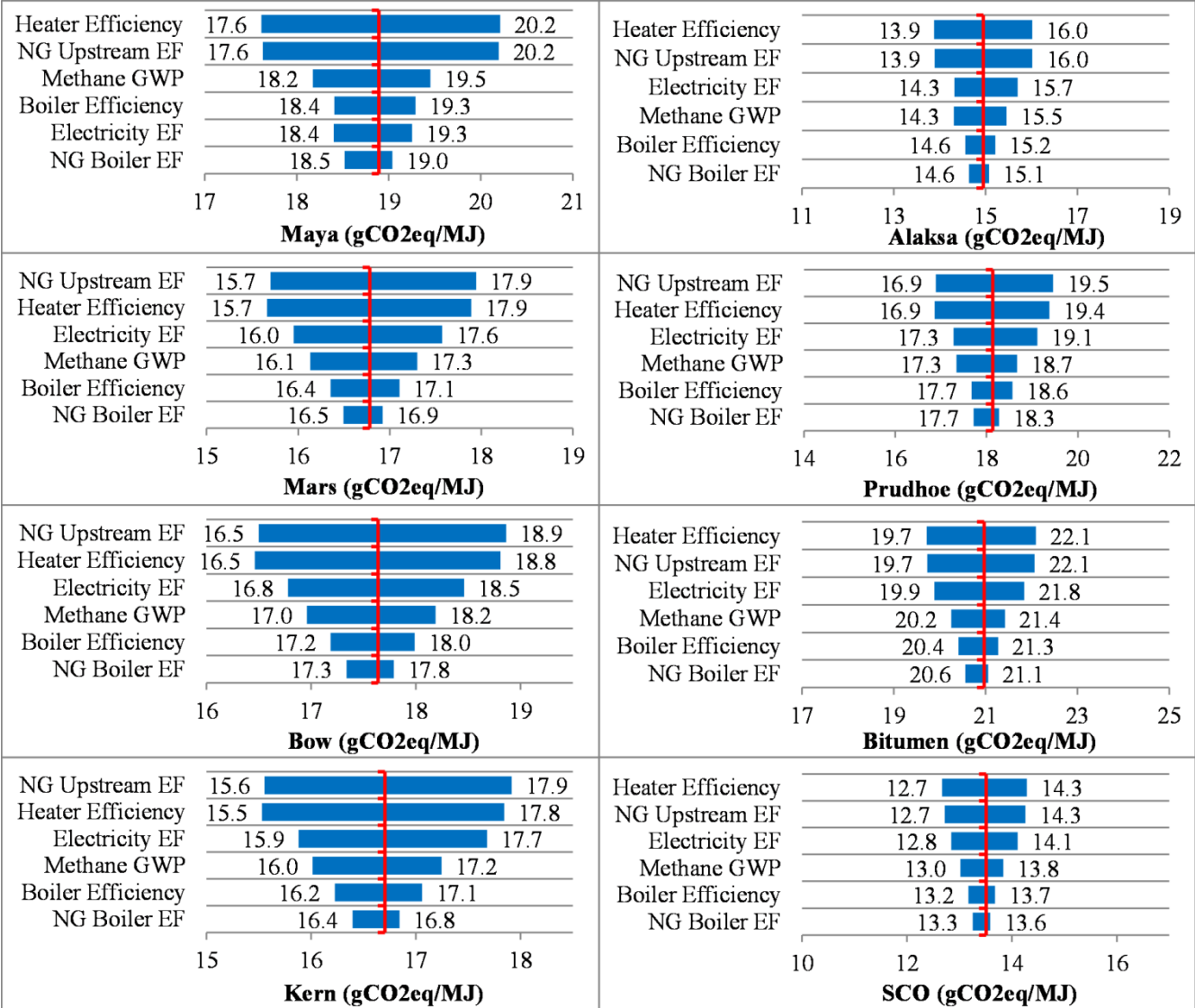


Figure A7: Refinery emission tornado plots for gasoline

Table A10: Refinery emission tornado plots for diesel

gCO ₂ eq/MJ Diesel	Maya		Mars		Bow		Alaska		Prudhoe		Kern		Bitum
Input	Min	Max	Min	Max	Min	Max	Min	Max	Min	Max	Min	Max	Min
NG Boiler EF	15.0	15.5	12.3	12.7	13.7	14.1	10.6	10.9	14.7	15.1	12.1	12.4	16.8
Electricity EF	14.9	15.6	11.9	13.2	13.6	14.3	10.4	11.3	14.4	15.7	11.8	12.9	16.3
Boiler Efficiency	14.9	15.7	12.2	12.9	13.4	14.4	10.5	11.0	14.6	15.3	11.9	12.6	16.7
Methane GWP	14.7	15.8	12.1	13.0	13.3	14.6	10.4	11.1	14.4	15.4	11.8	12.7	16.6
Heater Efficiency	14.3	16.4	11.8	13.4	13.0	14.8	10.1	11.4	14.1	15.9	11.4	13.1	16.1
NG Upstream EF	14.3	16.4	11.8	13.4	13.0	14.9	10.1	11.4	14.1	15.9	11.4	13.2	16.1
Conditional mean	15.3		12.6		14.0		10.8		15.0		12.3		17.

Table A11: Refinery emission tornado plots for jet

gCO ₂ eq/MJ Jet	Maya		Mars		Bow		Alaska		Prudhoe		Kern		Bitum
Input	Min	Max	Min	Max	Min	Max	Min	Max	Min	Max	Min	Max	Min
NG Boiler EF	9.4	9.7	7.9	8.1	8.8	9.0	6.9	7.1	9.2	9.4	8.4	8.6	11.6
Electricity EF	9.3	9.7	7.7	8.4	8.6	9.4	6.7	7.3	9.0	9.7	8.2	9.0	11.3
Boiler Efficiency	9.3	9.8	7.8	8.2	8.7	9.2	6.8	7.1	9.1	9.6	8.3	8.8	11.5
Methane GWP	9.2	9.9	7.8	8.3	8.6	9.2	6.7	7.2	9.0	9.6	8.2	8.8	11.4
Heater Efficiency	9.0	10.2	7.5	8.6	8.4	9.5	6.6	7.4	8.8	9.9	8.0	9.1	11.1
NG Upstream EF	8.9	10.2	7.5	8.6	8.4	9.6	6.6	7.4	8.8	9.9	8.0	9.2	11.1
Conditional mean	9.6		8.1		9.0		7.0		9.4		8.6		11.

A6.3 VFF tornado plots

The VFF tornado plots in Figure A8 show which inputs have a significant effect on the VFF emission uncertainty. The results are the exact same for gasoline, diesel, and jet fuel.

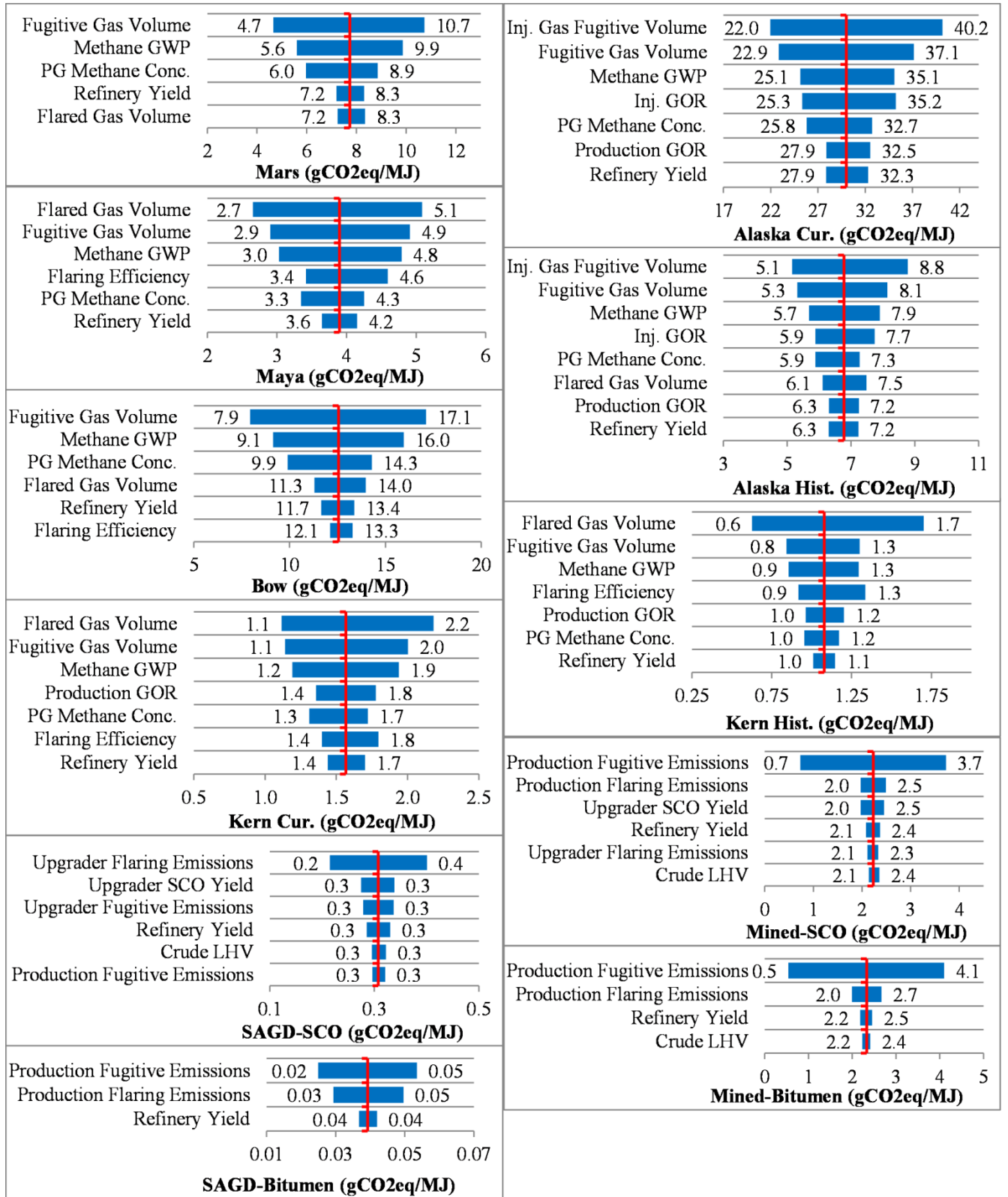


Figure A8: VFF emission tornado plots

A7. Abbreviations

°API	American Petroleum Institute gravity
API	American Petroleum Institute
EF	Emission factor
FUNNEL-GHG-CCO	FUNDamental ENgineering PrinciplEs-based ModeL for Estimation of GreenHouse Gases in Conventional Crude Oils
FUNNEL-GHG-OS	FUNDamental ENgineering PrinciplEs-based ModeL for Estimation of GreenHouse Gases in Oil Sands
GHG	Greenhouse gas
GOR	Gas-to-oil ratio (m^3/m^3)
REET	Greenhouse Gases, Regulated Emissions, and Energy Use in Transportation
GWP	Global warming potential
LHV	Lower heating value (MJ/kg)
OPGEE	Oil Production Greenhouse gas Emissions Estimator
P5	5th percentile
P95	95th percentile
PG	Produced gas
PRELIM	Petroleum Refinery Life Cycle Inventory Model
SAGD	Steam assisted gravity drainage
SCO	Synthetic crude oil
SOR	Steam-to-oil ratio (cold water equivalent m^3/m^3)
SP	Surface processing
VFF	Venting, flaring and fugitive
WOR	Water-to-oil ratio (m^3/m^3)
WTR	Well-to-refinery gate
WTT	Well-to-tank
WTC	Well-to-combustion

A8. References

1. Kidnay, A.J., W.R. Parrish, and D.G. McCartney, *Compression*, in *Fundamentals of Natural Gas Processing*. 2011, CRC Press: Boca Raton, Fl. p. 185-210.

2. Moshfeghian, M., *How to Estimate Compressor Efficiency?* July 1, 2015, John M. Campbell & Co: Norman, OK, <http://www.jmcampbell.com/tip-of-the-month/2015/07/how-to-estimate-compressor-efficiency/> (May 16, 2016).
3. *Gases - Specific Heat Capacities and Individual Gas Constants*. Bethlehem, PA [cited Feb. 22, 2016]; Available from: <http://catalog.conveyorspneumatic.com/Asset/FLS%20Specific%20Heat%20Capacities%20of%20Gases.pdf>.
4. Campell, J.M., *Gas Conditioning and Processing*. Vol. 2: The Equipment Modules. 1984, Norman, OK: Campell Petroleum Series.
5. El-Houjeiri, H.M., et al., *OPGEE* June 4, 2015, Stanford School of Earth, Energy & Environmental Sciences: Stanford, CA, <https://pangea.stanford.edu/researchgroups/eao/research/opgee-oil-production-greenhouse-gas-emissions-estimator> (May 16, 2016).
6. Gordon, D., et al., *Know Your Oil: Creating a Global Oil-Climate Index*. 2015, Carnegie Endowment for International Peace: Washington, http://carnegieendowment.org/files/know_your_oil.pdf (Feb. 18, 2016).
7. PetroWiki. *Real gases*. June 4, 2015 [cited Feb. 18, 2016]; Available from: http://petrowiki.org/Real_gases.
8. Division of Oil, Gas & Geothermal Resources. *2009 Annual Report of the State Oil & Gas Supervisor*. 2010, California Department of Conservation: Sacramento, CA, http://www.conservation.ca.gov/dog/pubs_stats/annual_reports/Pages/annual_reports.aspx (Feb. 18, 2016).
9. Di Lullo, G., M.M. Rahman, and A. Kumar. *Uncertainty analysis of transportation fuels from North American conventional oils GHG emissions*. in *65th Canadian Chemical Engineering Conference*. 2015. Calgary, Canada.
10. Desiderata Energy Consulting, *2014 Oil Sands Co-generation and Connection Report*. 2014, Oil sands community alliance: Fort McMurray, Alberta <http://www.oscaalberta.ca/wp-content/uploads/2015/08/2014-Oil-Sands-Cogeneration-Report-FINAL-18-Jun-2014.pdf>.
11. Holly, C., et al., *Oil sands production profile: 2004-2014*. 2016, Energy Technical Services Branch: Edmonton, Alberta, <http://www.energy.alberta.ca/Org/pdfs/InitiativeOSPP.pdf>.
12. Rahman, M.M., *Life Cycle Assessment of North American Conventional Crudes for Production of Transportation Fuels*, in *Mechanical Engineering*. 2014, University of Alberta: Edmonton.
13. Canter, C. and A. Kumar. *Impact of fugitive emissions on the greenhouse gas emissions of conventional crudes*. in *AIChE Annual Meeting*. 2014. Atlanta: AIChE.
14. Argonne, *GREET1*. 2015, Argonne National Laboratory: Argonne, IL, <https://greet.es.anl.gov/> (June 14, 2016).
15. Speight, J.G., *The Chemistry and Technology of Petroleum*. 4th ed. Chemical Industries. 2014, Hoboken: CRC Press.

16. Bergerson, J., *Petroleum Refinery Life Cycle Inventory Model*. 2015, University of Calgary: Calgary, AB, <http://ucalgary.ca/lcaost/prelim> (May 16, 2016).
17. Yeh, S., et al., *Land use greenhouse gas emissions from conventional oil production and oil sands*. *Environmental Science & Technology*, 2010. **44**(22): p. 8766-8772, doi: <http://dx.doi.org/10.1021/es1013278>.
18. Sigman, K., *Introduction to reducing variance in Monte Carlo simulations*. 2007, Department of Industrial Engineering and Operations Research: New York, <http://www.columbia.edu/~ks20/4703-Sigman/4703-07-Notes-ATV.pdf> (June 14, 2016).
19. Alaska Oil and Gas Conservation Commission. *Prudhoe Bay Feild, Prudhoe Oil Pool - EOR Injection*. 2004, Alaska Department of Administration: Anchorage, AK, http://doa.alaska.gov/ogc/annual/2004/Oil_Pools/Prudoe%20Bay%20-%20Oil/Prudhoe%20Bay,%20Prudhoe%20Bay/Cht_Inj_EOR.pdf (Apr. 29, 2016).
20. Alaska Oil and Gas Conservation Commission. *Prudhoe Bay Feild, Prudhoe Oil Pool - Production*. 2004, Alaska Department of Administration: Anchorage, AK, http://doa.alaska.gov/ogc/annual/2004/Oil_Pools/Prudoe%20Bay%20-%20Oil/Prudhoe%20Bay,%20Prudhoe%20Bay/Cht_Production.pdf (Apr. 29, 2016).
21. Alaska Oil and Gas Conservation Commission. *AOGCC Pool Statistics - Prudhoe Bay Unit, Prudhoe Oil Pool*. 2004, Alaska Department of Administration: Anchorage, AK, http://doa.alaska.gov/ogc/annual/current/18_Oil_Pools/Prudhoe%20Bay%20-%20Oil/Prudhoe%20Bay,%20Prudhoe%20Bay/1_Oil_1.htm (Apr. 29, 2016).
22. Keesom, W., S. Unnasch, and J. Moretta, *Life Cycle Assessment Comparison of North American and Imported Crudes prepared for Alberta Energy Research Institute*. July 2009, Jacobs Consultancy: Chicago, IL, <http://eipa.alberta.ca/media/39640/life%20cycle%20analysis%20jacobs%20final%20report.pdf> (June, 14, 2016).
23. Rosenfeld, J., et al., *Comparison of North American and Imported Crude Oil Lifecycle GHG Emissions - Final Report Prepared for Alberta Energy Reseach Institute*. July 6, 2009, TIAX LLC: Cupertino, CA, <http://eipa.alberta.ca/media/39643/life%20cycle%20analysis%20tiax%20final%20report.pdf> (Mar. 25, 2016).
24. *BP Crudes: Alaska North Slope*. July 2015 [cited July 20, 2016]; Available from: http://www.bp.com/en/global/bp-crudes/assays/americas/alaskan_north_slope.html.
25. Speight, J.G., *Crude Oil Assay Database*. Knovel, <http://app.knovel.com/hotlink/toc/id:kpCOAD0005/crude-oil-assay-database/crude-oil-assay-database> (Sept. 25, 2016).
26. Vose Software, *ModelRisk Software*. 2015, Vose Software: Belgium, <http://www.vosesoftware.com/> (May 16, 2016).
27. Myhre, G., et al., *Anthropogenic and Natural Radiative Forcing Supplementary Material*, in *Climate Change 2013: The Physical Science Basis. Contribution of Working Group to the Fifth Assessment Report of the Intergovernmental Panel on Climate Change*, T.F. Stocker, et al., Editors. 2013, Cambridge University Press: Cambridge and New York. p.

- 8SM-19, https://www.ipcc.ch/pdf/assessment-report/ar5/wg1/supplementary/WG1AR5_Ch08SM_FINAL.pdf (Nov. 15, 2016).
28. Myhre, G., et al., *Anthropogenic and Natural Radiative Forcing*, in *Climate Change 2013: The Physical Science Basis. Contribution of Working Group to the Fifth Assessment Report of the Intergovernmental Panel on Climate Change*, T.F. Stocker, et al., Editors. 2013, Cambridge University Press: Cambridge and New York, (Nov. 15, 2016).
 29. Weber, C.L. and C. Clavin, *Life cycle carbon footprint of shale gas: Review of evidence and implications*. *Environmental Science & Technology*, 2012. **46**(11): p. 5688-5695, doi: <http://dx.doi.org/10.1021/es300375n>.
 30. U.S. Energy Information Administration. *Natural Gas Gross Withdrawals and Production*. July 31, 2015, U.S. EIA: Washington, http://www.eia.gov/dnav/ng/ng_prod_sum_dcu_NUS_a.htm (Feb. 11, 2016).
 31. Turanskyj, L. and K. B.A., *Turbomachinery for the world's largest nitrogen plant: Enhanced Oil Recovery to increase the output in the Cantarell oil field, Mexico*. June 2001, MAN: Berlin, <https://www.yumpu.com/en/document/view/16563813/turbomachinery-for-the-worlds-largest-nitrogen-man-turbo-india/3> (Mar. 25, 2016).
 32. Environmental Protection Agency. *eGRID Data Files*. Jan. 4, 2016, Energy and the Environment: Washington, DC, <http://www.epa.gov/energy/egrid> (Feb. 11, 2016).
 33. Government of Canada. *National Inventory Report: Part 3*. Apr. 17, 2015, United Nations Framework Convention on Climate Change: Ottawa, ON. p. 85, http://unfccc.int/national_reports/annex_i_ghg_inventories/national_inventories_submissions/items/8812.php (Feb. 18, 2016).
 34. U.S. Energy Information Administration. *Alaska - State Profile and Energy Estimates*. Feb. 18, 2016, EIA: Washington, <http://www.eia.gov/state/?sid=AK#tabs-4> (Mar. 25, 2016).
 35. Cleaver Brooks., *Boiler Efficiency Guide: Facts about Firetube Boilers and Boiler Efficiency*. Mar. 2010, Cleaver Brooks: Thomasville, GA, <http://www.cleaver-brooks.com/reference-center/insights/boiler-efficiency-guide.aspx> (June 14, 2016).
 36. Stark, C., *Reducing Energy Cost Through Boiler Efficiency*. 2015, Department of Poultry Science North Carolina State University: Raleigh, NC, https://www.ncsu.edu/project/feedmill/pdf/E_Reducing%20Energy%20Cost%20Through%20Boiler%20Efficiency.pdf (Mar. 25, 2016).
 37. Energy Technology Systems Analysis Program., *Industrial Combustion Boilers*, in *IEA ETSAP - Technology Brief I01*. May 2010, International Energy Agency: Paris, FR, http://www.iea-etsap.org/web/e-techds/pdf/i01-ind_boilers-gs-ad-gct1.pdf (June 14, 2016).
 38. Council of Industrial Boiler Owners., *Energy Efficiency & Industrial Boiler Efficiency: An Industry Perspective*. 2015, Council of Industrial Boiler Owners: Warrenton, VA, <http://www.swagelokenergy.com/download/EEIBE.pdf> (Feb. 18, 2016).

39. Devco Process Heaters. *Our Heaters*. [cited Feb. 16, 2016]; Available from: <http://www.devcoheaters.com/our-heaters/>.
40. Wildy, F., *Fired Heater Optimization*. AMETEK Process Instruments: Pittsburgh, PA, <http://www.etaassociates.com/Fired%20Heater%20Optimization%20ISA%20AD.pdf> (Mar. 25, 2016).
41. Evans, J., *Centrifugal Pump Efficiency—What Is Efficiency?*, in *Pumps & Systems*. 2012, Pumps & Systems: Birmingham, AL, <http://www.pumpsandsystems.com/topics/pumps/pumps/centrifugal-pump-efficiency-what-efficiency> (March 30, 2016).
42. Rahman, M.M., C. Canter, and A. Kumar, *Greenhouse gas emissions from recovery of various North American conventional crudes*. *Energy*, 2014. **74**: p. 607-617, doi: <http://dx.doi.org/10.1016/j.energy.2014.07.026>.
43. Karassik, I.J., et al., *2.1 Centrifugal Pump Theory*, in *Pump Handbook*. 2015, McGraw Hill Professional: New York, <http://accessengineeringlibrary.com/browse/pump-handbook-fourth-edition> (January 26, 2016).
44. Wright, W., *Simple Equations to Approximate Changes to the Properties of Crude Oil with Changing Temperature*. Apr. 1, 2014, John M. Campbell Consulting: Norman, OK, <http://www.jmccampbell.com/tip-of-the-month/2014/04/simple-equations-to-approximate-changes-to-the-properties-of-crude-oil-with-changing-temperature/> (Feb. 17, 2016).
45. Manning, F.S. and R.E. Thompson, *Oilfield Processing of Petroleum: Crude Oil*. Vol. 2. 1995, Tulsa, OK: PennWell Books.
46. Stewart, M. and K. Arnold, *Chapter 2 - Crude Stabilization*, in *Emulsions and Oil Treating Equipment*. 2009, Gulf Professional Publishing: Burlington. p. 81-106.
47. Vlasopoulos, N., et al., *Life cycle assessment of wastewater treatment technologies treating petroleum process waters*. *Science of The Total Environment*, 2006. **367**(1): p. 58-70, doi: <http://dx.doi.org/10.1016/j.scitotenv.2006.03.007>.
48. Enbridge Pipelines Inc., *Q2 2015 Service Levels On the Enbridge Liquids Pipeline Mainline Network*. June 2015, Enbridge: Calgary, AB, http://www.enbridge.com/~/_media/Rebrand/Documents/Shippers/Enbridge_Mainline_Service_Levels.pdf?la=en (June 14, 2016).
49. Di Lullo, G., H. Zhang, and A. Kumar, *Evaluation of uncertainty in the well-to-tank and combustion greenhouse gas emissions of various transportation fuels*. *Applied Energy*, 2016. **184**: p. 413-426, doi: <http://dx.doi.org/10.1016/j.apenergy.2016.10.027>.
50. Psaraftis, H.N. and C.A. Kontovas, *Ship Emission Study prepared for Hellenic Chamber of Shipping*. May 2008, National Technical University of Athens Laboratory for Maritime Transport: Pireas, Greece, <http://www.nee.gr/downloads/66ship.emissions.study.pdf> (June 14, 2016).
51. Man Diesel & Turbo., *Basic Principles of Ship Propulsion*. Dec. 2011, MAN Diesel & Turbo: Copenhagen, Denmark, <https://marine.man.eu/docs/librariesprovider6/propeller-aftship/basic-principles-of-propulsion.pdf?sfvrsn=0> (June 14, 2016).

52. Lindstad, H., B.E. Asbjørnslett, and A.H. Strømman, *Reductions in greenhouse gas emissions and cost by shipping at lower speeds*. Energy Policy, 2011. **39**(6): p. 3456-3464, doi: <http://dx.doi.org/10.1016/j.enpol.2011.03.044>.
53. Hamilton, T.M., *Oil tanker sizes range from general purpose to ultra-large crude carriers on AFRA scale*, in *Today in Energy*. 2014, U.S. Energy Information Administration.
54. U.S. Energy Information Administration, *Crude Oil Production*. EIA: Washington, http://www.eia.gov/dnav/pet/pet_crd_crpdn_adc_mbbl_a.htm (Feb. 17, 2016).
55. U.S. Energy Information Administration. *International-Total Petroleum and Other Liquids Production*. EIA: Washington, <http://www.eia.gov/beta/international/?fips=MX#pet> (Feb. 17, 2016).
56. U.S. Energy Information Administration. *Crude Oil Production*. EIA: Washington, http://www.eia.gov/dnav/pet/pet_crd_crpdn_adc_mbbl_a.htm (May 20, 2016).
57. National Energy Board. *ARCHIVED - Estimated Production of Canadian Crude Oil and Equivalent*. 2016, NEB: Ottawa, <https://www.nerb-one.gc.ca/nrg/sttstc/crdlndprtlmprdct/stt/archive/stmtdprdcnrchv-eng.html> (Feb. 18, 2016).
58. U.S. Energy Information Administration. *Crude Oil Production*. 2015, EIA: Washington, http://www.eia.gov/dnav/pet/pet_crd_crpdn_adc_mbbl_a.htm (Sept. 26, 2016).
59. U.S. Energy Information Administration. *Natural Gas Gross Withdrawals and Production*. 2015, EIA: Washington, http://www.eia.gov/dnav/ng/ng_prod_sum_dcu_NUS_a.htm (Sept. 26, 2016).
60. Charpentier, A.D., et al., *Life Cycle Greenhouse Gas Emissions of Current Oil Sands Technologies: GHOST Model Development and Illustrative Application*. Environmental Science & Technology, 2011. **45**(21): p. 9393-9404, doi: 10.1021/es103912m.
61. Alberta Energy Regulator. *ST60B: Upstream Petroleum Industry Flaring and Venting Report*. 2014, AER: Edmonton, <https://www.aer.ca/documents/sts/ST60B-2014.pdf>.
62. Bergerson, J.A., et al., *Life cycle greenhouse gas emissions of current oil sands technologies: surface mining and in situ applications*. Environmental Science & Technology, 2012. **46**(14): p. 7865-7874, doi: 10.1021/es300718h; M3: DOI: 10.1021/es300718h; 04 10.1021/es300718h.
63. Alberta Environment and Parks. *Fugitive Emissions for SGER Oil Sands Facilities: 2011 - 2014*. 2015, Alberta Government: Edmonton, <http://aemeris.aemera.org/library/Dataset/Details/263>.
64. (S&T)² Consultants Inc., *GHGenius*. 2012, (S&T)² Consultants Inc: Delta, BC, <http://www.ghgenius.ca/downloads.php> (May 16, 2016).
65. Modern Power Systems, *Integrated solution key to success of world's largest oil-field N2 plant*. Nov. 16, 2001, Global Trade Media: London, <http://www.modernpowersystems.com/features/featureintegrated-solution-key-to-success-of-world-s-largest-oil-field-n2-plant/> (Mar. 25, 2016).

66. Cerce, M.A. and V.P. Patel. *Selecting Steam Turbines for Pump Drivers*. in *Twentieth International Pump Users Symposium*. 2003. Houston, TX: Turbomachinery Laboratory of the Texas A&M University.
67. Limón-Hernández, T., G. Garza-Ponce, and C. Lechuga-Aguiñaga. *Status of the Cantarell field development program: An overview*. in *Offshore Technology Conference*. 2001. Houston, TX: Offshore Technology Conference, <https://www.onepetro.org/download/conference-paper/OTC-13175-MS?id=conference-paper%2FOTC-13175-MS> (May 16, 2016).
68. Clemente, J., *Cantarell is not Mexico's only oil production problem*. *Pipeline & Gas Journal*, 2008(August, 2008): p. 52-54.
69. Weeden, S. *Meteoric History Of Cantarell Field Continues For Pemex*. *Exploration and Production*, May 1, 2015, 2015. Houston, TX: Hart Energy, <http://www.epmag.com/meteoric-history-cantarell-field-continues-pemex-792716#p=full> (Feb. 17, 2016).
70. Keesom, W., S. Unnasch, and J. Moretta, *Life Cycle Assessment Comparison of North American and Imported Crudes prepared for Alberta Energy Research Institute*. 2009, Jacobs Consultancy: Chicago, IL, <http://www.eipa.alberta.ca/media/39640/life%20cycle%20analysis%20jacobs%20final%20report.pdf> (February 18, 2016).
71. Sousa, L.d., *Deepwater GOM: Reserves versus Production - Part 1: Thunder Horse & Mars-Ursa*. Sept. 30, 2011, *The Oil Drum*. p. 30, http://www.theoil Drum.com/pdf/theoil Drum_8366.pdf (Mar. 25, 2016).
72. Lach, J., *IOR for Deepwater Gulf of Mexico* Dec. 15, 2010, Research Partnership to Secure Energy for America: Houston, TX. p. 329, http://www.knowledge-reservoir.com/pdf/rpsea_report.pdf (Feb. 18, 2016).
73. Bureau of Safety and Environmental Enforcement. *Oil and Gas Operations Reports - Part A (OGOR-A) Well Production 1996 - 2015*. 2016, BSEE: Washington, https://www.data.bsee.gov/homepg/pubinfo/freeasci/product/freeprod_ogora.asp (Feb. 18, 2016).
74. Lach, J., *IOR for Deepwater Gulf of Mexico* 2010, Research Partnership to Secure Energy for America: Houston, TX. p. 329, http://www.knowledge-reservoir.com/pdf/rpsea_report.pdf (February 18, 2016).
75. *Oil and Gas Operations Reports - Part A (OGOR-A) Well Production 1996 - 2015*. 2015, Bureau of Safety and Environmental Enforcement,; Washington, https://www.data.bsee.gov/homepg/pubinfo/freeasci/product/freeprod_ogora.asp (February 18, 2016).
76. Sousa, L.d., *Deepwater GOM: Reserves versus Production - Part 1: Thunder Horse & Mars-Ursa*. 2011, *The Oil Drum*. p. 30, http://www.theoil Drum.com/pdf/theoil Drum_8366.pdf (March 25, 2016).
77. Weiland, J., et al. *Case History Review of the Application of Pressure Transient Testing and Production Logging in Monitoring the Performance of the Mars Deepwater Gulf Of*

- Mexico Field*. in *SPE Annual Technical Conference and Exhibition*. 2008. Denver, CO: Society of Petroleum Engineers.
78. Alberta Energy Regulator. *Alberta's Energy Reserves & Supply/Demand Outlook*. 2015, AER: Edmonton, <https://www.aer.ca/data-and-publications/statistical-reports/st98> (Feb. 18, 2016).
 79. *Conventional Heavy Oil Resources of the Western Canada Sedimentary Basin*. 2011, National Energy Board: Calgary, <https://www.nerb-one.gc.ca/nrg/sttstc/crdlndprtlmprdct/rprt/archive/cnvntnlhvylrsrscs2001/TRhvylWCSB2001-eng.pdf> (February 18, 2016).
 80. Galas, C., et al., *Identification of Enhanced Oil Recovery Potential in Alberta - Phase 2 Final Report*. 2012, Energy Resource Conservation Board: Calgary, http://www.ags.gov.ab.ca/publications/pdf_downloads/ercb-eor-report2.pdf (February 18, 2016).
 81. Fedenczuk, L., P. Pedersen, and M. Pedersen. *Analyzing Waterflood Responses for Pekisko B*. in *Digging Deeper, Finding a Better Bottom Line*. 1999. Calgary, AB: The Petroleum Society.
 82. Renouf, G. and P. Nakutnyy, *Success of Heavy Oil Waterfloods - Factors and Predictions Phase II*. 2009, Petroleum Technology Research Centre: Regina. p. 121, http://steps.ptrc.ca/concrete/files/8914/0554/3411/SRC-001-00094_Final_Report_Phase_I.pdf (March 25, 2016).
 83. Renouf, G., et al., *Heavy Oil Waterflooding Scoping Study*. 2004, Petroleum Technology Research Centre: Regina, http://steps.ptrc.ca/concrete/files/3514/0546/3331/Heavy_Oil_Waterflooding_Scoping_Study_-_Final_Report.pdf (March 25, 2016).
 84. *Monthly Production Reports*. 2015, Alaska Oil and Gas Conservation Commission, Alaska Department of Administration: Anchorage, AK, <http://doa.alaska.gov/ogc/production/pindex.html> (April 29, 2016).
 85. Alaska Oil and Gas Conservation Commission. *Alaska Oil and NGL Production - December 2015*. Feb. 2, 2016, Alaska Department of Administration: Anchorage, AK, http://doa.alaska.gov/ogc/ActivityCharts/Production/2015_12-ProdChart.pdf (Apr. 29, 2016).
 86. *Prudhoe Bay Field, Prudhoe Oil Pool - EOR Injection*. 2004, Alaska Oil and Gas Conservation Commission, Alaska Department of Administration: Anchorage, AK, http://doa.alaska.gov/ogc/annual/2004/Oil_Pools/Prudoe%20Bay%20-%20Oil/Prudhoe%20Bay,%20Prudhoe%20Bay/Cht_Inj_EOR.pdf (April 29, 2016).
 87. *Prudhoe Bay Field, Prudhoe Oil Pool - Production*. 2004, Alaska Oil and Gas Conservation Commission, Alaska Department of Administration: Anchorage, AK, http://doa.alaska.gov/ogc/annual/2004/Oil_Pools/Prudoe%20Bay%20-%20Oil/Prudhoe%20Bay,%20Prudhoe%20Bay/Cht_Production.pdf (April 29, 2016).
 88. *Alaska Oil and NGL Production - December 2015*. Alaska Oil and Gas Conservation Commission, Alaska Department of Administration: Anchorage, AK,

- http://doa.alaska.gov/ogc/ActivityCharts/Production/2015_12-ProdChart.pdf (April 29, 2016).
89. Alaska Oil and Gas Conservation Commission. *Monthly Production Reports*. 2015, Alaska Department of Administration: Anchorage, AK, <http://doa.alaska.gov/ogc/production/pindex.html> (Apr. 29, 2016).
 90. Alaska Oil and Gas Conservation Commission. *Conservation Order 341D*. Nov. 30, 2001, Alaska Department of Administration: Anchorage, AK, http://doa.alaska.gov/ogc/orders/co/co300_399/co341d.htm (Apr. 29, 2016).
 91. Kaltenbach, B., et al. *North Slope of Alaska Facility Sharing Study*. May 2004, Alaska Department of Natural Resources: Anchorage, AK, http://dog.dnr.alaska.gov/publications/Documents/OtherReports/NorthSlope_Facility_Sharing_Study.pdf (Feb. 18, 2016).
 92. (S&T)² Consultants Inc., *Shale Gas Update for GHGenius*. 2011, Natural Resources Canada Office of Energy Efficiency: Ottawa, <http://www.ghgenius.ca/reports/ShaleGasUpdateFinalReport.pdf>.
 93. El-Houjeiri, H.M., et al., *OPGEE V1.1 Draft E*. 2015, Stanford School of Earth, Energy & Environmental Sciences: Stanford, CA, <https://pangea.stanford.edu/researchgroups/eao/research/opgee-oil-production-greenhouse-gas-emissions-estimator> (May 16, 2016).
 94. *2009 Annual Report of the State Oil, & Gas Supervisor*. 2010, Division of Oil, Gas & Geothermal Resources, California Department of Conservation: Sacramento, CA, http://www.conservation.ca.gov/dog/pubs_stats/annual_reports/Pages/annual_reports.aspx (February 18, 2016).
 95. Edmond, R., D. W., and T. Nass Chas, *Cogeneration improves thermal EOR efficiency*. Oil and Gas Journal, 1990. **88**(42).
 96. Çengel, Y. and M.A. Boles, *Thermodynamics: An Engineering Approach*. 7th ed. 2011, New York: McGraw-Hill.
 97. Alberta Energy Regulator. *Thermal In Situ (TIS) Water Publication June 15*. AER: Edmonton, <https://aer.ca/data-and-publications/activity-and-data/thermal-in-situ-tis-water-publication> (Aug. 28, 2016).
 98. Ordorica-Garcia, J.G., *Development of Optimal Energy Infrastructures for the Oil Sands Industry in a CO₂-constrained World in Chemical Engineering 2007*, University of Waterloo: Waterloo, Canada.
 99. Kearney, O., *The use of a mechanical vapour recompression (energy-saving) evaporator to concentrate acid casein whey* 1989, {Canadian Association of Petroleum Producers., 2012 #72} Commission of the European Communities: Luxembourg, <https://www.google.ca/url?sa=t&rct=j&q=&esrc=s&source=web&cd=2&ved=0CCMQFjABahUKEwjex7nX6vTGAhVHnYgKHfEnAX0&url=http%3A%2F%2Fbookshop.europa.eu%2Fsv%2Fthe-use-of-a-mechanical-vapour-recompression-energy-saving-evaporator-to-concentrate-acid-casein-whey-pbCDNA12157%2Fdownloads%2FCD-NA-12-157-EN->

112. Englander, J.G. and A. R.Brandt, *Oil Sands Energy Intensity Analysis for GREET Model Update Technical Documentation*. 2014, Department of Energy Resources Engineering Stanford: Stanford, <https://greet.es.anl.gov/publication-lca-update-oil-sands>.
113. Alberta Environment and Parks. *Industrial Emissions Management*. [cited Nov. 11, 2016]; Available from: <http://aep.alberta.ca/climate-change/programs-and-services/industrial-emissions-management.aspx>.
114. Rahman, M.M., *Life Cycle Assessment of North American Conventional Crudes for Production of Transportation Fuels*, in *Mechanical Engineering*. 2014, University of Alberta: Edmonton, Canada.
115. *GREET1*. 2013, Argonne National Laboratory: Argonne, IL, <https://greet.es.anl.gov/> (May 16, 2016).
116. U.S. Energy Information Administration. *Natural Gas Gross Withdrawals and Production*. 2013 February 11, 2016 [cited Feb. 11, 2016]; Available from: http://www.eia.gov/dnav/ng/ng_prod_sum_dcu_NUS_a.htm.
117. ICF Consulting Canada., *Life Cycle Greenhouse Gas Emissions of Natural Gas: A Literature Review of Key Studies Comparing Emissions from Natural Gas and Coal* 2012, The Canadian Natural Gas Initiative: Fairfax, VA.
118. Di Lullo, G.R., *Uncertainty in Life Cycle Assessments of Well-to-Wheel Greenhouse Gas Emissions of Transportation Fuels Derived from Various Crude Oils*, in *Mechanical Engineering*. 2016, University of Alberta: Edmonton, AB.
119. Turanskyj, L. and K. B.A., *Turbomachinery for the world's largest nitrogen plant: Enhanced Oil Recovery to increase the output in the Cantarell oil field, Mexico*. 2001, MAN: Berlin, <https://www.yumpu.com/en/document/view/16563813/turbomachinery-for-the-worlds-largest-nitrogen-man-turbo-india/3> (March 25, 2016).
120. *National Inventory Report: Part 3*. 2015, Government of Canada: Ottawa, ON. p. 85, cited in http://unfccc.int/national_reports/annex_i_ghg_inventories/national_inventories_submissions/items/8812.php (February 18, 2016).
121. U.S. Energy Information Administration. *Alaska - State Profile and Energy Estimates*. 2016 February 18, 2016 [cited Mar. 25, 2016]; Available from: <http://www.eia.gov/state/?sid=AK#tabs-4>.
122. Flowserve., *Pipeline Transportation Pumps*. Jan. 2015, Flowserve: Irving, TX. p. Brochure, <http://www.flowserve.com/files/Files/Literature/ProductLiterature/Pumps/fpd-8-e.pdf> (May 16, 2016).
123. U.S. Energy Information Administration. *International-Total Petroleum and Other Liquids Production*, EIA, Editor. 2016: Washington, <http://www.eia.gov/beta/international/?fips=MX#pet> (Feb. 17, 2016).
124. Bergerson, J., *Petroleum Refinery Life Cycle Inventory Model v1.0*. 2015, University of Calgary: Calgary, AB, <http://ucalgary.ca/lcaost/prelim> (May 16, 2016).
125. *Integrated solution key to success of world's largest oil-field N2 plant*. Modern Power Systems, Nov. 16, 2001, 2001. London: Global Trade Media,

- <http://www.modernpowersystems.com/features/featureintegrated-solution-key-to-success-of-world-s-largest-oil-field-n2-plant/> (Mar. 25, 2016).
126. Limón-Hernández, T., G. Garza-Ponce, and C. Lechuga-Aguiñaga. *Status of the Cantarell Field Development Program: An Overview*. in *Offshore Technology Conference*. 2001. Houston, TX: Offshore Technology Conference.
 127. Galas, C., et al. *Identification of Enhanced Oil Recovery Potential in Alberta - Phase 2 Final Report*. Mar. 2012, Energy Resource Conservation Board: Calgary, http://www.agr.gov.ab.ca/publications/pdf_downloads/ercb-eor-report2.pdf (Feb. 18, 2016).
 128. *Prudhoe Oil Pool: Modification to pool rules*. 2001, Alaska Oil and Gas Conservation Commission, Alaska Department of Administration: Anchorage, AK, http://doa.alaska.gov/ogc/orders/co/co300_399/co341d.htm (April 29, 2016).
 129. Moshfeghian, M. *How to Estimate Compressor Efficiency?* 2015 February 22, 2016 [cited May 16, 2016]; Available from: <http://www.jmcampbell.com/tip-of-the-month/2015/07/how-to-estimate-compressor-efficiency/>.
 130. (S&T)² Consultants Inc., *Shale Gas Update for GHGenius*. Aug. 31, 2011, Natural Resources Canada Office of Energy Efficiency: Ottawa, <http://www.ghgenius.ca/reports/ShaleGasUpdateFinalReport.pdf> (June 14, 2016).
 131. Alaska Oil & Gas Conservation Commission. *AOGCC: 50 years of Service to Alaska*. 2008, AOGCC: Juneau, AK, <http://doa.alaska.gov/ogc/WhoWeAre/50th/aogcc50thBooklet.pdf> (Sept. 26, 2016).
 132. Division of Oil, Gas & Geothermal Resources, *2009 Annual Report of the State Oil, & Gas Supervisor*. 2010, California Department of Conservation: Sacramento, CA, http://www.conservation.ca.gov/dog/pubs_stats/annual_reports/Pages/annual_reports.aspx.
 133. Alberta Department of Energy. *Bitumen Assay Program Aggregate Assay Information*, Energy Technical Services, Editor. 2016: Edmonton, www.energy.alberta.ca/Org/docs/BitumenAssayProgramAggregate.xlsx (Nov. 28, 2016).
 134. Crude Quality Inc. *Suncor Synthetic A Assay*. 2016 [cited Nov. 28, 2016]; Available from: CrudeMonitor.ca.
 135. Bureau of Safety and Environmental Enforcement. *Field Values for PACIFIC OGOR*. 2016, BSEE: Washington, <https://www.data.bsee.gov/homepg/pubinfo/pacificfreeascii/product/zipped/fixed/PacificOgorFixeddom.asp#Product> (May 16, 2016).